Analyses of Upwelling Events in the Gulf of Guinea using Satellite Observational Data and Model Outputs.

By

Patrick Dwomfuor

(10220881)

Supervised by

Dr. Joseph K. Ansong

Prof. Brian K. Arbic

Dr. Dimitris Menemenlis

August 2023

THIS THESIS IS SUBMITTED TO THE UNIVERSITY OF GHANA, LEGON IN PARTIAL FULFILMENT OF THE REQUIREMENTS FOR THE AWARD OF PHD IN MATHEMATICS DEGREE.

DECLARATION

This thesis was carried out in the Department of Mathematics, University of Ghana, Legon from May 2017 to August 2023 in partial fulfilment of the requirements for the award of Doctor of Philosophy degree in Mathematics under the supervision of Dr. Joseph K. Ansong of the University of Ghana, co-supervised by Prof. Brian Arbic of University of Michighan and Dr. Dimitris Menemenlis of JPL, NASA.

I hereby declare that except where due acknowledgement is made, this work has never been presented wholly or in part for the award of a degree at the University of Ghana or any other University.

Signature: .....

Student: Patrick Dwomfuor (10220881)

Signature: .....

Dr. Joseph K. Ansong (Principal Supervisor)

Signature: .....

Prof. Brian K. Arbic (Supervisor)

Signature: .....

Dr. Dimitris Menemenlis (Supervisor)

ABSTRACT

This thesis presents the analysis of upwelling events in the Gulf of Guinea and the Equatorial Atlantic region. The upwelling events in the West African subregion are usually experienced in the Gulf of Guinea, impacting the West African coastlines. During upwelling events, the wind blows across the water surface; a vacuum is created and filled with cold water and nutrient from the deep part of the ocean's surface. This process leads to heat distribution in the ocean, preserving the ocean's temperature. Classically, the upwelling events in the Gulf of Guinea were assumed to be generally caused by wind, Coriolis force, and Ekman transport. However, this research demonstrates that the wind that blows along the coast is usually in the north-northeastern direction. This means the correlation between the local wind stress and sea surface temperature (SST) anomaly in the Gulf of Guinea is considerably smaller.

Early research on the upwelling events in the eastern and tropical Atlantic region used trends and patterns from observations and mathematical numerical models to examine the cause of upwelling in the Atlantic region. [14] and [3] hypothesized that upwelling in the Gulf of Guinea is associated with Kelvin waves propagating eastward from the Brazillian coast along the equator. The Kelvin waves are trapped along the coast once they reach Equatorial Guinea as coastally-trapped Kelvin waves. A major goal of this study is to test this hypothesis using satellite observational data and output from the state-of-the-art Estimating the Circulation and Climate of the Ocean (ECCO) model.

We first investigate classical mathematical theory to understand the dynamics of upwelling. Exploring the classical theory of Ekman transport, Ekman pumping and suction will aid in explaining the reasons for the upwelling in the Gulf of Guinea. Based on [3], some mathematical derivations of the Kelvin waves theory will be used to find the features of the eastward propagating Kelvin waves on the ocean's surface.

Data collected from the Prediction and Research Moored Array in the Atlantic (PI-

RATA) will aid the understanding of the interactions between the ocean and atmosphere in the tropical Atlantic region. Temperature as a function of depth and time is collected from four different locations to understand how the ocean's temperature varies with depth. The rise of the thermal structure along the Atlantic region makes the thermocline shallower, leading to coastal upwelling, as discussed by [2] and [3]. June, July, August, and September usually are associated with low sea surface temperature (SST). However, the low SST is not enough evidence of what causes upwelling in the Gulf of Guinea, even though SST is important.

Sea surface height (SSH) signals from observations (satellite) and model data (ECCO) are composed of various waves whose characteristics and structures are different in terms of their period, wavelength, frequency, amplitude, and phase speeds. The Kelvin waves extracted from satellite data are examined and compared with the Kelvin waves extracted from model data. The phase speed of the Kelvin waves from observations and model data is about 1.8 m/s which is consistent with the result of [7]. The lag correlation between Kelvin waves from observation and ECCO for some specific years is good. The question is, how does the observational data compare with the model data, and can the model data be useful for future predictions? It is observed from analyzing the results that the error between Kelvin waves from observations and ECCO was getting smaller in recent years. This result shows a marginal improvement in the model.

Some selected parameters in a few areas of relevance in the Atlantic region, such as wind stress from the Brazilian region and SST from the Guinea-west region, were considered to examine the upwelling analysis used by [6], to explain the remote influence of upwelling in the Gulf of Guinea region. The results obtained by [6] were reproduced using recent observational data. In addition to the work by [6], model data from ECCO is used to produce similar results, supporting the hypothesis of [14].

DEDICATION

To my lovely wife and children.

ACKNOWLEDGEMENTS

"Surely, God is my help; the Lord is the one who sustains me. Psalm 54:4".I am grateful to God for helping me complete my research and my entire PhD studies. Even though it was difficult at first, the research ended well.

This research was conducted at the Mathematics Department, University of Ghana, Legon, with support from the Building a New Generation of Academics in Africa (BANGA-Africa). I would like to express my heartfelt gratitude to Dr Joseph K. Ansong, who is my principal supervisor, has been extremely supportive and helpful throughout the process of choosing a topic and navigating my thesis. He has also provided me with significant corrections for my thesis. I am grateful to Dr Ebenezer Nyadjro for his helpfulness and support during the early stages of my study on upwelling events in West Africa.

The motivation for this research started with a summer school organized by Estimating the Circulation and Climate of the Ocean (ECCO) on May 19-31, 2019, at Friday Harbor, Washington, USA. During a presentation at the summer school, Dr Michael McPhaden proposed a hypothetical idea behind upwelling dynamics in the Gulf of Guinea. I am very grateful to Dr Michael McPhaden for his suggestions and insightful view of the upwelling dynamics in the equatorial Atlantic region.

I am also grateful to Prof. Brian K. Arbic and Dr Dimitris Menemenlis, who are co-supervisors of this research, for their enthusiasm, unconditional support, and sacrifice towards this research. The beginning part of my research was a struggle; their collaborative effort, encouragement, and monthly meetings aided and guided my research. Special thanks to Prof. Paulo S. Polito for making available the code used in [9] to characterize Rossby waves. Modifying Paulo's code allowed for extracting the Kelvin waves in the equatorial Atlantic region. Special thanks to the Coastal Ocean Environment Summer School in Ghana (COESSING) organizers for their impact in the early part of this research. Through this organization, I learnt valuable tools for

researching upwelling events in the Gulf of Guinea.

I would like to extend my gratitude to the various sources that freely provided the data, including the following sources. SST data were obtained from https://www.metoffice.gov.uk/hadobs/hadisst/ provided under http://www.nationalarchives.gov.uk/doc/non-commercial-government-licence/version/2/. The observational sea level anomaly (SLA) data used in this research was obtained from E.U. Copernicus Marine Service Information; https://doi.org/10.48670/moi-00145. SST and SSH data were obtained from NASA Jet Propulsion Laboratory at https://ecco.jpl.nasa.gov/drive/files/Version5/Alpha/latlon_daily/SST.nc and https://ecco.jpl.nasa.gov/drive/files/Version5/Alpha/latlon_daily/SST.nc. The ERA5 wind product and SST were obtained from Copernicus Climate Change Service (C3S) Climate Data Store (CDS) at https://cds.climate.copernicus.eu/cdsapp#!/dataset/reanalysis-era5-single-levels?tab=form. The NOAA Optimum Interpolation 1/4 Degree Daily Sea Surface Temperature (OISST) Climate Data Record (CDR) used in this research was acquired from NOAA's National Climatic Data Center (http://www.ncdc.noaa.gov). Richard Reynolds and colleagues originally developed this CDR for NOAA's CDR Program. The PIRATA data for temperature was obtained from the Global Tropical Moored Buoy Array (GTMBA) Project Office of the National Oceanic and Atmospheric Administration (NOAA)/ Pacific Marine Environmental Laboratory (PMEL).

Furthermore, I want to thank my wife, Mrs Angelina Dwomfuor, and my son, Matthew Dwomfuor, for supporting me and giving me strength during the time I worked on my thesis.

Finally, I want to thank everyone who has helped and inspired me in many different ways.

Contents

Chapter 1

Introduction and Motivation

1.1 Introduction - Upwelling

Upwelling is the process whereby cold water and nutrient from the deep part of the ocean is displaced to the surface of the coastlines and along the equator. In the West African subregion, upwelling events are usually experienced in the Gulf of Guinea, impacting the West African coastlines. Classically, upwelling events are generally caused by wind, Coriolis force, and Ekman transport. Ideally, when the wind blows across the water's surface, a vacuum is created and filled with cold water and nutrient from the deep part of the ocean's surface. The dynamic process whereby the cold water and nutrient move to the ocean's surface is by conservation of mass. This process leads to heat distribution in the ocean, thereby preserving the ocean's temperature.

Figure 1.1a shows how the temperature in the ocean changes with depth; it is warmer on the surface and cooler at the bottom. During upwelling, the cooler waters in the deeper part of the ocean move to the ocean's surface, causing heat distribution in the ocean. Figure 1.1b, demonstrates how the wind pushes the surface water.

The different types of upwelling include coastal upwelling, equatorial upwelling (large-scale wind-driven upwelling in the ocean interior), upwelling associated with eddies, and upwelling due to Kelvin waves.

Coastal upwelling is the most common known upwelling process, which occurs when the wind direction is parallel to the coastline and generates wind-driven currents. In Figure 1.2, when the wind blows by the coast, the Ekman transport goes in a direction

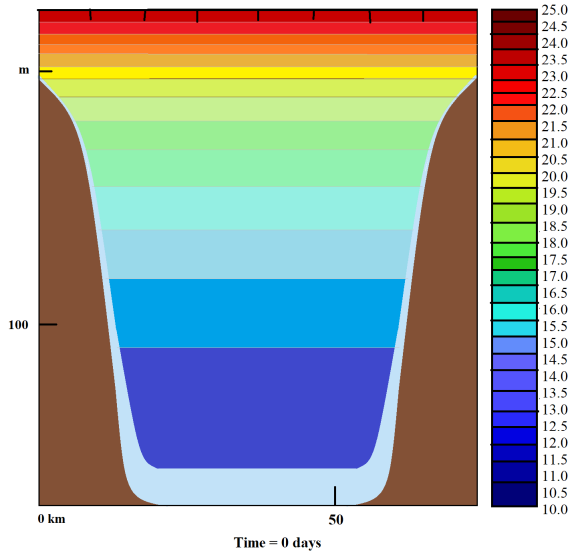

(a) Change in temperature with depth

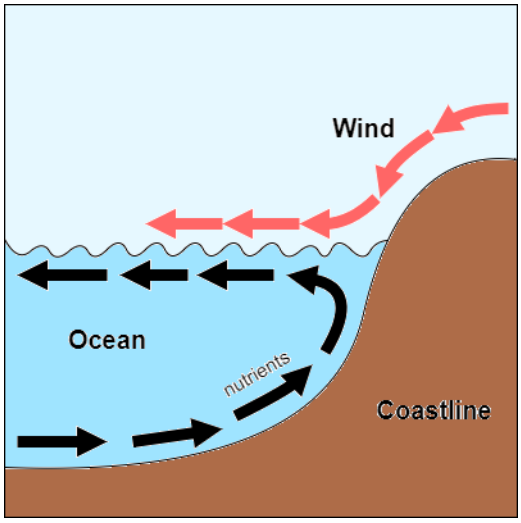

(b) Interaction of the wind with Upwelling

Figure 1.1: Upwelling Dynamics

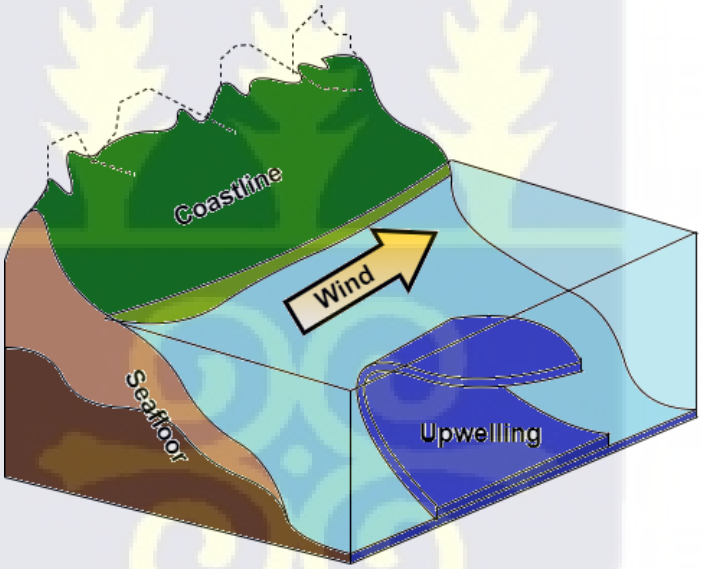

Figure 1.2: Upwelling

that is at a right angle to the wind. This means that there will either be water moving downwards or upwards at the coast to provide the Ekman layer with water. Ekman transport is the net movement of fluid on the ocean's surface layer in the direction of 90 degrees to the wind. At the coastline, Ekman transport can either converge or diverge at the coast.

Equatorial upwelling happens because of the westward wind (trade winds), which

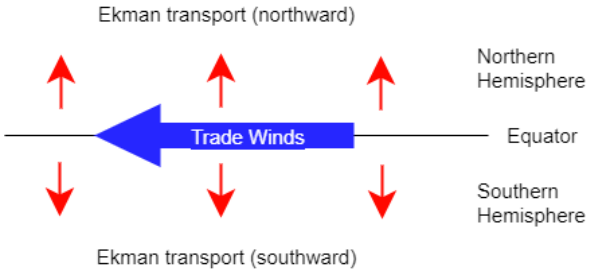

Figure 1.3: The Ekman Transport

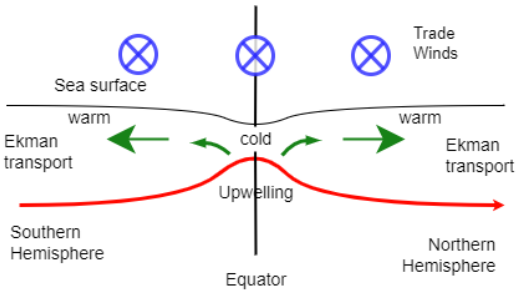

Figure 1.4: Effect on the thermocline and surface temperature

causes Ekman transport as seen in Figure 1.3 and 1.4. In Figure 1.3, the westward trade wind pushes the ocean surface water leading to Ekman transport in both the northward and southward direction. The process causes cold water and nutrients from the deep ocean to rise up to the ocean surface, as shown in Figure 1.4. The cold surface water leads to low SST, while the wind pushing the ocean surface water leads to low SSH. The low SST and SSH become necessary signatures or characteristics serving as indicators for upwelling triggered by the wind. The equatorial zone acts like a tunnel for waves, which means they get stuck near the equator and cannot easily move away. The equatorial Kelvin wave shows us that the equator acts like a boundary for the northern and southern hemispheres. This makes the wave similar to the Kelvin waves that are trapped near the coastlines. This means that even though the wind strength is not very strong, there is movement of deep water towards the surface near the equator because of the Coriolis effect. Eddies occur due to the circular mixing of the ocean forming circular currents. The wind patterns generated during slow-moving eddies (whirlpools) can also blow surface water aside, leading to upwelling.

Upwelling associated with Kelvin waves is due to the pushing of water by the wind in the westward direction of the ocean, which later impacts are experienced in the eastward direction of the ocean as Kelvin waves. If the Kelvin waves are trapped along the equator, they are called equatorial trapped Kelvin waves, while if the Kelvin waves are trapped along the coast, the process is known as coastally trapped Kelvin waves. Upwelling and downwelling both describe mass movements of the ocean, which are essential in stirring the ocean, delivering oxygen to depth, distributing heat, and bringing nutrients to the surface.

The upwelling event in the Gulf of Guinea has a significant impact on the coastal surroundings of West Africa. Coastal upwelling events are primarily experienced in

the coastal areas around the world. Along the Gulf of Guinea, upwelling events are usually experienced in June, July, August, and September, characterised by seasonally low Sea Surface Temperature (SST) of the ocean. During upwelling events, there is an increase in biological activities like phytoplankton and zooplankton in the ocean, which are nutrient-rich, serving as food for fish and other living organisms ([74]; [81]). The number of fish increases in areas that experience coastal upwelling, thereby increasing the economic revenue for the people and the country. Secondly, the cold water from upwelling impacts the environment and local climate by cooling the weather. Finally, upwelling dramatically affects the local climate and the environment since the coastal ocean surface conditions in the Gulf of Guinea influence the West African climate ([15]). [82] examined the reasons why the waters along the coast in the Northern Gulf of Guinea, specifically caused by the Niger River, are getting warmer. Their research shows that the Niger River warms the water along the coast of the northern Gulf of Guinea. However, they haven't yet studied or fully understood why this happens. The studies indicate that the Niger River's warming is a result of water movement in both vertical and horizontal directions. Also, the rising temperatures of the mean climatological state in the northern Gulf of Guinea's coastal waters are anticipated to have consequences for the marine ecosystem, according to [82]. This can make more plants grow and have a good effect on the environment in that region. However, the number and availability of fish species may decrease and have a negative impact on fishing in the region.

The influence of upwelling on SST explains why we have the cool weather in early August; the question is whether it is locally or remotely forced, as shown by [3]. Since the upwelling event changes seasonally, there is some impact on the weather. The low sea surface temperature (SST) during upwelling along the Gulf of Guinea accounts for some cool weather around June, July, August, and September. Annually, the Gulf of Guinea has cold weather from June to September, warm weather from October to May, and brief or light cold weather in January and February. The weak cold weather is usually associated with minor upwelling, and the strong cold weather is linked to major upwelling events. The minor upwelling season can last for three weeks, whiles the major upwelling season can last for about three months. According to [4], the coastal temperature data recorded between 1962 and 1982 indicate that the propagation of sea surface temperature signal was running east to west concerning the major upwelling season of June through September. This shows two types of upwelling seasons annually: minor upwelling and major upwelling.

1.1.1 Causes of Upwelling in the Gulf of Guinea

[24] suggested that the direction in which water on the surface moves can be affected by the presence of winds running alongside the coastline. When the divergence increases, it results in the upward movement of cold water to the top layer in order to maintain balance. Their results suggest that a decrease in the SST is a viable means of quantifying upwelling, as shown in Figure 1.2. [18] did some studies on the winds by analysing the winds and calculating the wind's angles with the coast to trigger upwelling events. Since the wind is not parallel to the coast, upwelling in the Gulf of Guinea may not be linked with local wind forcing alone but may be due to other factors.

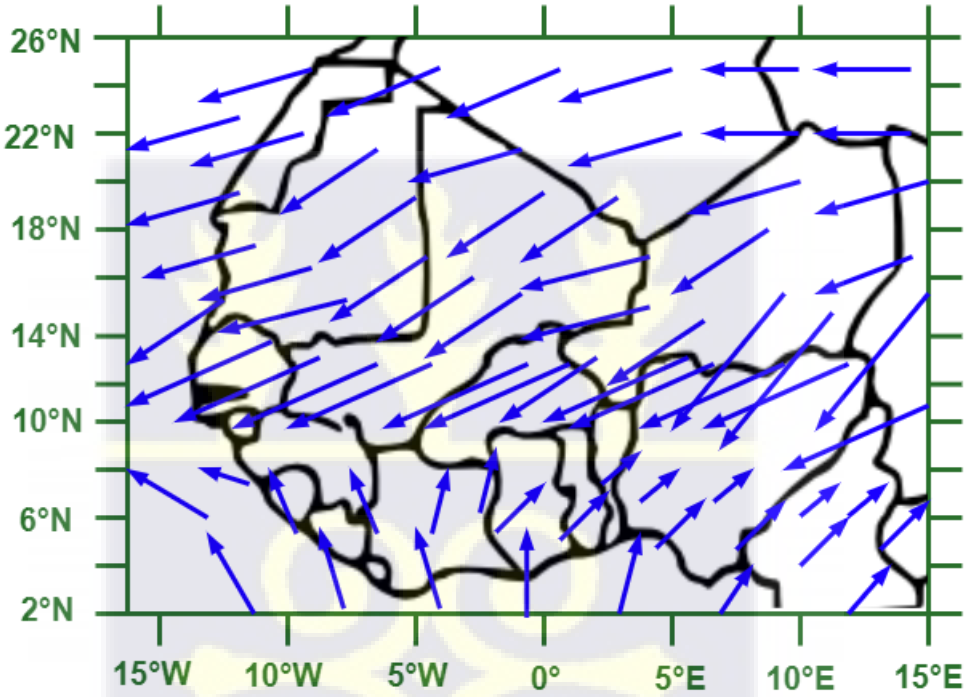

Figure 1.5: Mean wind speed and direction around West Africa (1956 to 2015) modified from [19]

The coastline of West Africa is bounded by the Gulf of Guinea in the northern hemisphere. The wind that blows along the coast is usually in the north-northeastward, as seen in Figure 1.5, causing the Gulf of Guinea surface current in the northern hemisphere to move 90 degrees to the eastward direction. This means upwelling in the Gulf of Guinea is not entirely connected in any obvious way to the local winds, as explained by [30] and [1]. Instead, the Gulf of Guinea upwelling is a large-scale event characterised throughout the region and lasts for several months.

One hypothesis is that the local wind is not responsible for upwelling; instead, it is due to remote influence. [14] suggested an explanation for the upwelling events in the Gulf of Guinea. They assumed that there was a sudden increase in wind strength in the Brazilian region. They also indicated that the wind has a complicated structure that changes over time and space, and it keeps getting stronger. In the past, due to limited observational and global model data, regional numerical models have been used to study the processes leading to how the ocean reacts to wind action. However, past research has indicated that the upwelling events along the Gulf of Guinea are probably due to Kelvin wave propagation. These Kelvin waves propagate eastward from the Brazilian coast along the equator ([3]). They split into two coastal waves that are trapped along the coast once they reach Equatorial Guinea. The trapped signal propagates along the coastline; one is to the southern direction and another to the northern direction in the Gulf of Guinea. Suppose the upwelling events are due to remote influence, is it a phenomenon that happens in the Equatorial Atlantic and later experienced on the West African coast? Is it predictable? This phenomenon will have a significant impact on tourism and fisheries. A major goal of this study is to test this hypothesis using satellite observational data and output from the state-of-the-art Estimating the Circulation and Climate of the Ocean (ECCO) model.

Observational and model data will be utilised to answer issues concerning upwelling in the Gulf of Guinea region. One approach is to compare model and observational (or PIRATA) data. Before the year 2000, scientists didn't have powerful models that ran for a very long time and they didn't have a lot of data to visualise some processes. Most past research had some famous equations on theoretical ideas, and there were not enough figures to support these ideas. However, we will look at these equations in this research and try implementing some solutions suggested in previous research.

1.2 Motivation

The motivation for this research is to fill a gap in our knowledge of the upwelling phenomenon in the Gulf of Guinea. There are several unanswered scientific questions regarding upwelling in the Gulf of Guinea. Unlike classical coastal upwelling caused by Ekman transport, the predominant wind direction in the surface waters of the Gulf of Guinea suggests that the usual conditions of water movement may not apply in the Gulf of Guinea.This idea made [14] hypothesize that the upward movement of cold water in the Gulf of Guinea is probably caused by waves that start near the coast of

Brazil and travel to the Gulf of Guinea. [3] used a simple numerical setup to generate Kelvin waves that propagated towards the Gulf of Guinea in a manner suggested by [14], thereby giving credence to the hypothesis. However, these earlier studies lacked enough observational and realistic model data to validate or evaluate the hypothesis of remote forcing. [6] analyzed historical observational data, employing lag correlation analysis, to show evidence of remote forcing of the Gulf of Guinea upwelling. It has been four decades since the study by [6], and there have been a lot more observational data collected and major improvements in realistic/operational numerical models. At the same time, some studies continue to implicate local forcing for the Gulf of Guinea upwelling (example [24] and others). A major goal of this study is to revisit and test the hypothesis of [14] using relatively recent satellite observational data and output from state-of-the-art numerical models like the Estimating the Circulation and Climate of the Ocean (ECCO) model. Other studies also suggest that the Gulf of Guinea upwelling is likely caused by a combination of local and remote forcing ([20]). However, the fraction of upwelling due to local and/or remote forcing is unknown.

Another motivation is that upwelling yields a rich ecosystem along the coast due to nutrients brought up to the surface from deeper waters. Thus, it would be important to be able to predict significant upwelling events using realistic ocean models like ECCO.

Chapter 2

Literature Review and Research Plan

2.1 Literature Review

There have been different kinds of research and studies to understand the upwelling dynamics in the Gulf of Guinea, but there are no clear-cut reasons to what is causing it. There are various theories and hypotheses about mechanisms that cause upwelling in the Gulf of Guinea (GoG). Some of the classical theories used to study upwelling in the Gulf of Guinea were that when the wind blows on the ocean's top layer, it creates surface currents. This leads to water from the bottom upwelling or rising to fill the water that moved away. This classical idea of explaining upwelling events in the Gulf of Guinea fails because there is no apparent connection between the local winds and upwelling in the Gulf of Guinea. A thorough investigation of the reasons why the classical idea of upwelling is inadequate is given by earlier theories and hypotheses based on previous studies regarding the numerous mechanisms causing upwelling in the Gulf of Guinea. [14] set the pace for the evolution of the remote influence of upwelling. His research used observations (not from satellites) to explain why the upwelling event in the Gulf of Guinea wasn't associated with the local winds.The observational data used in [14] were collected from GATE (summer 1974), a Soviet ship, the R.V. Passat, stationed on the equator at 10° west of the Eastern Atlantic region. It measures the temperature of the ocean's surface, which is usually low before the yearly upwelling starts in the Gulf of Guinea.Recording low sea surface temperature from a time series was not enough to conclude the onset of upwelling in the Gulf of Guinea.

[14] used a simple linear model to explain teleconnections between the eastward Kelvin waves and westward wind stress in the eastern Atlantic region. In the linear model, the wind stress was confined to the western ocean and switched on at some initial time; the linear model then generate eastward Kelvin waves with an average phase speed of 2.5 meters per second. One of the obvious challenges with using a simple linear model is that it does not capture nonlinearities, which amplifies the Kelvin waves and prolongs upwelling events.

[14] hypothesised that the upwelling event in the Gulf of Guinea results from intense westward wind stress applied in the western Atlantic. The idea was to generate an equatorially trapped Kelvin wave that moves eastward along the equator. The trapped Kelvin wave on reaching Africa in the eastward direction propagates along the coastal boundary of West Africa. This process of making water move upwards in the Gulf of Guinea is similar to how El Niño acts in the Pacific Ocean. However, their research had some limitations concerning limited observations to address whether an equatorial upwelling event occurs. Their research did not provide the theoretical background on the simple linear models to explain some of the dynamics of upwelling in the Eastern Atlantic region.

[2] and [3], provided enough mathematical and theoretical concepts necessary to understand how upwelling events occur in the Gulf of Guinea. Their work uses a linear model on an equatorial β-plane to simulate and explain the physical events linked with the seasonal upwelling in the Gulf of Guinea. The model is forced with an increase in the westward wind stress of 0.025 Nm^{-2} in the Western Atlantic to excite an equatorially trapped Kelvin wave that propagates eastward along the equator. The trapped Kelvin wave on reaching Africa in the eastward direction is propagated along the coastal boundary of West Africa. This creates a movement of deep, cold water rising up to the surface in the Gulf of Guinea. [3] used a linear model and numerical simulation to argue that the rise of cold water in the Gulf of Guinea was not caused by the winds and Ekman transport. Nonlinearities in the model were used to amplify the effects of the Kelvin wave and prolong the upwelling event, an improved version of the simple linear models used in [14].

[3] presented good background information using a research paper by [31] to find that during the summer of 1974, there was an increase in the oceanic zonal pressure gradient in the western equatorial Atlantic. This led to a high correlation between the zonal pressure gradient and the zonal wind stress.

In explaining why the local winds were insufficient to drive upwelling in the Gulf

of Guinea, [3] examined a study conducted by the Ghana Fishery Research Unit to measure the movement of cool water to the surface during the summer in the Gulf of Guinea. There are only a few specific areas along the coast where the local winds are in the right direction to cause an upward movement of water due to the wind. Still, there is a poor correlation between the local winds and upwelling. Studies by [30] and [1] explain how there is no time delay in the temperatures along the coastal areas near Tema to suggest that local ocean circulation advect the colder water to other regions. Instead, the Gulf of Guinea upwelling is a large-scale event characterised throughout the entire region and lasts for several months. Meaning there is no correlation between local winds and nearshore drop in temperature. [3] used a theoretical model to explain how upwelling due to a Kelvin wave becomes significant when the westward zonal wind stress increases in an unbounded ocean occurring 3000 km from the Gulf of Guinea coast.

In analysing the nonlinear model, [3] included a standardised linear case which considers an increase in wind stress of 0.025 Nm^{-2} in the western direction over 1500 km in the west of the basin. They also implemented a nonlinear case similar to the standard linear case, which included advective effects, local depth in the stress, and nonlinearities in the continuity equation with a reduction in the western wind stress. The west basin flow was adjusted so that the pressure gradient balances the wind stress. The equatorial Rossby waves propagate westward with a phase speed of 1/3 the Kelvin wave speed. The inclusion of the nonlinear terms has two effects on the Kelvin waves: to reduce the phase speed and amplify the wave's impact to prolong upwelling.

[81] examined how the Atlantic Ocean's eastern boundary upwelling area changes during different times of the year. They accomplished this by examining data gathered over several years from both moorings and satellites. Scientists found evidence of Kelvin waves by observing changes in sea level that are connected to changes in sea surface temperature, but with a 14 day delay.

Despite some improvements in understanding the dynamics of upwelling events in the Gulf of Guinea, some challenges are not well addressed in [3]. The challenges include the fact that the irregular geometry of the equatorial Atlantic basin, which extends approximately 5000 km zonally and 1500 km on either side of the equator, was not captured. The numerical simulation of the oceanic response used by [3] was done by considering a 2-layer model on the β-plane with an increase in westward wind stress integrated over the tropical Atlantic Ocean to predict and study the Kelvin waves.

This study utilizes a realistic ocean model that models the irregular geometry of the Gulf of Guinea basin and has 50 vertical levels.

[1] suggested that the movements of the Guinea Current (G.C) and the Ekman transport cause the water to rise up along the West African coast. [20] demonstrated that the amplitude of upwelling caused by G.C is insignificant when compared to observations. However, current studies by [12] noted the importance of G.C in generating coastal upwelling.

[6] studied the relationship between the temperature of the ocean's surface in the Gulf of Guinea and the strength of the wind in the Brazilian region in specific parts of the tropical Atlantic. Their study indicates that remote forcing in the western equatorial Atlantic ocean affects the temperature of the sea surface in the eastern part of the Atlantic Ocean. Their findings showed a strong connection between the temperature of the ocean's surface and the strength of the wind.

[4] used observations, theories, and models to analyse SST recorded from 16 coastal sites around the Gulf of Guinea and offer evidence of horizontal and vertical propagation of remotely driven seasonal upwelling in the eastern Atlantic. Their research work indicated some challenges that need to be considered, such as the predictability of his model in real life and how it compares to other models. [4] examined the hypothesis that an intensified westward wind in the equatorial Atlantic Ocean can lead to the accumulation of water near the coastline of Brazil. They found that the water buildup creates a pressure difference that is balanced by the wind stress. This process triggers Kelvin waves which propagate eastward at a speed of $c = \sqrt{g'H}$ where g' is the reduced gravity, and H is the height of the water column. The eastward trapped Kelvin waves split at the eastern boundary with waves going poleward along the coast in both hemispheres as coastally trapped Kelvin waves.

[4] found that the equatorial ocean has a far-reaching effect by creating equatorial Kelvin waves. These waves then produce trapped waves near the coast of Africa. Their calculation indicates that the coastal upwelling propagates poleward in both hemispheres starting from the equator.

[7] investigated oceanic Kelvin waves from the equator to the West African coast. They applied a 25 to 95 days bandpass filter to the sea surface height (SSH) product from TOPEX/POSEIDON altimeter. Their estimate for the phase speed of the Kelvin waves ranges from 1.5 to 2.1 m/s along the eastern Atlantic region. [75] discovered a new way to predict the strength of waves along the coast. The observation made by

[75] and [76] suggests that waves that become trapped in the vicinity of the coast can be removed as they are significant in determining the movement and circulation of the ocean. [76] studies in the southeastern Pacific and Atlantic oceans demonstrate how their approach is able to understand and describe the coastally trapped waves and their relationship to the changes in the equatorial region.

[79] studied how the Atlantic ocean near the equator affects the coastal area of Angola-Namibia over several years, between 1998 and 2012. Their findings indicated a significant correlation between the monthly height anomalies detected by the Prediction and Research Moored Array in the Tropical Atlantic (PIRATA), the anomalies observed in sea surface height measured by altimeters on a monthly basis, and the anomalies derived from an ocean model. Their results can be used as a starting point to understand the PIRATA records by using the equatorial Kelvin waves as a reference.

In the Gulf of Guinea, coastal upwelling can be attributed to four hypotheses, which are listed in [12]. The first hypothesis was that the eastward–flowing Guinea Current at the coast was associated with the upwelling process in the Gulf of Guinea. The hypothesis was supported by [63], [1], and [64]. They suggested that the movement of water in the ocean near the coast is caused by the adjustment of the Guinea Current and the way the wind pushes the water. However, the recent warming of the Atlantic Ocean ([6]) is concomitant to the decreasing of coastal upwelling ([11]) and to the intensification of Gulf of Guinea marine heatwaves ([13]). [65] suggested that these eddies are causing the sea surface temperature to be lower during the summer. They indicated that the Capes and Guinea current interactions generated cyclonic eddies. However, [11] have shown that coastal upwelling continues to occur even when there are no cyclonic eddies, contradicting this hypothesis. Thirdly, [64] proposed that another potential factor contributing to upwelling in the Gulf of Guinea might be the Ekman pumping brought on by the wind stress curl. This concept was initially proposed by [66], [67], and [68] based on the outputs of a tropical Atlantic model induced by climatology wind from 1982 to 1984. Finally, [14], [69], [6], and [4] found that the nature of the equatorial ocean can create waves that travel along the African coast. These waves are caused by the movement of equatorial Kelvin waves. [4] urged for further thermal structure measurements and other investigations using observation and model data to properly support this hypothesis.

2.2 Research Plan

We have already examined some limitations of most previous research on understanding upwelling events in the Eastern Atlantic region. Therefore, in mapping out the bigger picture of upwelling along the Gulf of Guinea in the tropical Atlantic region, the following needs to be considered: First, the mathematics and dynamics of upwelling will be explored in Chapter 4. Secondly, there are several theories and hypotheses regarding the various factors generating upwelling in the Gulf of Guinea (GoG). Explaining the upwelling process in the Gulf of Guinea is still contentious today. An analysis of the Kelvin waves extracted from the sea level anomaly (SLA), sea surface temperature (SST), and surface wind speeds are used to clearly understand what explains the upwelling events in the Gulf of Guinea. Some theories and hypotheses have suggested upwelling events associated with equatorially trapped Kelvin waves. Still, there hasn't been a clear understanding of how the Kelvin waves are associated with upwelling events in the West Africa region. Kelvin waves are extracted from sea level anomaly (SLA) at a specific period between 30 to 180 days and a wavelength of about 1,000 to 20,000 km to understand this phenomenon better.

Although [3] and other research papers use theoretical Kelvin wave models to predict the phase speed, it is not enough to give the Kelvin waves higher predictability on upwelling in the Gulf of Guinea. There have been better and well-equipped observational and model data in recent times.

The plan is to study the classical theory of upwelling and determine whether the winds in the Gulf of Guinea are connected to the upwelling process using modern satellite observational data and model outputs. Furthermore, we will review the dynamics and theory of upwelling in subsequent chapters, as this is the central focus of this research. We will use satellite (observational) data and current model (ECCO) data to extract Kelvin waves. The Kelvin waves extracted from observation and model data will be compared relatively to see how they correlate with each other in specific years. [7] filtering techniques use a 25 to 95 days bandpass filter to estimate the frequency of the eastward propagating Kelvin waves along the equator and the coastal region of West Africa. However, the filtering techniques used in this research consider both the Kelvin waves' wavelength and frequency. This approach provides an explicit characteristic and structure of the Kelvin waves. Extracting the Kelvin waves by this method will be implemented on observation and current model data. Now the scientific question is, how does the observational data compare with the model data,

and can the model data be useful for future predictions? These ideas will be further explored and analyzed in subsequent chapters.

2.3 Observational Data

We obtain altimeter grided Sea Level Anomalies (SLA) data from Copernicus Marine and Environment Monitoring Service (CMEMS). CMEMS are responsible for the processing and distributing Duacs grided "allsat" Sea Level Anomaly (SLA), formally distributed by Aviso as seen in [55]. The SLA was sampled daily from the 1/4 degree $\times$ 1/4 degree resolution data and spans from 01-01-1993 to 03-06-2020. The Kelvin waves were extracted from the SLA by using techniques presented by [9] on the characterization of Rossby waves. This was done for several spectral bands for the equatorial Atlantic basin ranging from 15° North to 15° South and 50° West to 15° East. A finite impulse response (FIR) filter of [9] was applied to the global SLA to extract the Kelvin waves for the Atlantic region.

Kelvin waves have wavelengths of about 1,000 to 20,000 km long and have a period of 25 to 95 days, as stated in [7]. The FIR filter uses both the spatial extent(wavelength) and time (period) to extract the Kelvin waves. We use lag correlation analyses to understand the connection between kelvin waves and upwelling events in the Gulf of Guinea.

The wind and SST products are obtained from ERA5, a fifth-generation ECMWF (European Centre for Medium-Range Weather Forecasts) reanalysis of the global climate and weather for the past 40 to 70 years as stated in [59]. Wind stress computed using $\tau = \rho_a C_d |\mathbf{U}|\mathbf{U}$, τ is the surface wind stress (units = Nm^{-2}), ρ_a is the air density (1.225 kgm^{-3}), C_d is the drag coefficient (1.43×10^{-3}), and $\mathbf{U}$ is the wind speed in ms^{-1}. 36-year time series from 1981 to 2016 of monthly means of wind and SST was used as monthly climatology to find the wind stress and SST anomalies. More data from more extended time series used in computing climatology for SLA, SST, and wind stress affects the lag correlation in the Brazilian, Guinea North, and Guinea West regions.

2.4 Model Data (ECCO)

Model output is obtained from ECCO. The model uses ideas similar to conventional ocean reanalysis to reconstruct the ocean states with the help of observational data from satellites like Topex Poseidon or in-situ measurements to fit the model to agree with observations. What makes ECCO different from other ocean reanalysis is that it can explain the physical causes and dynamics behind the behaviour and characteristics of the ocean. Data fitting is done by altering a set of ocean model initial conditions, parameters, and atmospheric boundary conditions that obey the laws of physics and thermodynamics. The version of the ECCO product used was ECCO LLC270 (1/3 degree), which was interpolated to a 1/4 degree latitude-longitude (lat-lon) grid. SST and SSH were obtained from the ECCO LLC270 output product. SLA from Aviso and SSH from ECCO are both 1/4 degree. Using Paulo's extraction code, Kelvin waves were extracted from both observation and model at periods of about one month, three months, and six months, respectively.

Chapter 3

General Theory of Fluids

3.1 Introduction to Fluid Mechanics

Fluid Mechanics is a branch of science that studies how fluids behave and how forces, movements, and static conditions interact in a continuous material. Fluid mechanics is the study of how fluids behave when they are not moving, or when they are moving without pressure forces, and when they are moving with pressure forces. Most of the mass in the universe is in a liquid form. This means that it is not possible to have life without liquids. This field of study focuses on different problems, like how liquids make a skin on top, how liquids move inside closed spaces, how liquids move around solid objects, how liquids stay steady, and more. Fluid mechanics is a fascinating field of study that has both scientific and practical significance. Fluid mechanics is a field of study that helps us understand how fluids move and behave. By studying fluid mechanics, we can use different methods to learn about the natural world and find ways to make life better for people.

Mathematical analysis and computer simulations are used to study fluid mechanics. They help us find solutions to simplify problems, which we can use to gain insights and understanding.

A fluid is a substance that always changes shape when it is pushed or pulled, no matter how much force is applied. There are two types of fluids: liquids and gases. A gas spreads out to fill its container, but liquids don't spread out as much and cannot fill big containers. Fluids have zero stiffness, which means that they cannot resist any force that causes them to change shape. When a solid is subjected to shear stress,

it does not change shape smoothly. However, it does have a natural shape, and it returns when the forces are removed. When a solid is subjected to a sideways force, if it is very flexible, it goes back to its normal shape when the force is removed. A liquid can change its shape when even a tiny force is applied to it. When the force that causes the fluid to slide past each other is taken away, the fluid does not go back to its original shape, and it continues to move. However, certain solid materials can bend and change shape if a certain amount of pressure is applied. This type of solid is called a *plastic*. Fluid and solid mechanics are not clearly different from each other because some solids can also change shape constantly. For instance, certain substances like paints, jelly, putty, and egg whites can act like both solids and liquids at the same time. We say that an elastic solid remembers its original shape very well because it always returns to that shape when it is not being stretched. An ordinary thick liquid does not have a memory because it does not bounce back when it is no longer being pushed or squeezed. Egg whites and similar substances can be called *viscoelastic* because they partially bounce back when not carrying any weight. When forces push or pull on solids and fluids, they act differently when experiencing shear stress but act similarly when experiencing normal compressive stresses. Solids can handle pulling and pushing forces, while fluids expand or change form when pulled. Certain liquids can withstand a small amount of stretching force. This depends on how tightly the molecules are connected and how long the stretching force is applied.

3.1.1 Properties of fluids

- Density or Mass density (ρ): It is the ratio of mass (m) of fluid to the volume (v) of fluid. Mathematically, $\rho = \frac{m}{V}$, and the SI unit is kilogram per meter cubed.
- Weight Density or Specific weight (ω): It is the ratio of the weight (w) of fluid to the volume (V) of fluid, and the SI unit is kilogram per meter cubed.
- Specific volume (V): It is the ratio of volume per unit mass.
- Specific gravity (S): It is the ratio of the weight density of the liquid to the weight density of the standard liquid (water) or the ratio of the mass density of the liquid to the mass density of water.

Viscosity (Dynamic viscosity): It is the resistance offered to a layer of fluid when it moves over another layer of fluid, and the SI is Newton-second per meter squared.

The rate of shear stress is directly proportional to the velocity gradient. Consider a fixed surface or base and let a fluid flow over the fixed surface with a fixed height in the y-direction as seen in Figure 3.1.

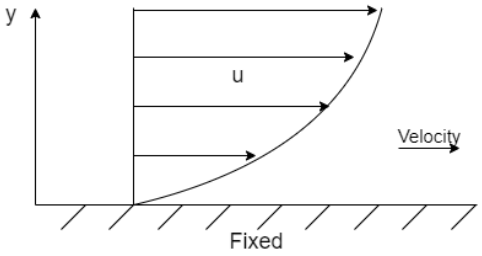

Figure 3.1: Velocity profile

Since the base surface is fixed, the velocity is zero there, and it resists the flow of fluid. We get a maximum velocity at the top of the fluid flow. We can better explain the fluid flow using the velocity profile in Figure 3.1 by considering a small element dy. When the layers move over each other with different velocities, the layer is likely to shear or slip. The slipping action is the rate at which the fluid shear (shear stress) is directly proportional to the velocity gradient.

Kinematic Viscosity: It is the ratio of dynamic viscosity to the density (mass density) of fluid.

$$\nu = \frac{\mu}{\rho},$$

where μ is the *dynamic viscosity* with units of $\mathrm{kgm^{-1}s^{-1}}$, ρ is the mass density of the fluid with units $\mathrm{kgm^{-3}}$, and ν is the *kinematic viscosity* with units $\mathrm{m^2s^{-1}}$.
Fluids that follow Newton's law of viscosity are called Newtonian fluids. **Newtonian fluid** is a fluid in which the shear stress arising from the fluid flow at every point is directly proportional to the rate of shear strain (the rate of change of its deformation over time). Newtonian fluids are the simplest mathematical models of fluids that account for viscosity. Fluids that perfectly fit this definition include water, oil, gasoline, alcohol, and air. The viscous stress is related to the strain rate by

$$\tau = \mu \frac{\mathrm{d}u}{\mathrm{d}y}, \tag{3.1}$$

where τ is the shear stress or drag in the fluid, μ is the shear viscosity of the fluid, also known as dynamic viscosity, and $\dfrac{\mathrm{d}u}{\mathrm{d}y}$ is the derivative of the velocity component that is parallel to the direction of shear or rate of shear strain as shown in Figure 3.1.
A fluid is said to be **incompressible** if the density of the fluid does not change with

pressure. If the fluid is incompressible and the viscosity is constant across the fluid, Equation 3.1 can be written in the two-dimensional form in terms of an arbitrary coordinate system as

$$\tau_{i,j} = \mu \left(\frac{\mathrm{d}u_i}{\mathrm{d}y_j} + \frac{\mathrm{d}u_j}{\mathrm{d}y_i} \right), \tag{3.2}$$

where y_j is the jth spatial coordinate, u_i is the fluid's velocity in the direction of ith axis, $\tau_{i,j}$ is the jth component of the stress acting on the faces of the fluid element perpendicular to the ith axis.

3.1.2 Types of fluids

Fluids can be classified into five types that is, Ideal fluid, Real fluid, Newtonian fluid, Non-newtonian fluid and Ideal plastic fluid. An ideal fluid is an incompressible fluid whose viscosity is low (close to zero), such as water, petrol, etc. Real fluid is a compressible fluid whose viscosity is non-zero. Newtonian fluid is a fluid in which shear stress is directly proportional to the velocity gradient. Non-newtonian fluid is a fluid in which shear stress is not directly proportional to the rate of shear strain. Ideal-plastic fluid is a fluid in which the shear stress is more than the yield value, and the shear stress is directly proportional to the shear strain.

3.1.3 Surface tension

Surface tension is a tensile force acting on the surface of a liquid in contact with air (gas) or between two immiscible liquids. It is denoted by σ. Surface tension and pressure force relation for a water droplet is

$$P = \frac{4\sigma}{d},$$

where P is the pressure force (intensity of pressure) with units Nm^{-2}, σ is the surface tension with units Nm^{-1} and d is the diameter of the water droplet.
Whenever two substances that cannot mix together, like air and water, come into contact, there can be a difference in how dense they are at the place where they meet. In simpler terms, when the forces between molecules on the surface are not balanced, the surface acts like a stretched membrane under tension. This is similar to when air bubbles in water form round shapes.

Capillarity happens because of surface tension. We know that when a tube with liquid inside is put in another container filled with liquid, the top surface of the liquid in the tube either goes up or down. These tiny tubes are called capillary tubes. The pressure in a still liquid can be explained by the hydrostatic law. Hydrostatic forces on surfaces are the forces applied by a still fluid. For hydrostatic forces to occur, the liquid must not be moving and the weight of the liquid will push on the object.
Hydrostatic law states that the increase of pressure intensity at a point in a static fluid is directly proportional to the weight density of the fluid. The intensity of pressure is given by $P = wh$, where P is the intensity of pressure at a particular depth in a fluid, w is the specific weight or weight density, and h is the height from the free surface of the liquid to the point of interest.

3.1.4 Pressure

In a fluid that is not moving, the **pressure** at a certain point is the amount of force divided by the area. Ordinary pressure is sometimes known as *absolute pressure*,P_a , which is different from *gauge pressure* (measured with an instrument), P_{gauge}, defined as absolute pressure (counted from the absolute vacuum) minus the atmospheric pressure, P_{atm}:

$$P_{\text{gauge}} = P_a - P_{\text{atm}},$$

where atmospheric pressure is the pressure in the surrounding atmosphere.

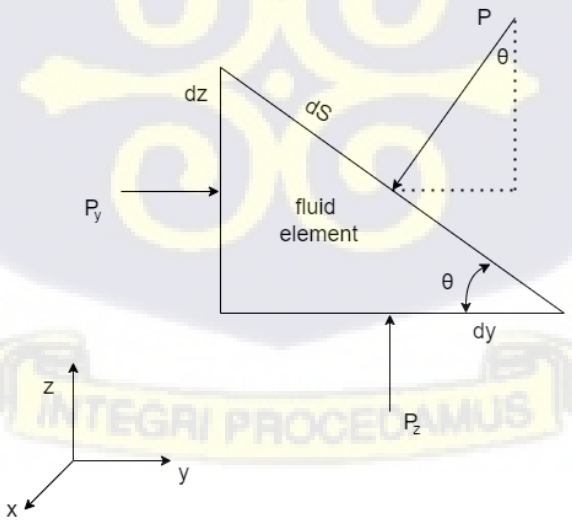

Figure 3.2: Pressure at a point in a fluid

In a static fluid, the tangential viscous stresses are absent and the only force acting on the adjacent surfaces is normal to the surface. Using this idea, we can demonstrate that the pressure at a point in a fluid is the same from any direction to the point. Consider a small volume of fluid with a triangular cross-section of unit thickness, and let P_y, P_z and P be the pressures on the three faces as shown in Figure 3.2. The only forces acting on the fluid are the pressure forces normal to the faces and the weight of the fluid.

Since in a static fluid there is no flow in the horizontal direction, y, the sum of forces in the y-direction is zero, that is,

$$P_y(dz)(1) - P(\sin\theta ds)(1) = 0.$$

Since $dz = \sin\theta ds$, we get $P_y = P$. A balance of forces in the z-direction gives

$$P_z(dy)(1) - P(\cos\theta ds)(1) - \frac{1}{2}\rho g dz dy = 0.$$

Since $dy = \cos\theta ds$, we get

$$P_z - P - \frac{1}{2}\rho g dz = 0.$$

As the static fluid in the Figure 3.2 is shrunk to a point, $dz \to 0$ with $\theta =$ constant, the gravitational force term drops out, leaving $P_z = P$. Thus, it doesn't matter which way you look at the pressure. This means the pressure at a point in a static fluid is the same in all directions, that is, $P_y = P_z = P$, also known as the **Pascal's law**.

We next determine the *spatial distribution* of pressure in a static fluid. Consider a static fluid in a cube of sides dx, dy, and dz, with one of the cube's faces looking as in Figure 3.3.

All the forces point into the cube since pressure is compressive stress; the forces push on the fluid. Let P be the pressure in the middle of the cube and the weight, wt $= \rho g dx dy dz$.
A balance of forces in the x and y directions gives

$$\left(P - \frac{\partial P}{\partial x}\frac{dx}{2}\right) dydz - \left(P + \frac{\partial P}{\partial x}\frac{dx}{2}\right) dydz = 0, \tag{3.3}$$

$$\left(P - \frac{\partial P}{\partial y}\frac{dy}{2}\right) dxdz - \left(P + \frac{\partial P}{\partial y}\frac{dy}{2}\right) dxdz = 0. \tag{3.4}$$

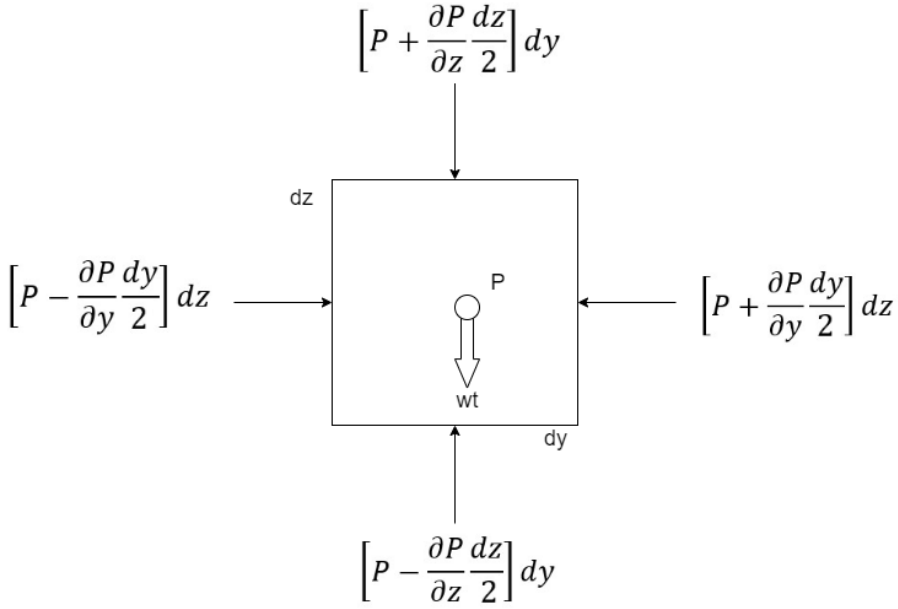

Figure 3.3: Pressure changing with depth

Simplifying Equations (3.3) and (3.4) gives $\frac{\partial P}{\partial x} = \frac{\partial P}{\partial y} = 0$. This shows that pressure doesn't vary along the co-ordinate axis of x and y. The sum of vertical forces along the positive z direction gives

$$\left(P - \frac{\partial P}{\partial z}\frac{dz}{2}\right)dxdy - \left(P + \frac{\partial P}{\partial z}\frac{dz}{2}\right)dxdy - \rho g dxdydz = 0,$$

which simplifies to

$$\frac{\partial P}{\partial z} = -\rho g.$$

This shows that pressure changes in the z-direction; that is, pressure in a static fluid subject to a constant gravitational field increases downward. For a fluid with uniform density, we can integrate to get

$$P = P_0 - \rho g z, \tag{3.5}$$

where P_0 is the pressure at $z = 0$. This is a well-known result of *hydrostatics* and indicates that fluid pressure increases *linearly* with decreasing height.

3.2 Some important Laws of Conservation

Fluid motions are governed by some fundamental physical principles known as conservation laws: these conservation laws include the conservation of mass, conservation of momentum, and conservation of energy.
The environment is made of matter, that is, solid, liquid, gas, and plasma. The conservation laws explain these states and their characteristics. The field of continuum fluid mechanics focuses on the study of the basic constituents that make up these states of matter. Continuum fluid mechanics is concerned with measuring materials on the move, such as liquids and gases. A control volume is a space in which there are different particles with different amounts of mass, momentum, and energy at different points in time. Transport in a continuous medium in a fixed position means moving things around in a substance that doesn't change position. This can be explained in a way that focuses on the speed of the movement, which stays the same in relation to the coordinates. The amount of mass, movement, and energy will be influenced by the movement of fluid through the edges of the control area. A material variable has a Lagrangian frame if its coordinates move with particles over time. So, the area where we are measuring things moves with the fluid, always staying with the same particles of fluid. The Lagrangian frame is often chosen over the Eulerian frame because it allows us to measure objects that are moving, such as Newton's laws of motion and the motion of two objects relative to each other.
By focusing on a small section of the fluid, we can determine the conservation laws with the use of the Lagrangian frame. The Eulerian frame is utilized to solve a situation where the connections between variables in a field are established through equations containing partial derivatives.x, y, z, and t are the independent variables present in these equations.

3.2.1 Material Derivative

To effectively utilize the conservation laws within the Eulerian frame, it is essential to identify the relationship between the changes in a field variable over time during movement, and its alterations at a particular point. Let $T = T(x, y, z, t)$ be a field variable such as temperature and differentiate the field variable $\vec{u}$ with respect to time

t using the chain rule to get

$$\frac{DT}{Dt} = \frac{\partial T}{\partial t} + \frac{\partial T}{\partial x}\frac{dx}{dt} + \frac{\partial T}{\partial y}\frac{dy}{dt} + \frac{\partial T}{\partial z}\frac{dz}{dt}. \tag{3.6}$$

If we let $\frac{dx}{dt} = u$, $\frac{dy}{dt} = v$ and $\frac{dz}{dt} = w$, where u, v and w are the velocity components in the x, y and z directions respectively, then Equation 3.6 becomes

$$\frac{DT}{Dt} = \frac{\partial T}{\partial t} + \left(u\frac{\partial T}{dx} + v\frac{\partial T}{\partial y} + w\frac{\partial T}{\partial z} \right), \tag{3.7}$$

where $\frac{D}{Dt}$ is the *total* or the *material* derivative whiles $\frac{\partial}{\partial t}$ is the *local* derivative. It explains how a specific material changes over time and tells us how the material and its local derivative are connected. Using vector notation, Equation 3.7 can be written as

$$\frac{DT}{Dt} = \frac{\partial T}{\partial t} + V \cdot \vec{\nabla} T, \tag{3.8}$$

where $\vec{V} = u\vec{i} + v\vec{j} + w\vec{k}$ is the velocity vector and $V \cdot \vec{\nabla} T$ is temperature *advection*.

3.2.2 Conservation of Mass

The conservation of mass is a way to understand how the amount of fluid stays the same as it moves. We study how fluid keeps its mass through two different methods. The first method uses an Eulerian control volume, and the second method uses a Lagrangian control volume. In the Eulerian control volume, we have a stationary volume where fluid moves through. In the Lagrangian control volume, the volume moves along with the flowing fluid.

To determine how the mass changes within the control volume, we will look at a control volume that stays in one place and has dimensions dx, dy, and dz. This control volume has a volume of $dV = dxdydz$, and its centre is located at the origin, as shown in Figure 3.4. We will call the face located at a distance $dy/2$ from the centre in the y-direction an outward-facing normal directed in the positive y-direction.

Let the mass flow rate of the fluid, $\dot{m} = \rho A \|\vec{v}\|$, the volume flow rate of the fluid, $Q = A\vec{v}$ and the velocity vector of the fluid, $\vec{v} = u\vec{i} + v\vec{j} + w\vec{k}$, where A is the area of the control volume. We can rewrite the mass flow rate of the fluid as $d\dot{m} = \rho\vec{v} \cdot \hat{\vec{n}} dA$

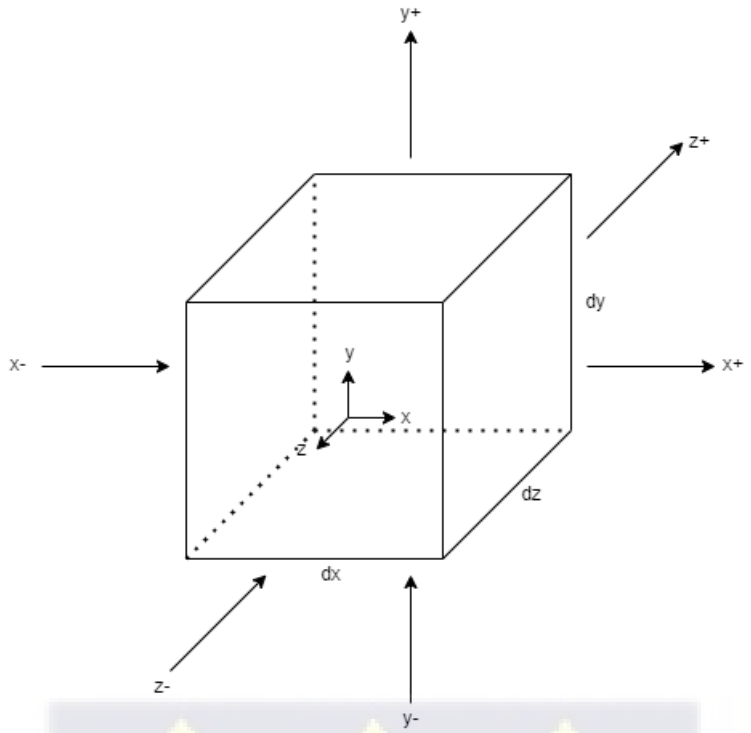

Figure 3.4: Control volume (CV)

and the volume flow rate of the fluid $dQ = \vec{v} \cdot \hat{\vec{n}} dA$. The fluid flow rate at the point (x, y, z) in the x-direction per unit area is the mass flux given as ρu. At the centre of the control volume, the flow rate of fluid per unit area in the positive x-direction is

$$\rho u + \left(\frac{\partial \rho u}{\partial x} \cdot \frac{dx}{2} \right) + \textbf{Higher order terms} \tag{3.9}$$

when you apply Taylor's series to ρu. Similarly, the flow rate of fluid per unit area in the negative x-direction is

$$\rho u - \left(\frac{\partial \rho u}{\partial x} \cdot \frac{dx}{2} \right) + \textbf{Higher order terms}. \tag{3.10}$$

The higher-order terms are negligible since we assume the control volume region is relatively small. For a fixed Eulerian control volume, the rate of mass entering the control volume must be the same as the rate of mass building up inside the control volume. Thus, in general, the mass flow rate of a fluid can be written as

$$\boxed{\begin{array}{l}\text{Rate of mass} \\ \text{increase}\end{array}} + \boxed{\begin{array}{l}\text{Rate of mass} \\ \text{leaving CV}\end{array}} - \boxed{\begin{array}{l}\text{Rate of mass} \\ \text{entering CV}\end{array}} = 0. \tag{3.11}$$

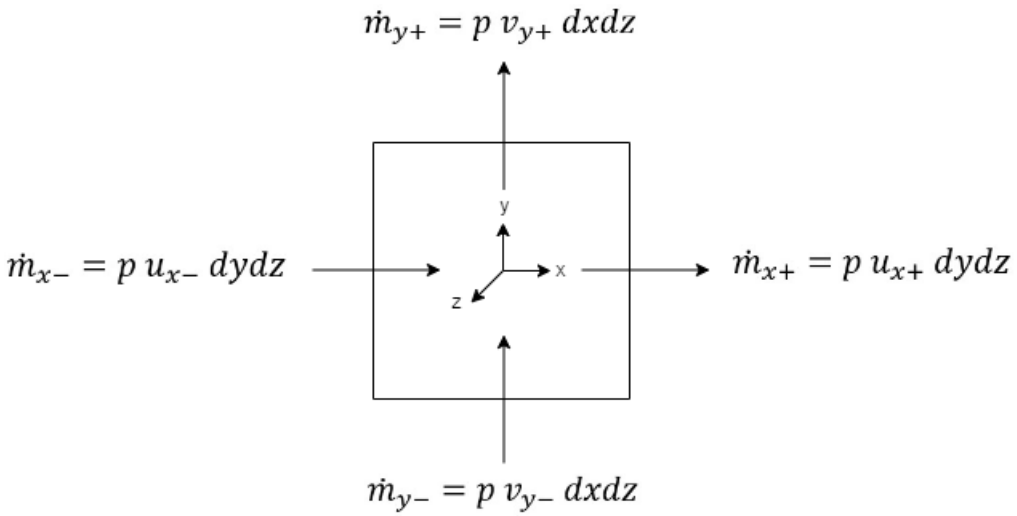

Figure 3.5: Two-dimensional slice of the control volume (CV)

Consider a two-dimensional slice of Figure 3.4 as shown in Figure 3.5, we can observe the rate of change in the mass flow in both the x and y axis. The velocity of fluid flowing in and out of the control volume's surfaces can be written as in Table 3.1.

Face	Direction	Rate of mass passing through the face
x^+	out of CV	$\dot{m}_{x^+} = \rho u_{x^+} dydz = \left[\rho u + \left(\frac{\partial \rho u}{\partial x} \cdot \frac{dx}{2}\right)\right] dydz$
x^-	into CV	$\dot{m}_{x^-} = \rho u_{x^-} dydz = \left[\rho u - \left(\frac{\partial \rho u}{\partial x} \cdot \frac{dx}{2}\right)\right] dydz$
y^+	out of CV	$\dot{m}_{y^+} = \rho v_{y^+} dxdz = \left[\rho v + \left(\frac{\partial \rho v}{\partial y} \cdot \frac{dy}{2}\right)\right] dxdz$
y^-	into CV	$\dot{m}_{y^-} = \rho v_{y^-} dxdz = \left[\rho v - \left(\frac{\partial \rho v}{\partial y} \cdot \frac{dy}{2}\right)\right] dxdz$
z^+	out of CV	$\dot{m}_{z^+} = \rho w_{z^+} dxdy = \left[\rho w + \left(\frac{\partial \rho w}{\partial z} \cdot \frac{dz}{2}\right)\right] dxdy$
z^-	into CV	$\dot{m}_{z^-} = \rho w_{z^-} dxdy = \left[\rho w - \left(\frac{\partial \rho w}{\partial z} \cdot \frac{dz}{2}\right)\right] dxdy$

Table 3.1: Table of the velocity of mass flow of fluid at the six faces of the control volume in Figure 3.4.

Note that in Table 3.1, we applied relations (3.9) and (3.10), and similar ones for the other directions. The mass flow rate defined in (3.11) yields:

$$\frac{\partial \rho}{\partial t} dxdydz + \left[\rho u + \left(\frac{\partial \rho u}{\partial x} \cdot \frac{dx}{2}\right) dydz + \rho v + \left(\frac{\partial \rho v}{\partial y} \cdot \frac{dy}{2}\right) dxdz + \rho w + \left(\frac{\partial \rho w}{\partial z} \cdot \frac{dz}{2}\right)\right] dxdy \ldots$$
$$- \left[\rho u - \left(\frac{\partial \rho u}{\partial x} \cdot \frac{dx}{2}\right) dydz + \rho u - \left(\frac{\partial \rho u}{\partial y} \cdot \frac{dy}{2}\right) dxdz + \rho w - \left(\frac{\partial \rho w}{\partial z} \cdot \frac{dz}{2}\right)\right] dxdy = 0. \tag{3.12}$$

Equation (3.12) simplifies to

$$\frac{\partial \rho}{\partial t} dxdydz + \left(\frac{\partial \rho u}{\partial x} + \frac{\partial \rho v}{\partial y} + \frac{\partial \rho w}{\partial z} \right) dxdydz = 0. \tag{3.13}$$

Divide Equation 3.13 by $dV = dxdydz$, to get

$$\frac{\partial \rho}{\partial t} + \left(\frac{\partial \rho u}{\partial x} + \frac{\partial \rho v}{\partial y} + \frac{\partial \rho w}{\partial z} \right) = 0. \tag{3.14}$$

Equation 3.14 is equivalent to the mass divergence form of the mass conservation given as

$$\frac{\partial \rho}{\partial t} + \vec{\nabla} \cdot \rho \vec{v} = 0, \tag{3.15}$$

where $\vec{\nabla} \cdot () = \frac{\partial ()}{\partial x} + \frac{\partial ()}{\partial y} + \frac{\partial ()}{\partial w}$ and it states that the *local* rate of change of the density equals negative the mass divergence.

In steady form, the amount of fluid leaving the control volume per unit time is equal to the amount of fluid entering the control volume per unit time, that is, $\frac{\partial \rho}{\partial t} = 0$, which implies Equation 3.15 become

$$\vec{\nabla} \cdot (\rho \vec{v}) = 0. \tag{3.16}$$

In an incompressible fluid flow, the density, ρ along the entire control volume is constant, that is, $\frac{\partial \rho}{\partial t} = 0$ implies Equation 3.16 becomes

$$\vec{\nabla} \cdot \vec{v} = 0, \tag{3.17}$$

which is referred to as the continuity equation. We can link the divergence form

$$\vec{\nabla} \cdot (\rho \vec{v}) = \rho \vec{\nabla} \cdot \vec{v} + \vec{v} \cdot \vec{\nabla} \rho$$

and the material derivative

$$\frac{D}{Dt} = \frac{\partial}{\partial t} + \vec{v} \cdot \vec{\nabla}$$

to write (3.15) as

$$\frac{1}{\rho} \frac{D\rho}{Dt} + \vec{\nabla} \cdot \vec{v} = 0. \tag{3.18}$$

This is the velocity divergence form of the continuity equation which states that the fractional rate of increase of the density following the motion of the fluid parcel is equal to the negative of the velocity divergence.

Alternatively, the mass conservation law can be shown using Lagrangian control volume of fixed mass δm that moves with the fluid. Let $\delta V = \delta x \delta y \delta z$ be the volume and $\delta m = \rho \delta V = \rho \delta x \delta y \delta z$ is conserved as it follows the motion of the fluid, that is,

$$\frac{1}{\delta m}\frac{D}{Dt}(\delta m) = \frac{1}{\rho \delta V}\frac{D}{Dt}(\rho \delta V) = \frac{1}{\rho}\frac{D\rho}{Dt} + \frac{1}{\delta V}\frac{D}{Dt}(\delta V) = 0. \tag{3.19}$$

Using the product rule, we can write

$$\frac{1}{\delta V}\frac{D}{Dt}(\delta V) = \frac{1}{\delta x}\frac{D}{Dt}(\delta x) + \frac{1}{\delta y}\frac{D}{Dt}(\delta y) + \frac{1}{\delta z}\frac{D}{Dt}(\delta z). \tag{3.20}$$

The velocity in the x-direction of Figure 3.4 can be denoted as $u_{x^-} = Dx/Dt$ and $u_{x^+} = D(x + \delta x)/Dt$ respectively. The difference in velocity of the two faces is $\delta u = u_{x^+} - u_{x^-} = D(\delta x)/Dt$. Similarly, $\delta v = D(\delta y)/Dt$ and $\delta w = D(\delta z)/Dt$. Therefore, Equation 3.20 becomes

$$\frac{1}{\delta V}\frac{D}{Dt}(\delta V) = \frac{1}{\delta x}\delta u + \frac{1}{\delta y}\delta v + \frac{1}{\delta z}\delta w. \tag{3.21}$$

Now taking the limit of Equation 3.21 as $\delta x \to 0$, $\delta y \to 0$, and $\delta z \to 0$, we get

$$\lim_{\delta x, \delta y, \delta z \to 0}\left[\frac{1}{\delta V}\frac{D}{Dt}(\delta V)\right] = \frac{\partial u}{\partial x} + \frac{\partial v}{\partial y} + \frac{\partial w}{\partial z} = \nabla \cdot \vec{v}. \tag{3.22}$$

Equation 3.19 and Equation 3.22 can be combined to get

$$\frac{D\rho}{Dt} + \nabla \cdot (\rho \vec{v}) = 0, \tag{3.23}$$

which is the mass conservation.

3.2.3 Conservation of Momentum

To find the flow passing through a surface, we determine the part of the velocity that is at a right angle to the surface. We define everywhere on the surface of the control volume as an outward normal orthogonal to the surface. So the component of the flow that carries momentum out or through the surface is the part that is perpendicular to the surface.

Considering Figure 3.4 and Table 3.1, the x-momentum through the six faces of the control volume can be written as

Face	Direction	Rate of momentum passing through the face
x^+	out of CV	$\left[\rho uu + \left(\frac{\partial \rho uu}{\partial x} \cdot \frac{dx}{2}\right)\right] dydz$
x^-	into CV	$\left[\rho uu - \left(\frac{\partial \rho uu}{\partial x} \cdot \frac{dx}{2}\right)\right] dydz$
y^+	out of CV	$\left[\rho uv + \left(\frac{\partial \rho uv}{\partial y} \cdot \frac{dy}{2}\right)\right] dxdz$
y^-	into CV	$\left[\rho uv - \left(\frac{\partial \rho uv}{\partial y} \cdot \frac{dy}{2}\right)\right] dxdz$
z^+	out of CV	$\left[\rho uw + \left(\frac{\partial \rho uw}{\partial z} \cdot \frac{dz}{2}\right)\right] dxdy$
z^-	into CV	$\left[\rho uw - \left(\frac{\partial \rho uw}{\partial z} \cdot \frac{dz}{2}\right)\right] dxdy$

Table 3.2: Table of x- momentum of fluid at the faces

Similarly, the y-momentum through the six faces of the control volume can be written as

Face	Direction	Rate of momentum passing through the face
x^+	out of CV	$\left[\rho vu + \left(\frac{\partial \rho vu}{\partial x} \cdot \frac{dx}{2}\right)\right] dydz$
x^-	into CV	$\left[\rho vu - \left(\frac{\partial \rho vu}{\partial x} \cdot \frac{dx}{2}\right)\right] dydz$
y^+	out of CV	$\left[\rho vv + \left(\frac{\partial \rho vv}{\partial y} \cdot \frac{dy}{2}\right)\right] dxdz$
y^-	into CV	$\left[\rho vv - \left(\frac{\partial \rho vv}{\partial y} \cdot \frac{dy}{2}\right)\right] dxdz$
z^+	out of CV	$\left[\rho vw + \left(\frac{\partial \rho vw}{\partial z} \cdot \frac{dz}{2}\right)\right] dxdy$
z^-	into CV	$\left[\rho vw - \left(\frac{\partial \rho vw}{\partial z} \cdot \frac{dz}{2}\right)\right] dxdy$

Table 3.3: Table of y- momentum of fluid at the faces

Finally, the z-momentum through the six faces of the control volume can be written as

Face	Direction	Rate of momentum passing through the face
x^+	out of CV	$\left[\rho wu + \left(\frac{\partial \rho wu}{\partial x} \cdot \frac{dx}{2}\right)\right] dydz$
x^-	into CV	$\left[\rho wu - \left(\frac{\partial \rho wu}{\partial x} \cdot \frac{dx}{2}\right)\right] dydz$
y^+	out of CV	$\left[\rho wv + \left(\frac{\partial \rho wv}{\partial y} \cdot \frac{dy}{2}\right)\right] dxdz$
y^-	into CV	$\left[\rho wv - \left(\frac{\partial \rho wv}{\partial y} \cdot \frac{dy}{2}\right)\right] dxdz$
z^+	out of CV	$\left[\rho ww + \left(\frac{\partial \rho ww}{\partial z} \cdot \frac{dz}{2}\right)\right] dxdy$
z^-	into CV	$\left[\rho ww - \left(\frac{\partial \rho ww}{\partial z} \cdot \frac{dz}{2}\right)\right] dxdy$

Table 3.4: Table of z- momentum of fluid at the faces

We can compute the rate of x-momentum through the six faces of the control volume as

Rate of momentum increase in CV	+	Rate of momentum leaving CV	−	Rate of momentum entering CV	=	Sum of forces applied to CV in the x direction.

Using the idea of Equation 3.12, the rate of x-momentum through the six faces of the control volume can be simplified to get

$$\frac{\partial \rho u}{\partial t} dxdydz + \left[\frac{\partial \rho uu}{\partial x} + \frac{\partial \rho uv}{\partial y} + \frac{\partial \rho uw}{\partial z}\right] dxdydz = \sum F_x. \tag{3.24}$$

Using the product rule

$$\frac{\partial \rho uu}{\partial x} = u\frac{\partial \rho u}{\partial x} + \rho u\frac{\partial u}{\partial x}, \tag{3.25}$$

we can write

$$\left[\frac{\partial \rho uu}{\partial x} + \frac{\partial \rho uv}{\partial y} + \frac{\partial \rho uw}{\partial z}\right] = u\left[\frac{\partial \rho u}{\partial x} + \frac{\partial \rho v}{\partial y} + \frac{\partial \rho w}{\partial z}\right] + \rho\left[u\frac{\partial \rho u}{\partial x} + v\frac{\partial \rho u}{\partial y} + w\frac{\partial \rho u}{\partial z}\right]. \tag{3.26}$$

Substitute into Equation 3.24 and divide by the volume $dV = dxdydz$ to get

$$\frac{\partial \rho u}{\partial t} + u\left[\frac{\partial \rho u}{\partial x} + \frac{\partial \rho v}{\partial y} + \frac{\partial \rho w}{\partial z}\right] + \rho\left[u\frac{\partial \rho u}{\partial x} + v\frac{\partial \rho u}{\partial y} + w\frac{\partial \rho u}{\partial z}\right] = \frac{\sum F_x}{dV}. \tag{3.27}$$

Also, from the product rule

$$\frac{\partial \rho u}{\partial t} = u\frac{\partial \rho}{\partial t} + \rho\frac{\partial u}{\partial t}, \tag{3.28}$$

substitute into Equation 3.27 and rearrange to get

$$u\left[\frac{\partial \rho}{\partial t} + \frac{\partial \rho u}{\partial x} + \frac{\partial \rho v}{\partial y} + \frac{\partial \rho w}{\partial z}\right] + \rho\left[\frac{\partial u}{\partial t} + u\frac{\partial u}{\partial x} + v\frac{\partial u}{\partial y} + w\frac{\partial u}{\partial z}\right] = \frac{\sum F_x}{dV}. \tag{3.29}$$

Recall from Equation 3.14 the conservation of mass

$$\frac{\partial \rho}{\partial t} + \frac{\partial \rho u}{\partial x} + \frac{\partial \rho v}{\partial y} + \frac{\partial \rho w}{\partial z} = 0$$

and applying to the conservation of momentum reduces Equation 3.29 to

$$\rho\left[\frac{\partial u}{\partial t} + u\frac{\partial u}{\partial x} + v\frac{\partial u}{\partial y} + w\frac{\partial u}{\partial z}\right] = \frac{\sum F_x}{dV}. \tag{3.30}$$

Using the material derivative, the conservation of momentum in the x-direction can be written as

$$\rho\frac{Du}{Dt} = \frac{\sum F_x}{dV}. \tag{3.31}$$

Similarly, the conservation of momentum in the y and z direction are

$$\rho\frac{Dv}{Dt} = \rho\left[\frac{\partial v}{\partial t} + u\frac{\partial v}{\partial x} + v\frac{\partial v}{\partial y} + w\frac{\partial u}{\partial z}\right] = \frac{\sum F_y}{dV} \tag{3.32}$$

and

$$\rho\frac{Dw}{Dt} = \rho\left[\frac{\partial w}{\partial t} + u\frac{\partial w}{\partial x} + v\frac{\partial w}{\partial y} + w\frac{\partial w}{\partial z}\right] = \frac{\sum F_z}{dV} \tag{3.33}$$

respectively.

Note that the Navier-Stokes equations are the sum of gravitational force, pressure force, and viscous forces, equal to the product of mass and acceleration. The three forces are similar to the force of gravity, normal, and friction. Subsection 3.2.4 gives a way of deriving the pressure force and viscous forces of the Navier-Stokes equations.

3.2.4 Derivation of Navier Stokes equations

The simplest relation for a Newtonian fluid is given by the fluid's *normal* and *tangential* or *shear* stresses in the control volume. The normal stress relation is

given by

$$\sigma_{xx} = -P + 2\mu\frac{\partial u}{\partial x}$$
$$\sigma_{yy} = -P + 2\mu\frac{\partial v}{\partial y}$$
$$\sigma_{zz} = -P + 2\mu\frac{\partial w}{\partial z},$$

where we have the pressure, $-P$, which is compressive and σ_{xx}, σ_{yy} and σ_{zz} are the normal stresses.

The tangential stress relation is given by Equation 3.2 as

$$\tau_{xy} = \tau_{yx} = \mu\left(\frac{\partial u}{\partial y} + \frac{\partial v}{\partial x}\right)$$
$$\tau_{zy} = \tau_{yz} = \mu\left(\frac{\partial v}{\partial z} + \frac{\partial w}{\partial y}\right)$$
$$\tau_{xz} = \tau_{zx} = \mu\left(\frac{\partial u}{\partial z} + \frac{\partial w}{\partial x}\right),$$

where the strain rates give the shear stresses in the other directions.

Substitute the normal and shear relations into Equation 3.31 and assume density and viscosity are constant (that is, we consider an incompressible flow). Consider the x component of the momentum equations

$$\rho\frac{Du}{Dt} = \rho g_x + \left[\frac{\partial \sigma_{xx}}{\partial x} + \frac{\partial \tau_{yx}}{\partial y} + \frac{\partial \tau_{zx}}{\partial z}\right], \tag{3.34}$$

where $\rho\frac{Du}{Dt}$ is the inertia force, ρg_x is the body force and $\frac{\partial \sigma_{xx}}{\partial x} + \frac{\partial \tau_{yx}}{\partial y} + \frac{\partial \tau_{zx}}{\partial z}$ are the stresses. Substituting the normal and shear stresses into Equation 3.34 to get

$$\rho\frac{Du}{Dt} = \rho g_x + \frac{\partial}{\partial x}\left[-P + 2\mu\frac{\partial u}{\partial x}\right] + \frac{\partial}{\partial y}\left[\mu\left(\frac{\partial u}{\partial y} + \frac{\partial v}{\partial x}\right)\right] + \frac{\partial}{\partial z}\left[\mu\left(\frac{\partial u}{\partial z} + \frac{\partial w}{\partial x}\right)\right]. \tag{3.35}$$

Rearranging and collecting like terms gives

$$\rho\frac{Du}{Dt} = \rho g_x - \frac{\partial P}{\partial x} + \frac{\partial}{\partial x}\left[\mu\left(\frac{\partial u}{\partial x} + \frac{\partial v}{\partial y} + \frac{\partial w}{\partial z}\right)\right] + \frac{\partial}{\partial x}\left[\mu\frac{\partial u}{\partial x}\right] + \frac{\partial}{\partial y}\left[\mu\frac{\partial u}{\partial y}\right] + \frac{\partial}{\partial z}\left[\mu\frac{\partial u}{\partial z}\right], \tag{3.36}$$

where the term $\frac{\partial u}{\partial x}+\frac{\partial v}{\partial y}+\frac{\partial w}{\partial z}$ was seen in Equation 3.17 of the continuity equation. The equation of motion in the x-direction now reduces to

$$\rho\frac{Du}{Dt}=\rho g_x-\frac{\partial P}{\partial x}+\frac{\partial}{\partial x}\left[\mu\frac{\partial u}{\partial x}\right]+\frac{\partial}{\partial y}\left[\mu\frac{\partial u}{\partial y}\right]+\frac{\partial}{\partial z}\left[\mu\frac{\partial u}{\partial z}\right], \tag{3.37}$$

If surface tension force is needed, it can be added to the equation of motion. However, assuming the viscosity is constant, we can simplify further Equation 3.37 to get the x component of the momentum

$$\rho\left[\frac{\partial u}{\partial t}+u\frac{\partial u}{\partial x}+v\frac{\partial u}{\partial y}+w\frac{\partial u}{\partial z}\right]=\rho g_x-\frac{\partial P}{\partial x}+\mu\left[\frac{\partial^2 u}{\partial x^2}+\frac{\partial^2 u}{\partial y^2}+\frac{\partial^2 u}{\partial z^2}\right]. \tag{3.38}$$

The y component of the momentum is given as

$$\rho\left[\frac{\partial v}{\partial t}+u\frac{\partial v}{\partial x}+v\frac{\partial v}{\partial y}+w\frac{\partial v}{\partial z}\right]=\rho g_y-\frac{\partial P}{\partial y}+\mu\left[\frac{\partial^2 v}{\partial x^2}+\frac{\partial^2 v}{\partial y^2}+\frac{\partial^2 v}{\partial z^2}\right], \tag{3.39}$$

while z component of the momentum is given as

$$\rho\left[\frac{\partial w}{\partial t}+u\frac{\partial w}{\partial x}+v\frac{\partial w}{\partial y}+w\frac{\partial w}{\partial z}\right]=\rho g_z-\frac{\partial P}{\partial z}+\mu\left[\frac{\partial^2 w}{\partial x^2}+\frac{\partial^2 w}{\partial y^2}+\frac{\partial^2 w}{\partial z^2}\right]. \tag{3.40}$$

We can also combine these component forms of the momentum into a convenient and compact vector form as

$$\rho\left[\frac{\partial\vec{V}}{\partial t}+\vec{V}\cdot\nabla\vec{V}\right]=\rho\vec{g}-\nabla P+\mu\nabla^2\vec{V}, \tag{3.41}$$

where ∇P is the gradient of the pressure and $\nabla^2\vec{V}$ is the Laplacian of $\vec{V}$. equation (3.41) is the vector form of the *Navier Stokes* equations. The vector form of the equation is very compact and useful. For instance, if one is interested in solving the equation in other coordinates, like cylindrical or spherical form.
Dividing Equation 3.41 by ρ gives an alternative form of the equation in which we obtain the acceleration instead of having the inertia force, that is

$$\frac{\partial\vec{V}}{\partial t}+\vec{V}\cdot\nabla\vec{V}=\vec{g}-\frac{1}{\rho}\nabla P+\frac{\mu}{\rho}\nabla^2\vec{V}, \tag{3.42}$$

where $\vec{g}$ and $\frac{1}{\rho}\nabla P$ are the force per unit mass density and $\frac{\mu}{\rho}$ is the kinematic viscosity. The inertia force or the change in momentum equals the total forces in the control

volume. Therefore, the rate of change of momentum per volume is equal to force per volume.

The complete set of the cartesian component form of the momentum equations and continuity equation (conservation of mass for an incompressible fluid) are:

$$x \text{ component} : \rho\left[\frac{\partial u}{\partial t} + u\frac{\partial u}{\partial x} + v\frac{\partial u}{\partial y} + w\frac{\partial u}{\partial z}\right] = \rho g_x - \frac{\partial P}{\partial x} + \mu\left[\frac{\partial^2 u}{\partial x^2} + \frac{\partial^2 u}{\partial y^2} + \frac{\partial^2 u}{\partial z^2}\right] \tag{3.43}$$

$$y \text{ component} : \rho\left[\frac{\partial v}{\partial t} + u\frac{\partial v}{\partial x} + v\frac{\partial v}{\partial y} + w\frac{\partial v}{\partial z}\right] = \rho g_y - \frac{\partial P}{\partial y} + \mu\left[\frac{\partial^2 v}{\partial x^2} + \frac{\partial^2 v}{\partial y^2} + \frac{\partial^2 v}{\partial z^2}\right] \tag{3.44}$$

$$z \text{ component} : \rho\left[\frac{\partial w}{\partial t} + u\frac{\partial w}{\partial x} + v\frac{\partial w}{\partial y} + w\frac{\partial w}{\partial z}\right] = \rho g_z - \frac{\partial P}{\partial z} + \mu\left[\frac{\partial^2 w}{\partial x^2} + \frac{\partial^2 w}{\partial y^2} + \frac{\partial^2 w}{\partial z^2}\right] \tag{3.45}$$

$$\text{Continuity equation} : \frac{\partial u}{\partial x} + \frac{\partial v}{\partial y} + \frac{\partial w}{\partial z} = 0, \tag{3.46}$$

where viscosity and density are assumed constant in a Newtonian fluid. Note that from Equation 3.43 and Equation 3.44, z is obviously the vertical as the hydrostatic balance was written along it, so it is implicit that x and y are horizontal and gravity does not apply in these directions. Hence, the horizontal gravity terms are negligible. These are known as the Navier-Stokes equations. There are four equations in four unknowns, that is, u, v, w and ρ. The Navier-Stokes equations become non-linear because of the acceleration term, which measures how momentum changes over time. The viscosity term makes the Navier-Stokes equations more complicated, turning them into second-order non-linear partial differential equations. These equations are used in computational fluid dynamics. We will look at some of the numerical and analytical solutions to gain good insight into the behaviour of fluids and some motivations for some parts of the thesis. The equations will be simplified in Chapter 4 to derive the classical theory of upwelling.

3.2.5 Importance of rotation in fluid

Understanding how the surrounding environment's rotation affects the fluid's movement is helpful. The surrounding rotation rate, denoted as Ω, is defined as:

$$\Omega = \frac{2\pi}{\text{time of one revolution}}.$$

The earth spins around itself once every day and goes around the sun once every year. So, the value of Ω has two parts, that is,

$$\frac{2\pi}{24 \text{ hours}} + \frac{2\pi}{365.24 \text{ days}} = 7.2921 \times 10^{-5}\text{s}^{-1} \tag{3.47}$$

The result of Equation 3.47 shows what happens when we look at a star that is always in the same place in the sky, but we observe it at different times. The day lasts almost 24 hours because the Earth moves around the sun, causing it to rotate a little more than once before facing the sun again. If a fluid moves slowly or for a long time, it will be affected by the spinning of its surroundings. Let's define the dimensionless quantity

$$\omega = \frac{\text{time of revolution}}{\text{motion time scale}} = \frac{2\pi/\Omega}{T} = \frac{2\pi}{\Omega T},$$

where T is the time scale of the flow. If T is more than 24 hours, then ω is equal to or less than 1, which means that rotation effects need to be taken into account. If the movement happens quickly, with ω greater than 1, rotation can also affect a large spatial pattern.

3.2.6 Importance of stratification in fluid

How does stratification in a fluid affect how it moves? Normally, a fluid is made up of different masses with different densities that stack on top of each other due to gravity. This helps the fluid reach a state where it has the least amount of stored energy. However, movement in the fluid constantly upsets this balance, causing the heavy fluid to rise up and the light liquid to go down. The fluid slows down because the potential energy increases while the kinetic energy decreases. Usually, the opposite happens. When potential energy turns into kinetic energy, the fluid movement becomes stronger until the unequal stratified fluid reaches equilibrium. We can understand how important stratification is by looking at how much energy is stored and how much energy is in motion.

Suppose $\Delta\rho$ is the difference in density within the fluid, H is the height of the fluid, and ρ_0 is the density of the lighter fluid element. The disturbance to the stratification involves increasing the fluid component of density $\rho_0 + \Delta\rho$ and reducing the less dense fluid component of density ρ_0 over the height H to maintain the total amount of fluid constant. The potential energy per unit volume is the equivalent change,

$(\rho_0 + \Delta\rho)gH - \rho_0 gH = \Delta\rho gH$. With a fluid velocity of U, the kinetic energy per unit volume is $\frac{1}{2}\rho_0 U^2$. The comparative energy ratio is

$$\sigma = \frac{\frac{1}{2}\rho_0 U^2}{\Delta\rho gH}.$$

If σ is around 1, then the potential energy is needed to disturb the stratification. The flow is limited when there isn't enough energy to disturb the layers of fluid, which happens when σ is less than one ($\sigma < 1$). Lastly, if the value of *sigma* is more than one, which means $\sigma > 1$, then changes in the potential energy will have a small impact on the kinetic energy. This means that stratification will not greatly affect the flow. So, we can't ignore the effects of stratification in the first two cases.
When both spinning and stratification influences are equally significant in fluids, neither is greater than the other. This happens when $\omega \sim 1$ and $\sigma \sim 1$. This gives us the following connections between the different scales:

$$L \sim \frac{U}{\Omega} \qquad \text{and} \qquad U \sim \sqrt{\frac{\Delta\rho}{\rho_0} gH}.$$

The factors 2π and $\frac{1}{2}$ are not important for analyzing dimensions or scales. Getting rid of the velocity U gives us the length scale:

$$L \sim \frac{1}{\Omega}\sqrt{\frac{\Delta\rho}{\rho_0} gH}.$$

In a fluid with an average density ρ_0 and a difference in density $\Delta\rho$, at height H spinning at a speed of Ω and experiencing a gravitational force of g, we can find the distance in which movements occur. On earth, $\Omega = 7.29 \times 10^{-5}\,\mathrm{s}^{-1}, g = 9.81\,\mathrm{m/s}^2$ and in the ocean of $\rho_0 = 1028\,\mathrm{kg/m}^3, \Delta\rho = 2\,\mathrm{kg/m}^3, H = 1000\,\mathrm{m}$ yield the natural length and velocity scales: L_{ocean} is about 60 km and U_{ocean} is about 4 m/s.

Even though these approximations are not very accurate, we can still identify the average size and speed of important movements in the ocean. Problems in fluid dynamics are mainly about how fluids move when they have rotating or layered characteristics. A mixture of different liquids or gases will naturally separate under gravity, with the denser substances sinking to the bottom and the less dense ones rising to the top. The way that the layers are arranged up and down causes differences in the speed of movement in that same direction. So, having layers makes the vertical rigidity caused

by rotation weaker. As a result, when a denser fluid is underneath a lighter fluid, it makes the system become more stable horizontally. This happens because the stratification separates the different densities of fluids. Gravity waves can happen inside the fluid when different densities of the fluid are stacked on top together. When the layers are arranged horizontally, other waves can occur, causing movement in balance. If they get bigger by using up the available energy, it can cause problems.

Consider a fluid that is not moving or changing. We assume that without any sideways forces, things cannot move. So, if everything is the same sideways, nothing will move. The fluid is stable if the heavier fluid is on the bottom and the lighter fluid is on top. If the heavier fluid is on top and the lighter fluid is on the bottom, then the fluid is unstable. To check this situation, imagine a small amount of fluid at a certain height z above a specific point where the fluid's density is $\rho(z)$. Move that fluid upwards to a higher level $z+h$ where the density is $\rho(z+h)$. If the fluid cannot be compressed, the parcel that was pushed away will still have the same thickness, even if there is a small change in the pressure. The new level is pushed down by gravity, but it also gets pushed up by the buoyancy force of the fluid it displaces. This is .

$$g[\rho(z) - \rho(z+h)]V,$$

where V represents the amount of fluid inside the parcel. This force is positive when it goes downwards. Newton's law (mass multiplied by acceleration equals upward force) yields.

$$\rho(z)V\frac{d^2h}{dt^2} = g[\rho(z) - \rho(z+h)]V. \tag{3.48}$$

After division by V, Equation 3.48 yields

$$\rho(z)\frac{d^2h}{dt^2} = g[\rho(z) - \rho(z+h)]. \tag{3.49}$$

To simplify, substitute $\rho(z)$ with the reference density ρ_0 in equation Equation 3.49. Then, use a Taylor expansion to estimate the difference in density on the right to get

$$\rho(z+h) - \rho(z) \approx \frac{d\rho}{dz}h. \tag{3.50}$$

Combining Equation 3.49 and Equation 3.50, leads to

$$\frac{d^2h}{dt^2} - \frac{g}{\rho_0}\frac{d\rho}{dz}h = 0, \tag{3.51}$$

which indicates two different situations that can happen. The coefficient $-\frac{g}{\rho_0}\frac{d\rho}{dz}$ can be either positive or negative. If $d\rho/dz > 0$, then the fluid above has higher densities than the fluid below. If the coefficient is positive, then the change in density with respect to height is decreasing. This indicates that the fluid below has a higher density than the fluid above. In this case, we can define a quantity N^2 as

$$N^2 = -\frac{g}{\rho_0}\frac{d\rho}{dz},$$

and Equation 3.51 reduces to

$$\frac{d^2h}{dt^2} + N^2h = 0. \tag{3.52}$$

When a heavier object is pushed upwards in a liquid, it will be pulled back down and will start to fall at a downward speed. When the particle goes back to its starting position, its inertia makes it go even lower than the original level. The quantity

$$N = \sqrt{-\frac{g}{\rho_0}\frac{d\rho}{dz}}$$

gives how often something moves back and forth and can be called the stratification frequency. N is often called the Brunt–Väisälä frequency, named after the two scientists who first realized its significance in layered fluids.

If N^2 in Equation 3.52 is less than zero, the solution of the differential equation shows a very fast increase, which means it is unstable. The object in the package moves upwards because it is surrounded by a heavier fluid. It becomes buoyant and goes further away from where it started. Any small change will ensure that the single moved package leaves where it started. The fluid will continue to flow until it settles, with the less dense fluid resting on top of the denser fluid. But let's imagine that the fluid is made unstable forever by heating it from the bottom or cooling it from the top. In that situation, it will make the fluid keep moving all the time leading to convection.

3.2.7 Coriolis force

All equations that describe how fluid moves can be explained in relation to a fixed point of reference. A person on earth sees the movement of the fluid compared to the rotating system. In a spinning frame, we have to consider forces that seem to exist but are actually due to the way we define our measurements based on Earth's

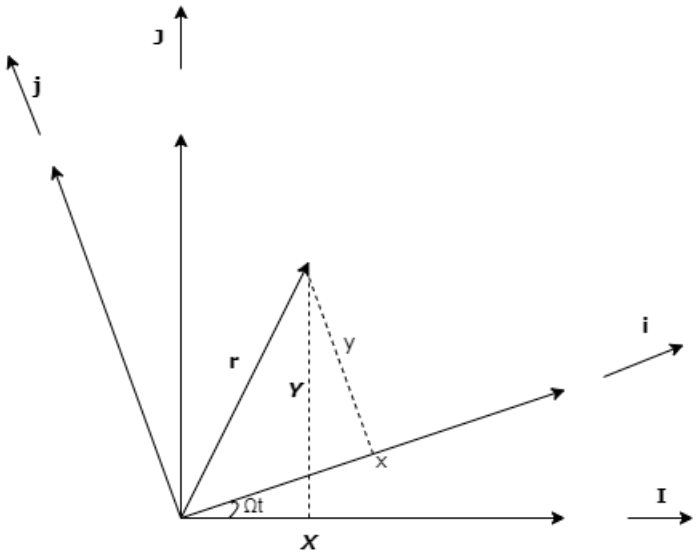

Figure 3.6: The Coriolis effect at a specific location (x, y) of a fluid

surface. The earth spins around in a circle at a certain speed. Coriolis forces are called apparent forces because they only exist when the frame of reference is moving. The Coriolis force is used to explain how a fluid moves in something that is spinning. The Coriolis force makes things move in a different direction because the Earth is spinning.

We will focus on understanding the Coriolis force and how it impacts fluid parcels. First, let's look at the situation when we only have two dimensions. In Figure 3.6, there are two frames of reference: the inertial frame with the X and Y axes and the rotating frame with the x and y axes. The x and y axes rotate at a certain speed called Ω, which is measured in a counterclockwise direction. Both frames have the same starting point or origin. The unit vectors are represented by $(\vec{I}, \vec{J})$ and $(\vec{i}, \vec{j})$ respectively. At any given time, t, the x axis spinning, moves at an angle of Ωt in relation to a fixed X axis. It follows that

$$\vec{\mathrm{i}} = \cos\Omega t\, \vec{\mathrm{I}} + \sin\Omega t\, \vec{\mathrm{J}} \qquad \vec{\mathrm{I}} = \cos\Omega t\, \vec{\mathrm{i}} - \sin\Omega t\, \vec{\mathrm{j}}$$
$$\vec{\mathrm{j}} = -\sin\Omega t\, \vec{\mathrm{I}} + \cos\Omega t\, \vec{\mathrm{J}} \qquad \vec{\mathrm{J}} = \sin\Omega t\, \vec{\mathrm{i}} + \cos\Omega t\, \vec{\mathrm{j}},$$

and the displacement vector $\vec{\mathrm{r}} = X\vec{\mathrm{I}} + Y\vec{\mathrm{J}} = x\vec{\mathrm{i}} + y\vec{\mathrm{j}}$ of any point within the plane are related by

$$x = \cos\Omega t\, X + \sin\Omega t\, Y \tag{3.53}$$
$$y = -\sin\Omega t\, X + \cos\Omega t\, Y. \tag{3.54}$$

The rate of change of the previous expressions is found by taking the derivative with respect to time to yield

$$\frac{dx}{dt} = \cos\Omega t \frac{dX}{dt} + \sin\Omega t \frac{dY}{dt} - \Omega X \sin\Omega t + \Omega Y \cos\Omega t \tag{3.55}$$

$$\frac{dy}{dt} = -\sin\Omega t \frac{dX}{dt} + \cos\Omega t \frac{dY}{dt} - (\Omega X \cos\Omega t + \Omega Y \sin\Omega t). \tag{3.56}$$

Multiply Equation 3.53 and (3.54) by Ω to get

$$\Omega y = -\Omega X \sin\Omega t + \Omega Y \cos\Omega t \tag{3.57}$$

and

$$\Omega x = \Omega X \cos\Omega t + \Omega Y \cos\Omega t. \tag{3.58}$$

The rates at which the coordinates change over time are represented by the first derivatives dx/dt and dy/dt. They are the parts that make up the relative velocity which is given as:

$$\vec{\mathrm{u}} = \frac{dx}{dt}\vec{\mathrm{i}} + \frac{dy}{dt}\vec{\mathrm{j}} = u\vec{\mathrm{i}} + v\vec{\mathrm{j}}. \tag{3.59}$$

Similarly, dX/dt and dY/dt show how much the absolute coordinates are changing over time and make up the absolute velocity:

$$\vec{\mathrm{U}} = \frac{dX}{dt}\vec{\mathrm{i}} + \frac{dY}{dt}\vec{\mathrm{j}} = U\vec{\mathrm{i}} + V\vec{\mathrm{j}}. \tag{3.60}$$

Expressing the vector $\vec{\mathrm{U}}$ using the rotating unit vectors provides

$$\vec{\mathrm{U}} = \left(\cos\Omega t \frac{dX}{dt} + \sin\Omega t \frac{dY}{dt}\right)\vec{\mathrm{i}} + \left(-\sin\Omega t \frac{dX}{dt} + \cos\Omega t \frac{dY}{dt}\right)\vec{\mathrm{j}} = U\vec{\mathrm{i}} + V\vec{\mathrm{j}}. \tag{3.61}$$

The velocity of an object in an inertial frame is represented by the values dX/dt and dY/dt. In a rotating frame, the same velocity is represented by the values U and V. When we put together equations (3.57), (3.58), and (3.61), we get the following relationships between absolute and relative velocities:

$$U = u - \Omega y, \qquad V = v - \Omega x.$$

These quantities mean that the total velocity is the combination of the relative velocity and the velocity caused by the rotation of the reference frame.
The second derivative of Equation 3.55 and (3.56) when we look at how they change

over time is:

$$\frac{d^2x}{dt^2} = \cos\Omega t\,\frac{d^2X}{dt^2} + \sin\Omega t\,\frac{d^2Y}{dt^2} + 2\Omega\left(-\sin\Omega t\,\frac{dX}{dt} + \cos\Omega t\,\frac{dY}{dt}\right) - \Omega^2(X\cos\Omega t + Y\sin\Omega t) \tag{3.62}$$

$$\frac{d^2y}{dt^2} = -\sin\Omega t\,\frac{d^2X}{dt^2} + \cos\Omega t\,\frac{d^2Y}{dt^2} - 2\Omega\left(\cos\Omega t\,\frac{dX}{dt} + \sin\Omega t\,\frac{dY}{dt}\right) - \Omega^2(-X\sin\Omega t + Y\cos\Omega t). \tag{3.63}$$

Using the relative and absolute accelerations, we can find the second derivative of Equation 3.62 and (3.63) as

$$\vec{a} = \frac{d^2x}{dt^2}\,\vec{i} + \frac{d^2y}{dt^2}\,\vec{j} = \frac{du}{dt}\,\vec{i} + \frac{dv}{dt}\,\vec{j} = a_1\vec{i} + a_2\vec{j} \tag{3.64}$$

$$\vec{A} = \frac{d^2X}{dt^2}\,\vec{I} + \frac{d^2Y}{dt^2}\,\vec{J} \tag{3.65}$$

$$= \left(\cos\Omega t\,\frac{d^2X}{dt^2} + \sin\Omega t\,\frac{d^2Y}{dt^2}\right)\vec{i} + \left(-\sin\Omega t\,\frac{d^2X}{dt^2} + \cos\Omega t\,\frac{d^2Y}{dt^2}\right)\vec{j} = A_1\vec{i} + A_2\vec{j}, \tag{3.66}$$

where

$$a_1 = A_1 + 2\Omega V - \Omega^2 x \tag{3.67}$$

and

$$a_2 = A_2 - 2\Omega U - \Omega^2 y. \tag{3.68}$$

d^2X/dt^2 and d^2Y/dt^2 are the components of the absolute acceleration $\vec{A}$ in the inertial frame, whiles A_1 and A_2 are the components of the same vector in the rotating frame. The absolute acceleration components can be obtained by solving for A_1 and A_2 in Equation 3.67 and Equation 3.68 to get

$$A_1 = a_1 - 2\Omega v - \Omega^2 x, \qquad A_2 = a_2 + 2\Omega u - \Omega^2 y.$$

We can notice that there are two parts to the distinct nature of absolute and relative acceleration. Coriolis acceleration is a measure of how an object's velocity relates to the Earth's rotation. It is directly proportional to Ω, which represents the Earth's rotation rate. The centrifugal acceleration, on the other hand, is directly proportional to Ω^2 and the coordinates of the object. These can be changed to forces when put in Newton's law. The centrifugal force pulls things away from the center. The Coriolis force is affected by the speed and direction of the relative motion.

The vector form of the rate of rotation can be described as

$$\vec{\Omega} = \Omega\vec{\mathrm{k}},$$

where $\vec{\mathrm{k}}$ is a unit vector in the third dimension that is the same in both reference systems. We can express the absolute velocity and acceleration using vectors:

$$\vec{\mathrm{U}} = \vec{\mathrm{u}} + \vec{\Omega} \times \vec{\mathrm{r}} \tag{3.69}$$

$$\vec{\mathrm{A}} = \vec{\mathrm{a}} + 2\vec{\Omega} \times \vec{\mathrm{u}} + \vec{\Omega} \times (\vec{\Omega} \times \vec{\mathrm{r}}), \tag{3.70}$$

where $\times$ represents the cross product. This means that when we take the time derivative of a vector in relation to the reference frame that doesn't move, it is similar to using the operator:

$$\frac{d}{dt} + \vec{\Omega}\times$$

within the spinning frame.

Let ϕ represent the latitude of the spinning earth. Let's say that the x-axis points to the east, the y-axis points to the north, and the z-axis points up. Then, according to [26], the direction in which the earth rotates can be represented by the vector:

$$\vec{\Omega} = \langle 0, \Omega\cos\phi, \Omega\sin\phi\rangle. \tag{3.71}$$

The rate at which the velocity vector changes in an inertia frame of reference can be substituted into Equation 3.42 of the momentum equations to get

$$\frac{\partial\vec{V}}{\partial t} + \vec{V}\cdot\nabla\vec{V} + 2\vec{\Omega}\times\vec{\mathrm{V}} + \vec{\Omega}\times(\vec{\Omega}\times\vec{\mathrm{r}}) = \vec{g} - \frac{1}{\rho}\nabla P + \frac{\mu}{\rho}\nabla^2\vec{V}. \tag{3.72}$$

Equation (3.72) can be simplified to get

$$\frac{\partial\vec{V}}{\partial t} + \vec{V}\cdot\nabla\vec{V} + 2\vec{\Omega}\times\vec{\mathrm{V}} = \vec{g^*} - \frac{1}{\rho}\nabla P + \frac{\mu}{\rho}\nabla^2\vec{V}, \tag{3.73}$$

where $\vec{g^*} = \vec{g} - \vec{\Omega}\times(\vec{\Omega}\times\vec{\mathrm{r}})$. We can compute

$$2\vec{\Omega}\times\vec{\mathrm{V}} = 2\langle 0, \Omega\cos\phi, \Omega\sin\phi\rangle \times \langle u, v, w\rangle \tag{3.74}$$

$$= \langle 2w\Omega\cos\phi - 2v\Omega\sin\phi, 2u\Omega\sin\phi, -2\Omega\cos\phi\rangle \tag{3.75}$$

The Coriolis parameter is represented by the equation $f = 2\Omega\sin\phi$. The term $2\Omega\cos\phi$

is unimportant and doesn't impact the Coriolis force. This reduces (3.75) to

$$2\vec{\Omega} \times \vec{\mathrm{V}} = \langle -fv, fu, 0 \rangle. \tag{3.76}$$

Combining Equation 3.73 and (3.76), the momentum equations now become

$$\frac{\partial \vec{V}}{\partial t} + \vec{V} \cdot \nabla \vec{V} + \langle -fv, fu, 0 \rangle = \vec{g^*} - \frac{1}{\rho}\nabla P + \frac{\mu}{\rho}\nabla^2 \vec{V}. \tag{3.77}$$

The momentum equations can be written in cartesian component form as:

$$\frac{\partial u}{\partial t} + u\frac{\partial u}{\partial x} + v\frac{\partial u}{\partial y} + w\frac{\partial u}{\partial z} - fv = g_x^* - \frac{\partial P}{\rho \partial x} + \frac{\mu}{\rho}\left[\frac{\partial^2 u}{\partial x^2} + \frac{\partial^2 u}{\partial y^2} + \frac{\partial^2 u}{\partial z^2}\right] \tag{3.78}$$

$$\frac{\partial v}{\partial t} + u\frac{\partial v}{\partial x} + v\frac{\partial v}{\partial y} + w\frac{\partial v}{\partial z} + fu = g_y^* - \frac{\partial P}{\rho \partial y} + \frac{\mu}{\rho}\left[\frac{\partial^2 v}{\partial x^2} + \frac{\partial^2 v}{\partial y^2} + \frac{\partial^2 v}{\partial z^2}\right] \tag{3.79}$$

$$\frac{\partial w}{\partial t} + u\frac{\partial w}{\partial x} + v\frac{\partial w}{\partial y} + w\frac{\partial w}{\partial z} = g_z^* - \frac{\partial P}{\rho \partial z} + \frac{\mu}{\rho}\left[\frac{\partial^2 w}{\partial x^2} + \frac{\partial^2 w}{\partial y^2} + \frac{\partial^2 w}{\partial z^2}\right]. \tag{3.80}$$

3.3 Waves in the Ocean

There are three main things that make waves in the ocean: wind, when a lot of water gets moved all at once (like when you jump into the ocean and make a big splash), and the forces between the Earth, Moon, and Sun. Waves made by the wind can be small and called capillary waves, or they can be bigger like swell, chop, or seiche. Some big waves are called seiche, and they can be caused by earthquakes or landslides. However, most of these waves are called tsunamis. We can see waves in the ocean when we go to the beach or look at pictures of the ocean. These waves carry energy. The energy travels to the top of the water far from where we can see the waves. This energy goes to the beach, where it moves the sand and makes the coast wear away. Surfers use this energy to ride waves without any cost. In certain areas, wave energy is used to make electricity for towns or industries. But, because wave energy fluctuates every day, it can't give a steady flow of energy. Having a good way to save energy for later is helpful.

Certain waves are created by winds that occur nearby. However, the majority of the waves we observe at the beach, known as swell, are actually caused by winds from storms that are very far away, sometimes even thousands of miles away. The regular waves in the ocean that happen twice a day are called tides. They are caused by the pull of gravity from different parts of the earth, moon, and sun.

3.3.1 How waves are formed

Over time, the upper parts of the ocean move faster than the lower parts due to the force of friction between the layers and the water surface. These upper layers move, causing circular whirlpools, which make the water surface form waves. This is how the patterns of waves are made on the surface of the ocean. When the wind blows, it creates shapes in the water called waves. These waves move forward with the wind, not the water itself. This waveform is similar to holding onto one end of a rope and quickly letting go of it. A wave moves along the rope, but the rope itself doesn't move like water. However, the passing wave shape can affect the movement of water. Water movement happens under wave crests instead of towards the coast. It happens in a circular back-and-forth motion of the wave particles. These back-and-forth movements reach a distance of about half the length of the wave. To understand how waves are formed, it is important to distinguish between two types of forces that make waves move. These forces are called the generating force and the restoring force. The force pushes water upwards where it meets the air. Waves that travel through the pycnoclines can affect underwater and marine creatures that live in that area. Imagine being inside a submarine that can survive extreme pressure of up to 1,000 meters underwater. If the submarine stays near the same depth as the pycnocline, it can be suddenly moved to deeper depths by a passing wave. Experts believe that strange submarine accidents might have occurred because of this phenomenon. This means that waves happen at the edges.The force that creates movement pushes water from one layer to another, while another force pulls it back to where it started, trying to keep things balanced. In the middle of the two layers, there is a back-and-forth movement. As long as the force that starts the movement keeps pushing, and the force that brings it back keeps pulling, the wave will keep forming where it was disturbed and send its energy in all directions. When the force that makes the waves stops, the waves will go away from where they started, and the water goes back to how it was before. Now, let's see a few examples.

When you blow air onto hot tea in a teacup, you make a little disturbance that moves the air into the water. The surface tension of the water creates the force that brings things back to their normal position in this situation. The surface tension is caused by the water molecules being connected through hydrogen bonding, creating a protective layer on top of the water. When you blow air over hot tea, little waves are created. When you stop blowing, the waves get smaller and then go away. The little waves created by the water's surface tension are called capillary waves. When you blow air

forcefully, it can make the hot tea go up into the air. This breaks the connections between water molecules, which are called hydrogen bonds. The water eventually falls down due to gravity and returns to its original shape. Gravity waves are waves that make water go back to its normal shape because of gravity. All waves in the ocean are either small or big, the size of the wave mostly depends on the forcing, as the restoring force always tries to damp waves. Even a gentle breeze creates tiny wavy ripples on the water's surface. But when the wind gets stronger, these ripples grow and become waves that move more forcefully.

Waves have certain characteristics. One of these is called the amplitude. It measures how far the wave goes from the equilibrium surface, either up to the highest point or down to the lowest point. The equilibrium surface basically means the ocean surface without any waves. The height is how tall the wave is from the top to the bottom, and it is twice the wave's amplitude. The wavelength is the distance between two low points or two high points on a wave or any point on the wave to where that point appears again. Wave base (motion created by deep water waves) is an important thing to know about a wave. The ocean and everything in it, such as fish and submarines, do not feel any movement or disturbances below a certain depth. They are not aware that there is a wave above them. To find the wave base, divide the wavelength by two and then measure the distance from the surface.

If the forces that make the waves are always there, then the waves will keep moving back and forth. Because some waves are stuck in a small area, they form a standing wave. Standing waves in waters are called seiches. These waves are usually found in small basins or lagoons. Children can cause a phenomenon called seiches by making waves in bathtubs. This happens when the water splashes out of the tub and floods nearby places. The biggest wave in terms of amplitude and wavelength in the ocean is called the tidal wave. Their generating force comes from the varying gravitational forces the moon and sun exert on different parts of the earth.

Tsunamis and wind-generated waves in the ocean are known as progressive waves. Progressive waves are waves that start in one place and move outward. As they travel, they lose their energy and eventually reach faraway shores. The force that creates these waves does not keep going all the time. Progressive waves come in two types: transverse waves that move sideways, like earthquake waves on land or in the ocean, and longitudinal waves that compress and expand air, like sound waves from a source to your ear. Waves are movements that happen when energy causes the air or water to move back and forth. The air doesn't transfer from the headphones to your ear. Instead, sound waves move through the air as it moves back and forth, carrying

energy.

The ocean waves usually move in circular patterns. These circles become smaller as you go down to the bottom of the waves. As we have seen before, we cannot usually notice the back and forth motion below the lowest point of a wave. So, things like seaweed that are above the point where waves reach and floating garbage will be moved in a circular motion. When surfers see curling waves, they are actually seeing waves moving in a circular pattern.

When a very strong wind like a hurricane or a big storm happens far away from the beach, the waves it creates in that area are called chop. When waves move away from the storm, they divide into groups of waves that are all the same size and shape. These groups of waves travel towards the beach to form swell.

One important feature of a wave is how fast it moves. The speed of a wave is how far it goes in a certain amount of time and is determined by its length and time. For example, a tsunami is a big wave that is about 200 kilometers long and takes about 15 minutes to pass by. It moves pretty fast, going about 800 kilometers per hour. On average, waves coming towards the ocean move at about 33 km/h. The speed of the wave decreases when it touches or goes into shallow water. Deep-water waves are waves that move through water that is deeper than their wave base. When deep-water waves give their energy to the rocks or dirt on the bottom of the sea, the energy will make the sediment move, wear down the rocks, and slow down the waves. The highest part of the wave will keep going fast, but the lower part is getting slower. This makes the waves closer together, taller, and the circular movements turn into oval shapes. As a wave gets closer to the coast, you will notice that the height becomes bigger, but the length and speed become smaller. The wave always takes the same amount of time to repeat.

3.3.2 Wave kinematics

Because many things in the ocean look like waves, we need to understand the basic properties of waves to study how the ocean works. Wave number refers to the number of waves per unit distance. Frequency is the number of waves that pass through a point per unit time. The dispersion relation is a mathematical equation that shows how the frequency of a wave relates to its wave number. Phase speed is the speed at which a point on a wave moves. Group velocity is the speed at which a wave packet (a group of waves) moves. These concepts are explained and understood in terms of their physical meanings.

Wavenumber and Wavelength

Consider a wave moving on a flat surface defined by the (x, y) coordinates. This wave changes over time and has straight lines along its peaks as shown in Figure 3.7.

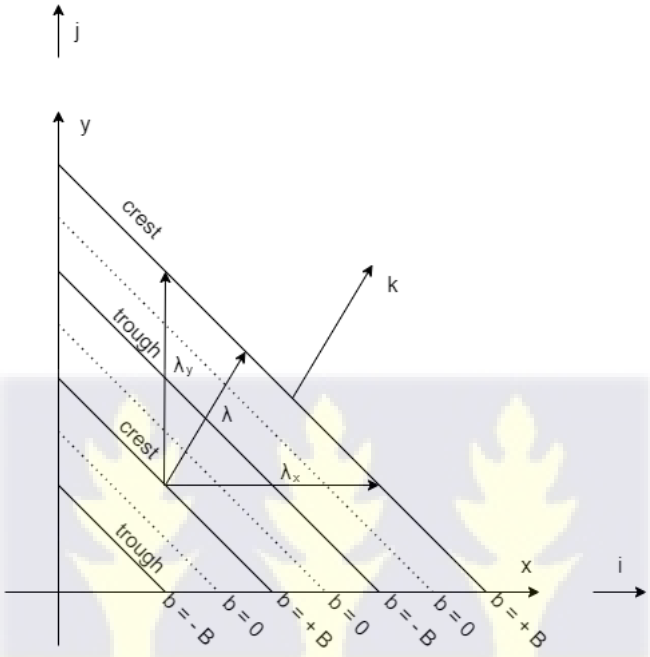

Figure 3.7: The phase lines that show different parts of a wave in a two-dimensional space.

Assume that there is a physical variable b given as

$$b(x, y, t) = B\cos(k_x x + k_y y - \omega t + \phi). \tag{3.81}$$

The coefficient B is the wave amplitude whereby $-B \leq b \leq B$, whiles the argument

$$\beta = k_x x + k_y y - wt + \phi \tag{3.82}$$

is known as the phase, and the constant ϕ is the reference phase. k_x is the wavenumber that tells us how quickly a wave is changing in the x-direction. k_y is a number that tells us how quickly a wave is changing in the y-direction. ω tells us how many waves are passing by in a given time period. They show how quickly the wave moves up and down in space and how quickly it moves back and forth in time.
The movement of the waves can be shown from Equation 3.81 as

$$b(x, y, t) = B_1 \cos(k_x x + k_y y - \omega t) + B_2 \sin(k_x x + k_y y - \omega t), \tag{3.83}$$

where $B_1 = B\cos\phi$ and $B_2 = -B\cos\phi$, and

$$b = \mathrm{Re}[B_c e^{\mathrm{i}(k_x x + k_y y - \omega t)}]. \tag{3.84}$$

The notation Re[ ] means "the real part of". The complex amplitude coefficient $B_c = B_1 - \mathrm{i}B_2$ which can be represented as $e^{\mathrm{i}\phi}$.

A wave crest is the highest point of a wave and a trough is the lowest point. The signal reaches its highest value at a certain time and is called a wave crest ($b = B$). On the other hand, when the signal reaches its lowest value, it is called a trough ($b = -B$). Phase lines are lines where the signal has the same value at a particular moment in time. They can be seen in Figure 3.7. In a plane wave, all the high points, low points, and other lines showing different parts of the wave are straight.

The pattern of peaks in the signal happens regularly because of the back-and-forth movement of the sinusoidal function. This is what makes the signal look wavy. The distance it repeats itself in the x direction is

$$\lambda_x = \frac{2\pi}{k_x}. \tag{3.85}$$

Similarly, the distance at which the signal repeats itself up and down in the y direction is

$$\lambda_y = \frac{2\pi}{k_y}. \tag{3.86}$$

λ_x and λ_y refer to the lengths of the waves in the zonal and meridional directions, respectively. These are lengths of waves that can be seen when someone looks through slits that are in line with the zonal and meridional directions. The actual wavelength of a wave, symbolized by λ, is the shortest distance between two adjacent crests. It is smaller than λ_x and λ_y.

Consider

$$\frac{1}{\lambda^2} = \frac{1}{\lambda_x^2} + \frac{1}{\lambda_y^2} = \frac{k_x^2 + k_y^2}{4\pi^2} \tag{3.87}$$

or the real length of the wave can be expressed as

$$\lambda = \frac{2\pi}{k}, \tag{3.88}$$

where k is referred to as the wavenumber, which is defined as

$$k = \sqrt{k_x^2 + k_y^2}. \tag{3.89}$$

Note that $\lambda^2 \neq \lambda_x^2 + \lambda_y^2$. Additionally, (λ_x, λ_y) does not represent a vector but can be used to define

$$\vec{k} = k_x\vec{\mathrm{i}} + k_y\vec{\mathrm{j}}, \tag{3.90}$$

and k is the size of the vector $\vec{k}$.
Phase lines at a specific time match up with lines that have the same value of $k_x x + k_y y = \vec{k} \cdot \vec{r}$, where $\vec{r} = x\vec{\mathrm{i}} + y\vec{\mathrm{j}}$ is the displacement vector.
These lines are phase line composed of point.The point has vectors that start at the origin and are the same length when measured against the wavenumber vector. These points form a line that is perpendicular to all the other lines, indicating the varying phases. The straight line follows the direction of the up-and-down movement.

Frequency, Phase speed, and Dispersion

Imagine that someone is watching a signal that moves back and forth in the same place (x, y). The time it takes for the signal to reach its highest point again is the same as the time it takes for the phase to increase by a full rotation. During this time, the phase increases by 2π. The time it takes for a wave to make one complete cycle is called the period. It is calculated using $T = \dfrac{2\pi}{\omega}$.
Consider a specific wave that has a height $b = B$ between one time t_1 and another time t_2. The time difference between t_2 and t_1 is called Δt. During this period, the highest point of a wave has moved from one place to another. The x axis moves a distance Δx in time Δt. The distance is calculated using $\Delta x = \dfrac{\omega t_2}{k_x} - \dfrac{\omega t_1}{k_x} = \dfrac{\omega \Delta t}{k_x}$.
This defines how fast the wave moves in the x direction:

$$c_x = \frac{\Delta x}{\Delta t} = \frac{\omega}{k_x}. \tag{3.91}$$

c_x is the speed of a wave in the direction of the x-axis. The distance of the wave is $\Delta y = \dfrac{\omega t_2}{k_y} - \dfrac{\omega t_1}{k_y} = \dfrac{\omega \Delta t}{k_y}$ and the time interval is Δt. The speed at which the signal travels in the y direction is

$$c_y = \frac{\Delta y}{\Delta t} = \frac{\omega}{k_y}. \tag{3.92}$$

But these speeds are only going fast in one way. The distance the crest line travels in a specific time Δt is Δs . The distance is measured perpendicular to the crest. Consider

$$\frac{1}{\Delta s^2} = \frac{1}{\Delta x^2} + \frac{1}{\Delta y^2} \tag{3.93}$$

which reduces to

$$\Delta s = \frac{\omega \Delta t}{k}, \tag{3.94}$$

where k represent the wavenumber expressed in Equation 3.89. The speed of the crest line is

$$c = \frac{\Delta s}{\Delta t} = \frac{w}{k}. \tag{3.95}$$

All phase lines move at the same speed, which is called *phase speed*, c. Also, $c^2 \neq c_x^2 + c_y^2$ because c is smaller than both c_x and c_y, and the pair (c_x, c_y) does not represent a physical vector. The phase travels in the same direction as the wavenumber vector $\vec{k}$.

Assume we have a system that doesn't change over time. It is either not moving or flowing steadily. Then, at time $t = 0$, we disturb it by changing its shape using a wavy pattern in the x and y directions. The size of the waves is determined by the values of k_x and k_y, and the overall change in shape is determined by the amplitude B for variable b. Usually, the value of ω depends only on k_x and k_y. If the frequency depends on the wavenumber components, then the phase speed also depends on them:

$$c = \frac{\omega(k_x, k_y)}{\sqrt{k_x^2 + k_y^2}} = c(k_x, k_y). \tag{3.96}$$

This means that when a signal is made up of different waves, those waves will all move at different speeds, which can cause the signal to change or become distorted over time. Specifically, a sudden increase in activity in a small area, which includes waves of different lengths, will spread out and become less concentrated over time. The phenomenon is referred to as dispersion. The relationship between the frequency ω and the wavenumber components k_x and k_y is referred to as the *dispersion relation*. In two dimensions, the dispersion relation can be shown as a group of curves on the k_x and k_y plane where ω stays the same. In one dimension, $k_x = k$ and $k_y = 0$. When the characteristics of a physical system remain consistent from all directions within a two-dimensional framework, and the frequency ω only depends on k, we only need

one curve that shows how ω changes with k.
Sometimes, the relationship between frequency and wavenumber can be simplified to a single proportional relationship. The phase speed is the speed at which waves move together without changing their shape over time. The wave that falls under this category is known as a *non-dispersive wave*.

Energy Propagation and Group Velocity

A wave is composed of multiple waves. Several waves are combined, which can either add up to make a bigger wave (constructive interference) or cancel each other out (destructive interference). When waves combine and make bigger waves, they have more energy. When waves mix and make smaller waves, they have less energy. The distribution of energy involves the dispersal of energy across various waveforms. Each wave contains an equal distribution of energy, so it is not solely dependent on a single wave. The manner in which energy travels through waves is determined by the movement of interference patterns, rather than the mean speed at which the waves travel. In order to comprehend the speed of energy transmission, we will analyze two straight waves. These waves have the same size and shape, and are almost the same length:

$$b = B\cos(k_1 x - \omega_1 t) + B\cos(k_2 x - \omega_2 t), \tag{3.97}$$

k_1 and k_2 are almost the same value as their average $k = \dfrac{k_1 + k_2}{2}$, and the change $\Delta k = k_1 - k_2$ is relatively smaller, that is $|\Delta k| \ll |k|$. Because waves follow the dispersion relation, that is, $\omega = \omega(k)$, it means that the two frequencies $\omega_1 = \omega(k_1)$ and $\omega_2 = \omega(k_2)$ will be close to the average $\omega = (\omega_1 + \omega_2)/2$ and the difference $\Delta\omega = \omega_1 - \omega_2$ is relatively smaller, that is, $|\Delta\omega| \ll |\omega|$. In Equation 3.97, the two reference phases were adjusted to have an initial value of zero. This can be achieved by choosing a favourable space and time. By trigonometric identities Equation 3.97 can be converted into

$$b = 2B\cos\left(\frac{\Delta k}{2}x - \frac{\Delta\omega}{2}t\right)\cos(kx - \omega t), \tag{3.98}$$

which looks like the result of combining two waves. The combined average of the wavenumber and frequency of the two waves is demonstrated in the second cosine function. The first cosine function has a lower wavenumber, which means it has a

longer wavelength and a lower frequency. The longer wave looks almost the same over time as the shorter wave. The (k, ω) wave looks like it is changing; its size $2B\cos[(\Delta kx - \Delta\omega t)/2]$ is changing slowly with space and time.

Even though the wave signal goes from its highest point to its lowest point and then to the next highest point in a distance equal to $\lambda = 2\pi/k$, the total length of the wave is actually much longer, that is, $\lambda' = \frac{1}{2}[2\pi/(\Delta k/2)] = 2\pi/\Delta k$. A collection of waves with a specific length termed as λ' constitutes the wave pattern. The speed c of the wave can be calculated by dividing the frequency ω by the wavelength k. The speed of the burst is equal to the change in frequency divided by the change in wavelength, that is, $c' = \Delta\omega/\Delta k$. A very small difference in the wavenumber of the wave is

$$c_g = \frac{dw}{dk}.$$

Group velocity is the term used to describe how fast a burst or collection of waves moves. Energy is interconnected with every group, hence the velocity at which waves move and transfer energy is referred to as group velocity.The earlier description indicates that the signal depends on having two waves that are the same size. When two waves have different strengths, like B_1 and B_2, they do not completely cancel each other out in destructive interference because the weaker wave is not strong enough to completely negate the stronger wave. The changing shape of the envelope goes up and down between the values of $B_1 + B_2$ and $|B_1 - B_2|$ on the high side and between $-(B_1 + B_2)$ and $-|B_1 - B_2|$ on the low side. Construction interference occurs in certain regions, causing higher energy levels to move at the group velocity.

This can also apply to waves that have more than one dimension. For instance, when dealing with two dimensions, we measure the speed of groups in both the horizontal (x) and vertical (y) directions as

$$c_{gx} = \frac{\partial\omega}{\partial k_x}, \qquad c_{gy} = \frac{\partial\omega}{\partial k_y},$$

since the frequency depends on the wavenumbers, denoted as $\omega(k_x, k_y)$. These terms show the parts of the slope of the function ω in the (k_x, k_y) space for wave numbers. They can also be thought of as the parts of a physical vector that represents how a group is moving.

$$\vec{c_g} = \nabla_k \omega,$$

where ∇_k is a mathematical operation that measures the changes in the variables k_x and k_y. Matching the horizontal and vertical axes with the corresponding k_x and k_y

axes of the plane helps us see which way energy is moving in space.

3.3.3 Gravity Waves

Gravity waves happen when the force of gravity tries to balance things in a fluid. They occur at the place where two fluids meet. This interface can be where the air meets the water, leading to waves on the water called wind waves. The phenomenon of gravity waves arises from the displacement of a fluid from its expected location. The fluid, upon reaching equilibrium, will exhibit a wave-like motion known as a **wave orbit**. Gravity waves on the surface of the ocean are called **surface gravity waves** or **surface waves**. The waves inside the water are called **internal waves**.

3.3.4 Internal–Wave Theory

To find the equations that govern internal waves, we first start by making certain key assumptions. There is no spinning; the domain is infinite, there is no way for energy to be lost, and the movement of the waves and size is tiny. This is done so that the governing equations can be simplified and linear. We add the term $\partial w/\partial t$ in the vertical momentum equation to properly account for the upward and downward movements in gravity waves. The fluid density can be expressed as

$$\text{Fluid density (actual)} = \rho_0 + \bar{\rho}(z) + \rho'(x, y, z, t), \tag{3.99}$$

where ρ_0 is the initial density, $\bar{\rho}(z)$ is the normal density in the environment, and $\rho'(x, y, z, t)$ is the change in density caused by the wave. The inequality $|\bar{\rho}| \ll \rho_0$ justifies the Boussinesq approximation required to linearize the wave problem. From Equation 3.14 of the mass conservation and the product rule, we obtain

$$\frac{\partial \rho}{\partial t} + \rho\left(\frac{\partial u}{\partial x} + \frac{\partial v}{\partial y} + \frac{\partial w}{\partial z}\right) + u\frac{\partial \rho}{\partial x} + v\frac{\partial \rho}{\partial y} + w\frac{\partial \rho}{\partial z} = 0. \tag{3.100}$$

Substitutes Equation 3.46 of the continuity equation into Equation 3.100 to get

$$\frac{\partial \rho}{\partial t} + u\frac{\partial \rho}{\partial x} + v\frac{\partial \rho}{\partial y} + w\frac{\partial \rho}{\partial z} = 0. \tag{3.101}$$

From Equation 3.99, Equation 3.101 reduces to

$$\frac{\partial \rho'}{\partial t} + w\frac{d\bar{\rho}}{dz} = 0. \tag{3.102}$$

The pressure caused by the fluid can be expressed as

$$\text{Actual pressure} = p_0(z) + p'(x, y, z, t), \tag{3.103}$$

where $p_0(z)$ is the hydrostatic pressure defined by Equation 3.5 and the change in pressure is $p'(x, y, z, t)$.
Based on the previous assumptions, we obtain the following equations:

$$\frac{\partial u}{\partial t} = -\frac{1}{\rho_0}\frac{\partial p'}{\partial x} \tag{3.104}$$

$$\frac{\partial v}{\partial t} = -\frac{1}{\rho_0}\frac{\partial p'}{\partial y} \tag{3.105}$$

$$\frac{\partial w}{\partial t} = -\frac{1}{\rho_0}\frac{\partial p'}{\partial z} - \frac{1}{\rho_0}g\rho' \tag{3.106}$$

$$\frac{\partial u}{\partial x} + \frac{\partial v}{\partial y} + \frac{\partial w}{\partial z} = 0. \tag{3.107}$$

$$\frac{\partial \rho'}{\partial t} + w\frac{d\bar{\rho}}{dz} = 0. \tag{3.108}$$

Equation (3.108) states that the change in density at a point is caused by the upward movement of the average density. The term $d\bar{\rho}/dz$ can be changed by considering the stratification frequency, which is known as the Brunt–Väisälä frequency (*buoyancy frequency*)

$$N^2 = -\frac{g}{\rho_0}\frac{d\bar{\rho}}{dz}$$

to obtain

$$\frac{\partial \rho'}{\partial t} - \frac{N^2\rho_0}{g}w = 0. \tag{3.109}$$

The buoyancy frequency $N(z)$ is a measure of how fast a fluid particle moves up and down when it is displaced vertically. It is measured in radians per second. This measurement is taken when there is no friction in the fluid, and the particle is released from a stationary position. This is discussed in Section 3.2.6.
We can simplify the above equations by only considering the vertical displacement w. This can be achieved by taking the time derivative of the continuity equation to get

$$\frac{\partial^2 u}{\partial t \partial x} + \frac{\partial^2 v}{\partial t \partial y} + \frac{\partial^2 w}{\partial t \partial z} = 0. \tag{3.110}$$

Use the horizontal momentum equations in (3.104) and (3.105) to eliminate u and v to obtain

$$\frac{\partial}{\partial x}\left\{\frac{\partial u}{\partial t}\right\}+\frac{\partial}{\partial y}\left\{\frac{\partial v}{\partial t}\right\}+\frac{\partial}{\partial z}\left\{\frac{\partial w}{\partial t}\right\}=0 \tag{3.111}$$

$$\frac{\partial}{\partial x}\left\{-\frac{1}{\rho_0}\frac{\partial p'}{\partial x}\right\}+\frac{\partial}{\partial y}\left\{-\frac{1}{\rho_0}\frac{\partial p'}{\partial y}\right\}+\frac{\partial^2 w}{\partial t\partial z}=0 \tag{3.112}$$

$$-\frac{1}{\rho_0}\left[\frac{\partial^2 p'}{\partial x^2}+\frac{\partial^2 p'}{\partial y^2}\right]=-\frac{\partial^2 w}{\partial t\partial z} \tag{3.113}$$

$$\frac{1}{\rho_0}\nabla_H^2 p'=\frac{\partial^2 w}{\partial t\partial z} \tag{3.114}$$

where $\nabla_H^2=\dfrac{\partial^2}{\partial x^2}+\dfrac{\partial^2}{\partial y^2}$ is the *horizontal* Laplacian operator.
Density perturbation ρ' can be eliminated by using Equation 3.114 and the vertical momentum equation in Equation 3.106 to get

$$\frac{1}{\rho_0}\frac{\partial^2 p'}{\partial t\partial z}=-\frac{\partial^2 w}{\partial t^2}-N^2 w. \tag{3.115}$$

Finally, the change in pressure, denoted as p', can be removed by finding the derivative of Equation 3.114 with respect to z and t and insert into Equation 3.115 to get

$$\frac{1}{\rho_0}\nabla_H^2\frac{\partial^2 p'}{\partial t\partial z}=\frac{\partial^2}{\partial t\partial z}\left\{\frac{\partial^2 w}{\partial t\partial z}\right\}$$

$$-\nabla_H^2\left[\frac{\partial^2 w}{\partial t^2}+N^2 w\right]=\frac{\partial^2}{\partial z^2}\left\{\frac{\partial^2 w}{\partial t^2}\right\}$$

$$\left[\nabla_H^2+\frac{\partial^2}{\partial z^2}\right]\frac{\partial^2 w}{\partial t^2}+\nabla_H^2 N^2 w=0,$$

which simplifies to

$$\frac{\partial^2}{\partial t^2}\nabla^2 w+N^2\nabla_H^2 w=0, \tag{3.116}$$

where $\nabla^2\equiv\dfrac{\partial^2}{\partial x^2}+\dfrac{\partial^2}{\partial y^2}+\dfrac{\partial^2}{\partial z^2}=\nabla_H^2+\dfrac{\partial^2}{\partial z^2}$ is the *Laplacian operator* in three dimension. We can use Equation 3.116 to find out the vertical velocity, w. This will help us learn about how internal gravity waves spread out. The fluid we are studying is divided into layers, and waves can move in any direction, even at an angle to the vertical. When it comes to which way the waves move, the wave number vector $\vec{\mathrm{K}}=k_x\,\vec{\mathrm{i}}+k_y\,\vec{\mathrm{j}}+k_z\,\vec{\mathrm{k}}$ becomes important. The relationship between the frequency of the waves (ω) depends on the wave number components (k_x, k_y, k_z).
Internal waves are waves that happen inside the water, not at the surface. When

these waves move, the pressure and density in the water change, but they do not mix together. Baroclinic processes (changes in density with respect to depth and height) in fluid create spinning motion in the fluid, which is measured by vorticity according to Kelvin's circulation theorem. So, waves inside a fluid with different layers are spinning. The Laplace equation is used to describe how fluids flow in different layers. However, it cannot be used to describe how waves move within a fluid that has different levels of density.

$$\eta(\vec{x},t) = a\cos(k_x\,x + k_y\,y + k_z\,z - \omega t) = a\cos(\vec{\mathrm{K}}\,\cdot\,\vec{x} - \omega t)$$

where $\mathrm{K} = |\,\vec{\mathrm{K}}\,| = \sqrt{k_x^2 + k_y^2 + k_z^2}$, $\vec{x} = x\,\vec{\mathrm{i}} + y\,\vec{\mathrm{j}} + z\,\vec{\mathrm{k}}$ and $\lambda = 2\pi\ \mathrm{K}$ for the vertical velocity

$$w = w_0 \mathrm{e}^{\vec{\mathrm{i}}(k_x\,x + k_y\,y + k_z\,z - \omega t)} = w_0 \mathrm{e}^{\vec{\mathrm{i}}(\vec{\mathrm{K}}\,\cdot\,\vec{x} - \omega t)} \tag{3.117}$$

in a fluid where the upward force remains constant. Substitute Equation 3.117 into Equation 3.116 with constant buoyancy frequency N leads:

$$\omega^2 = \frac{k_x^2 + k_y^2}{k_x^2 + k_y^2 + k_z^2} N^2. \tag{3.118}$$

For simplicity, let's use the x, z plane that includes $\vec{\mathrm{K}}$ and has k_y equal to zero. We can make this choice without any problems because the medium has the same properties in all directions, so now K_x represents the whole wave number in the horizontal direction and Equation 3.118 can be written as

$$\omega = \frac{k_x N}{\sqrt{k_x^2 + k_z^2}} = \frac{k_x N}{\mathrm{K}}. \tag{3.119}$$

Chapter 4

Introduction To Upwelling

We will look at how the classical theory fails to answer the question of upwelling in the Gulf of Guinea as discussed in Subsection 1.1.1 of Chapter 1. Later, we will also expand on the idea of Kelvin waves which have been hypothesised to be associated with upwelling in the Gulf of Guinea.

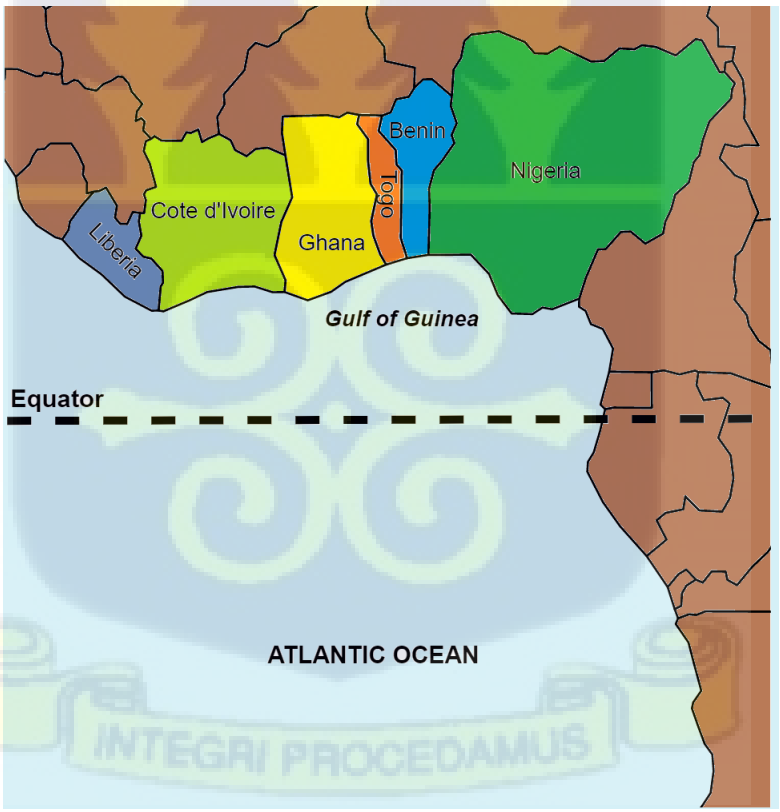

Figure 4.1: Map of Gulf of Guinea (GoG) region

Figure 4.1 shows a map of the Gulf of Guinea located in the eastern part of the

Atlantic ocean, where upwelling in the Gulf of Guinea is different from the classical theory of wind versus direction of Ekman transport. The question is, what is the cause of upwelling in the Gulf of Guinea? To answer this question, we dive into what constitutes the classical theory of upwelling.

4.1 Classical Theory of Upwelling

The full set of the cartesian component form of the momentum equations and continuity equation (conservation of mass for an incompressible fluid) from Equation (3.78), (3.78), (3.80), and (3.46) in Subsection 3.2.4 are:

$$\frac{\partial u}{\partial t} + u\frac{\partial u}{\partial x} + v\frac{\partial u}{\partial y} + w\frac{\partial u}{\partial z} - fv = -\frac{\partial P}{\rho \partial x} + \nu\left[\frac{\partial^2 u}{\partial x^2} + \frac{\partial^2 u}{\partial y^2} + \frac{\partial^2 u}{\partial z^2}\right] \tag{4.1}$$

$$\frac{\partial v}{\partial t} + u\frac{\partial v}{\partial x} + v\frac{\partial v}{\partial y} + w\frac{\partial v}{\partial z} + fu = -\frac{\partial P}{\rho \partial y} + \nu\left[\frac{\partial^2 v}{\partial x^2} + \frac{\partial^2 v}{\partial y^2} + \frac{\partial^2 v}{\partial z^2}\right] \tag{4.2}$$

$$\frac{\partial w}{\partial t} + u\frac{\partial w}{\partial x} + v\frac{\partial w}{\partial y} + w\frac{\partial w}{\partial z} = -\frac{\partial P}{\rho \partial z} + \nu\left[\frac{\partial^2 w}{\partial x^2} + \frac{\partial^2 w}{\partial y^2} + \frac{\partial^2 w}{\partial z^2}\right] \tag{4.3}$$

$$\frac{\partial u}{\partial x} + \frac{\partial v}{\partial y} + \frac{\partial w}{\partial z} = 0, \tag{4.4}$$

where the kinematic viscosity, $\nu = \dfrac{\mu}{\rho}$ and f is the Coriolis force. It can be observed that the term $\vec{g^*}$ from Equation (3.78), (3.78), and (3.80) which combines the buoyancy and centrifugal acceleration has been ignored since it does not play any role in the Ekman transport.

The classical idea behind upwelling is triggered by three main drivers, namely: wind, the Coriolis effect, and Ekman transport. Under the Ekman process, the following assumptions are made on the equations of motion.

- The flow is assumed steady, $\dfrac{\partial u}{\partial t} = 0$ and $\dfrac{\partial v}{\partial t} = 0$ where u is the zonal velocity (velocity along the x direction) and v is a meridional velocity (velocity along the y direction).
- A horizontal flow on the surface of the ocean, that is, $w = 0$, where w is the vertical velocity along the z direction.

- A homogeneous flow, where changes in spatial horizontal gradients are zero, that is

$$\frac{\partial u}{\partial x} = \frac{\partial u}{\partial y} = \frac{\partial v}{\partial x} = \frac{\partial v}{\partial y} = 0. \tag{4.5}$$

- A rotating earth leading to balance between frictional force and Coriolis effect.

Now consider flow in the $xz-$plane where the tangential stress to the boundary of the fluid, $\tau_{xz} = \rho\nu\frac{\partial u}{\partial z}$. $\rho\nu$ is the molecular viscosity and $\frac{\partial u}{\partial z}$ the velocity shear at the boundary. For an incompressible fluid, the frictional force per unit mass is given by

$$\begin{aligned}\nu\left[\frac{\partial^2 u}{\partial x^2} + \frac{\partial^2 u}{\partial y^2} + \frac{\partial^2 u}{\partial z^2}\right] &= \frac{\partial}{\partial x}\left(\nu\frac{\partial u}{\partial x}\right) + \frac{\partial}{\partial y}\left(\nu\frac{\partial u}{\partial y}\right) + \frac{\partial}{\partial z}\left(\nu\frac{\partial u}{\partial z}\right)\\ &= \frac{1}{\rho}\left[\frac{\partial(\tau_{xx})}{\partial x} + \frac{\partial(\tau_{xy})}{\partial y} + \frac{\partial(\tau_{xz})}{\partial z}\right]\\ &= \frac{1}{\rho}\frac{\partial(\tau_{xz})}{\partial z}\end{aligned}$$

Note that, $\frac{\partial(\tau_{xx})}{\partial x} = 0$ and $\frac{\partial(\tau_{xy})}{\partial y} = 0$, since there is no flow in the $xx-$plane and $xy-$plane. Similarly, if we consider flow in the $yz-$plane, where the molecular viscosity, $\rho\nu$ is the ratio of the stress, τ tangential to the boundary of the fluid and the velocity shear at the boundary. That is, $\tau_{yz} = \rho\nu\frac{\partial v}{\partial z}$. For an incompressible fluid, the frictional force per unit mass is given by

$$\begin{aligned}\nu\left[\frac{\partial^2 v}{\partial x^2} + \frac{\partial^2 v}{\partial y^2} + \frac{\partial^2 v}{\partial z^2}\right] &= \frac{\partial}{\partial x}\left(\nu\frac{\partial v}{\partial x}\right) + \frac{\partial}{\partial y}\left(\nu\frac{\partial v}{\partial y}\right) + \frac{\partial}{\partial z}\left(\nu\frac{\partial v}{\partial z}\right)\\ &= \frac{1}{\rho}\left[\frac{\partial(\tau_{yx})}{\partial x} + \frac{\partial(\tau_{yy})}{\partial y} + \frac{\partial(\tau_{yz})}{\partial z}\right]\\ &= \frac{1}{\rho}\frac{\partial(\tau_{yz})}{\partial z}\end{aligned}$$

Also, $\frac{\partial(\tau_{yx})}{\partial x} = 0$ and $\frac{\partial(\tau_{yy})}{\partial y} = 0$, since there is no flow in the $yx-$plane and $yy-$plane. Assume a constant vertical eddy viscosity, A_z. Consider wind stress in x and y direction as $\tau_x = \tau_{xz} = \rho A_z\frac{\partial u}{\partial z}$ and $\tau_y = \tau_{yz} = \rho A_z\frac{\partial v}{\partial z}$ respectively. The Eddy viscosity is a proportionality factor describing the circular mixing of the fluid particles forming internal friction as they shear against each other randomly. Due to the random movement of the water particles, the eddies are created, behaving as circular currents. They obey Newton's law of viscosity, meaning the fluid under consideration

is Newtonian.

Under these conditions, we have a flow with no x and y dependence given by

$$fv + \frac{1}{\rho}\frac{\partial \tau_x}{\partial z} = 0 \iff fv + A_z\frac{d^2u}{dz^2} = 0 \tag{4.6}$$

$$-fu + \frac{1}{\rho}\frac{\partial \tau_y}{\partial z} = 0 \iff -fu + A_z\frac{d^2v}{dz^2} = 0 \tag{4.7}$$

where ρ is the density of sea water and f is the Coriolis parameter. Consider wind stress on the surface of the water in the Northern direction, $\tau_x = 0$. Boundary conditions include:

- Below the base of Ekman layer $u(z) = v(z) = 0$ as $z \to -\infty$.
- At the surface of the ocean $\tau_y(0) = \rho A_z\dfrac{dv(0)}{dz} = \tau$ and $\tau_x(0) = 0$ at $z = 0$.

We derive solutions to these coupled differential Equation 4.6 and Equation 4.7 with the boundary conditions to get u and v as follows. From Equation 4.7

$$A_z\frac{d^2v}{dz^2} = fu \quad \Longrightarrow \quad u = \frac{A_z}{f}\frac{d^2v}{dz^2} \tag{4.8}$$

Put Equation 4.8 into Equation 4.6 to get

$$fv + A_z\frac{d^2}{dz^2}\left(\frac{A_z}{f}\frac{d^2v}{dz^2}\right) = 0 \tag{4.9}$$

$$f^2v + A_z^2\frac{d^4v}{dz^4} = 0 \tag{4.10}$$

Now Equation 4.10 is a fourth-order constant coefficient ordinary differential equation in v. Suppose there is a solution that is both complex and exponential in the following form $v = Be^{kz}$, where B is a constant.
Note that

$$\frac{d^4v}{dz^4} = k^4Be^{kz}. \tag{4.11}$$

Put Equation 4.11 and $v = Be^{kz}$ into Equation 4.10 to get

$$\begin{aligned} f^2 Be^{kz} + A_z^2 k^4 Be^{kz} &= 0 \\ (f^2 + A_z^2 k^4) Be^{kz} &= 0 \\ f^2 + A_z^2 k^4 &= 0, \quad \text{since } e^{kz} \neq 0 \\ \left(\frac{f}{A_z}\right)^2 + k^4 &= 0 \\ \implies k^4 &= -\left(\frac{f}{A_z}\right)^2. \end{aligned}$$

Also $k^4 = -\left(\frac{f}{A_z}\right)^2$ implies that $k = \pm\sqrt{\mathrm{i}}\sqrt{\left(\frac{f}{A_z}\right)}$, where $\mathrm{i} = \sqrt{-1}$. Let $\sqrt{\mathrm{i}} = x + \mathrm{i}y$, so that

$$\sqrt{\mathrm{i}} = x + \mathrm{i}y \tag{4.12}$$

$$\mathrm{i} = (x + \mathrm{i}y)^2 \tag{4.13}$$

$$\mathrm{i} = x^2 - y^2 + \mathrm{i}2xy. \tag{4.14}$$

Comparing the real and imaginary parts of Equation 4.14 implies that $x^2 - y^2 = 0$ and $2xy = 1$. For $x^2 - y^2 = 0$ then $y = x$ or $y = -x$. Put $y = x$ into $2xy = 1$ to get

$$\begin{aligned} 2x^2 &= 1 \\ x &= \pm\sqrt{\frac{1}{2}} \quad \text{similarly} \quad y = \pm\sqrt{\frac{1}{2}}. \end{aligned}$$

Also put $y = -x$ into $2xy = 1$ to get

$$\begin{aligned} 2x(-x) = -2x^2 &= 1 \\ x^2 &= -\frac{1}{2} \\ x &= \pm\mathrm{i}\sqrt{\frac{1}{2}} \quad \text{similarly} \quad y = \pm\mathrm{i}\sqrt{\frac{1}{2}}. \end{aligned}$$

We can choose $\sqrt{i} = \pm(1 + \mathrm{i})\sqrt{\frac{1}{2}}$. Then

$$k = \pm\sqrt{\mathrm{i}}\sqrt{\left(\frac{f}{A_z}\right)} = \pm(1 + \mathrm{i})\sqrt{\frac{1}{2}}\sqrt{\left(\frac{f}{A_z}\right)} = \pm(1 + \mathrm{i})\sqrt{\frac{f}{2A_z}}.$$

Let $a = \sqrt{\dfrac{f}{2A_z}}$ and $V(z) = u(z) + \mathrm{i}v(z)$ be the general form of the solution. The general complex solution is

$$V(z) = Ce^{a(1+\mathrm{i})z} + De^{-a(1+\mathrm{i})z}, \tag{4.15}$$

where C and D are constants to be determined from the boundary conditions. Note that

$$\sqrt{2}e^{(\pi/4)\mathrm{i}} = \sqrt{2}(\cos(\pi/4) + \mathrm{i}\sin(\pi/4)) = 1 + \mathrm{i} \tag{4.16}$$

As z approaches $-\infty$ from the boundary conditions, Equation 4.15 becomes

$$\begin{aligned}
\lim_{z\to-\infty} V(z) &= \lim_{z\to-\infty} (Ce^{a(1+\mathrm{i})z} + De^{-a(1+\mathrm{i})z}) \\
0 &= D \lim_{z\to-\infty} e^{-a(1+\mathrm{i})z}, \quad \text{since } \lim_{z\to-\infty} Ce^{a(1+\mathrm{i})z} = 0 \\
0 &= D, \quad \text{since } \lim_{z\to-\infty} e^{-a(1+\mathrm{i})z} \neq 0.
\end{aligned}$$

Since the constant term $D = 0$, Equation 4.15 reduces to

$$V(z) = Ce^{a(1+\mathrm{i})z}. \tag{4.17}$$

Differentiating Equation 4.17 with respect to z, we get

$$\frac{dV(z)}{dz} = Ca(1+\mathrm{i})e^{a(1+\mathrm{i})z}. \tag{4.18}$$

Multiplying through by ρA_z, we have

$$\rho A_z \frac{dV(z)}{dz} = \rho A_z Ca(1+\mathrm{i})e^{a(1+\mathrm{i})z}. \tag{4.19}$$

Considering flow at the surface of the ocean, we can substitute $z = 0$ to get

$$\rho A_z \frac{dV(0)}{dz} = \rho A_z Ca(1+\mathrm{i})e^{a(1+\mathrm{i})(0)} = \rho A_z Ca(1+\mathrm{i}). \tag{4.20}$$

Since $V(z) = u(z) + iv(z)$ and $\dfrac{dV(z)}{dz} = \dfrac{du(z)}{dz} + i\dfrac{dv(z)}{dz}$ implies that

$$\begin{aligned}
\frac{dV(0)}{dz} &= \frac{du(0)}{dz} + \mathrm{i}\frac{dv(0)}{dz} \\
\implies \rho A_z \frac{dV(0)}{dz} &= \rho A_z \frac{du(0)}{dz} + \mathrm{i}\rho A_z \frac{dv(0)}{dz} \\
\implies \rho A_z \frac{dV(0)}{dz} &= \tau_x(0) + \mathrm{i}\tau_y(0) \\
\implies \rho A_z \frac{dV(0)}{dz} &= 0 + \mathrm{i}\tau
\end{aligned}$$

This implies $\rho A_z \dfrac{dV(0)}{dz} = \rho A_z Ca(1+\mathrm{i}) = \mathrm{i}\tau$. From Equation 4.16: $1 + \mathrm{i} = \sqrt{2}e^{(\pi/4)\mathrm{i}}$. Therefore $\rho A_z Ca(1+\mathrm{i}) = \rho A_z Ca\sqrt{2}e^{(\pi/4)\mathrm{i}}$, and

$$\rho A_z Ca\sqrt{2}e^{(\pi/4)\mathrm{i}} = \mathrm{i}\tau.$$

Thus,

$$\begin{aligned}
C &= \frac{\mathrm{i}\tau}{\rho A_z a\sqrt{2}} \cdot e^{-(\pi/4)\mathrm{i}} \\
\implies C &= \frac{e^{(\pi/2)\mathrm{i}}\tau}{\rho A_z a\sqrt{2}} \cdot e^{-(\pi/4)\mathrm{i}} \quad \text{since } \mathrm{i} = \cos(\pi/2) + \mathrm{i}\sin(\pi/2) = e^{(\pi/2)\mathrm{i}} \\
\implies C &= \frac{\tau}{\rho A_z a\sqrt{2}} \cdot e^{(\pi/4)\mathrm{i}}
\end{aligned}$$

Putting C into the general solution of Equation 4.17, we get

$$\begin{aligned}
V(z) &= \frac{\tau}{\rho A_z a\sqrt{2}} e^{(\pi/4)\mathrm{i}} e^{a(1+\mathrm{i})z} \\
\implies V(z) &= \frac{\tau}{\rho A_z a\sqrt{2}} e^{az} e^{(az+\pi/4)\mathrm{i}} \\
\implies V(z) &= \frac{\tau}{\rho A_z a\sqrt{2}} e^{az}(\cos(az+\pi/4) + \mathrm{i}\sin(az+\pi/4)) \\
\implies V(z) &= \frac{\tau}{\sqrt{\rho^2 f A_z}} e^{az}(\cos(az+\pi/4) + \mathrm{i}\sin(az+\pi/4)) \\
\implies V(z) &= V_0 e^{az}(\cos(az+\pi/4) + \mathrm{i}\sin(az+\pi/4)).
\end{aligned}$$

$V = u + \mathrm{i}\,v$ implies that

$$u = V_0 e^{az}\cos(az+\pi/4) \quad \text{and} \quad v = V_0 e^{az}\sin(az+\pi/4),$$

where $V_0 = \dfrac{\tau}{\sqrt{\rho^2 f A_z}}$ and $a = \sqrt{\dfrac{f}{2A_z}}$.

Some implications from $V(z) = V_0 e^{az}(\cos(az + \pi/4) + \mathrm{i}\sin(az + \pi/4))$ is that, at the sea surface $z = 0$, $u(0) = V_0\cos(\pi/4)$ and $v(0) = V_0\sin(\pi/4)$. The surface current velocity in the northern hemisphere is shifted 45° to the right as seen in Figure 4.2 and to the left of the wind in the southern hemisphere.

For a complex velocity $V = u + iv$, the velocity decays exponentially with depth in different directions as you move below the surface. This forms the Ekman spiral, as seen in Figure 4.3. This means that the deeper you go below the sea surface, that is, a few 100 meters below the sea surface, the Ekman velocities approach zero. The

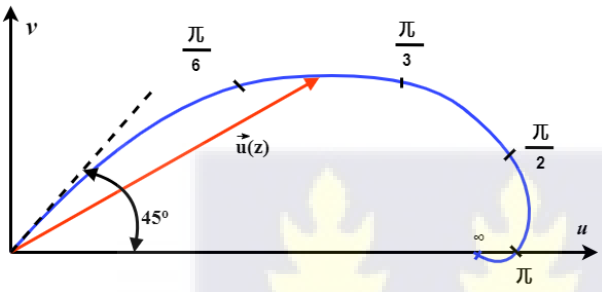

Figure 4.2: The Ekman velocity spiral

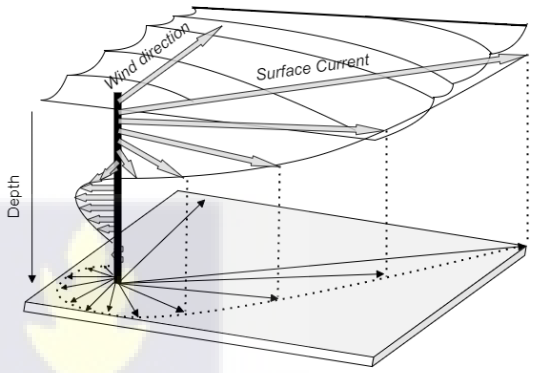

Figure 4.3: Ekman spiral

Ekman layer is a layer near the surface of the ocean where the force of friction is equal to the force of the Earth's rotation (Coriolis force). In this layer, there is movement of water that carries mass.

4.1.1 Ekman Transport

Ekman transport is the movement of the surface layer of water due to winds, causing surface currents at the top layer. By conservation of mass and non-homogeneous wind forcing, water from the bottom rises to fill the water that moved away. To get the net effect of Ekman transport, we integrate the mass transport over depth. Ekman transport is the net movement of fluid on the surface layer of the ocean in a direction 90° to the wind. The component of Ekman transport that results in areas of upwelling due to the divergence of water is called **Ekman suction** and the reverse

case is **Ekman pumping**. We can modify Equation 4.6 and (4.7) to get

$$\rho v = -\frac{1}{f}\frac{\partial \tau_x}{\partial z} \tag{4.21}$$

and

$$\rho u = \frac{1}{f}\frac{\partial \tau_y}{\partial z}. \tag{4.22}$$

From (4.21) and (4.22), the transport in x direction is

$$M_x = \int_{-\infty}^{0} \rho u dz = \frac{\tau_y(0)}{f} \tag{4.23}$$

and the transport in y direction is

$$M_y = \int_{-\infty}^{0} \rho v dz = -\frac{\tau_x(0)}{f}. \tag{4.24}$$

The transport is perpendicular to the wind stress, and to the right of the wind in the northern hemisphere. If the wind is to the north in the positive y direction (a south wind), then $\tau_x(0) = 0$, $M_y = 0$, and $M_x = \tau_y(0)/f$. In the northern hemisphere, $f > 0$ and the mass transport is in the x direction (to the east). The wind pushing against the ocean causes a current to flow in a direction that is perpendicular to the wind. This happens because we assume that friction only happens on a very thin surface.

4.1.2 Ekman Suction and Pumping

The spatial variability of the transport leads to convergence and divergence of vertical velocities in the Ekman layer. Convergence leads to downwelling of water out of the Ekman layer, whiles divergence leads to upwelling into the Ekman layer due to the conservation of mass. To find the vertical velocity W_E at the top of the Ekman layer, we integrate the continuity equation throughout the depth of the Ekman layer, represented by D_E. We assume that the velocity at which water is moving up or

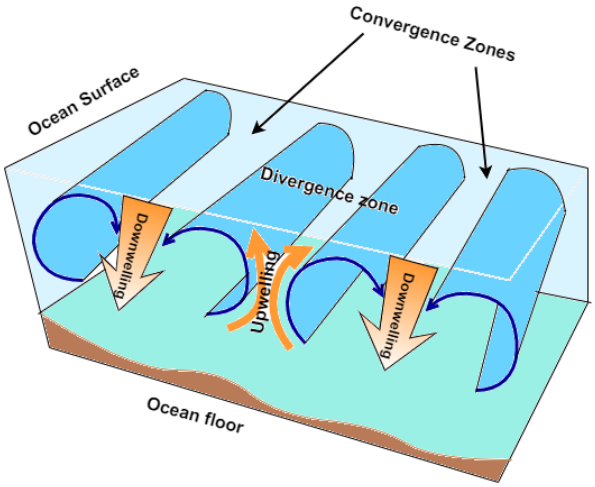

Figure 4.4: Relationship between convergence or divergence and upwelling or downwelling

down at the surface, $W(0)$, is equal to zero.

$$\rho \int_{D_E}^{0} \left(\frac{\partial u}{\partial x} + \frac{\partial v}{\partial y} + \frac{\partial W}{\partial z} \right) dz = 0 \tag{4.25}$$

$$\implies \frac{\partial}{\partial x} \int_{D_E}^{0} \rho u dz + \frac{\partial}{\partial y} \int_{D_E}^{0} \rho v dz = -\rho \int_{D_E}^{0} \frac{\partial W}{\partial z} dz \tag{4.26}$$

$$\implies \frac{\partial M_x}{\partial x} + \frac{\partial M_y}{\partial y} = -\rho[W(0) - W(D_E)] \tag{4.27}$$

$$\implies \frac{1}{\rho} \left[\frac{\partial M_x}{\partial x} + \frac{\partial M_y}{\partial y} \right] = W(D_E) \tag{4.28}$$

The vertical velocity $W_E = W(D_E) = 1/\rho \nabla_H \cdot \vec{M}$, where ∇_H is the horizontal divergence vector and $\vec{M} = \langle M_x, M_y \rangle$ is the vector of Ekman transport. From Equation 4.23 and (4.24), we can write Equation 4.28 as

$$W_E = \frac{1}{\rho} \left[\frac{\partial}{\partial x} \left(\frac{\tau_y}{f} \right) - \frac{\partial}{\partial y} \left(\frac{\tau_x}{f} \right) \right]. \tag{4.29}$$

The relation of the Ekman transport divergence to the wind stress is $W_E = \vec{k} \cdot \nabla \times (\vec{\tau}/\rho f)$, where $\vec{\tau} = \langle \tau_x, \tau_y \rangle$ and $\vec{k}$ is a unit vector in the vertical direction. If the vertical velocity, W_E is negative, it means the transport is converging, leading to downwelling. If the upward velocity at the bottom of the Ekman layer is positive, then the mass transport is diverging, which leads to upwelling, as seen in Figure 4.4. In the northern hemisphere, when there is a positive wind stress curl, it causes water to move upward into the Ekman layer. And when there is a negative wind stress curl, it causes water to move downward. In the southern hemisphere, the opposite happens.

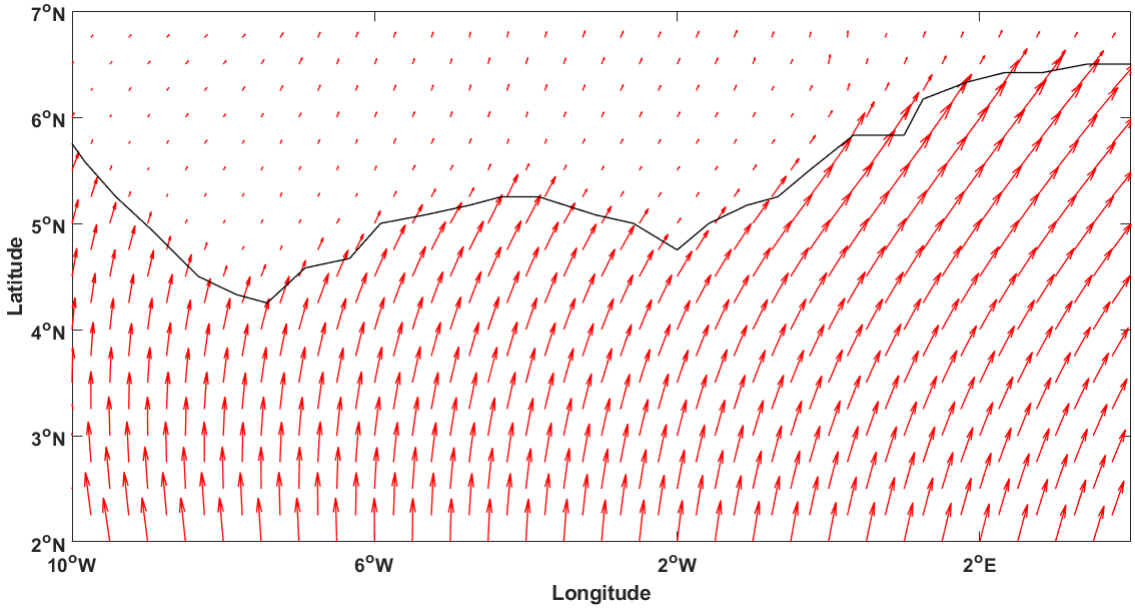

Figure 4.5: The vectors show the mean wind stress (in Nm^{-2}) averaged from 1993 to 2016 in the Gulf of Guinea region.

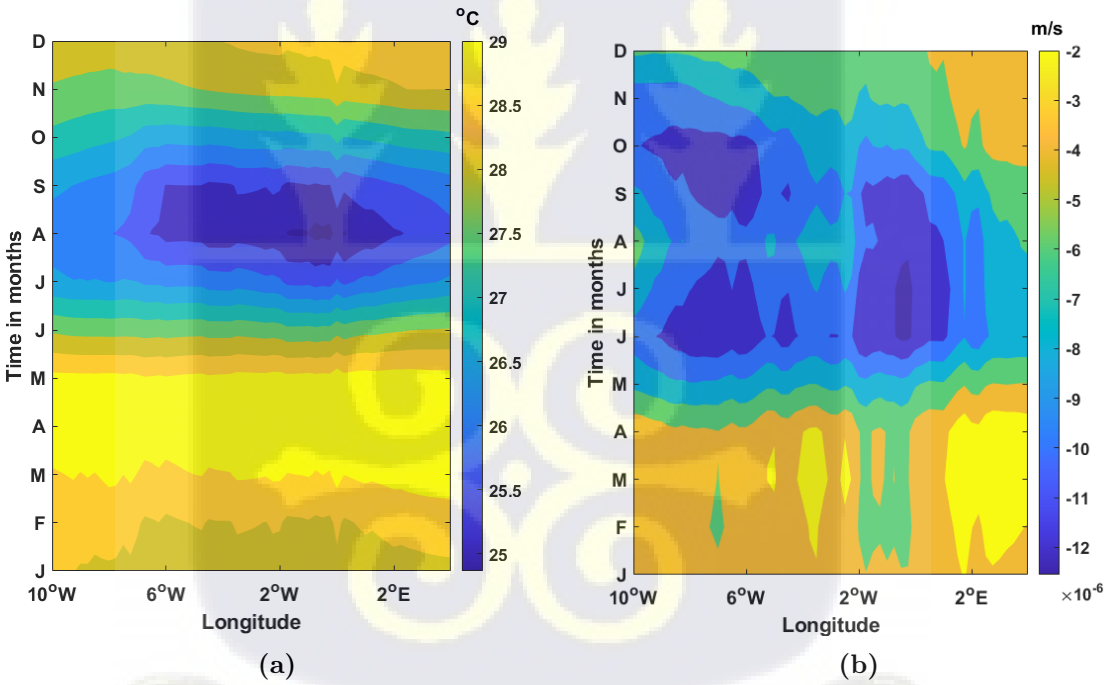

Figure 4.6: Monthly mean SST (in degrees Celsius) (left panel) and Ekman Pump (Vertical Velocity in ms^{-1}) (right panel) averaged from latitude 2°N to 7°N and longitude 10°W to 4°E (1993 to 2016) in the Gulf of Guinea region.

In Figure 4.5, we observe that the wind stress responsible for upwelling is mainly in the northeast direction along the coastline of West Africa bounded by latitude 2°N to 7°N and longitude 10°W to 4°E. The wind in the Gulf of Guinea region does not

favour upwelling in the classical sense. Because in the classical sense, if we wanted to get upwelling due to the local winds, the winds should be blowing to the east, which will generate Ekman transport to the right of the wind (that is, into the ocean), which will cause water to come up along the coast. Studying the contribution of wind stress to upwelling in the Gulf of Guinea, we observe in Figure 4.6a that the SST is relatively colder than the rest of the months from June to September. Using Equation 4.29, we can compute the Ekman vertical velocities to get Figure 4.6b. In Figure 4.6b, the vertical velocities are all negative, indicating that there is downwelling, meaning no upwelling. This is another evidence that if the local winds were causing the upwelling, we would have expected that the vertical velocities in this region would have been positive between June and September, which indicates that water is coming up because of divergence. But now we have negative velocities, which means that the rising of cold water in the Gulf of Guinea is not entirely the result of the winds. However, [12] indicated that upwelling events also take place east of Cape Three Points due to the winds. The upwelling event is not the result of Ekman divergence because the cross-equatorial winds contribute to the intensification of the upwelling and these winds are shown by Figure 4.5.

4.2 Kelvin waves Theory

The Kelvin wave is a kind of wave that is influenced by the Earth's rotation. Sir William Thompson, who later became Lord Kelvin, discovered the Kelvin wave in 1879. Kelvin wave propagates parallel to a fixed boundary such as a coastline or the equator, that is, they are trapped on the coastline or along the equator. They have their highest amplitude at the coast or equator. There are two types of Kelvin waves: **equatorial Kelvin waves** and **coastally-trapped Kelvin waves**. Kelvin waves move only towards the east at the equator and decay exponentially with increasing latitude. They send signals from the equator towards the poles. Kelvin waves are important for understanding how the ocean near the equator responds to changes in the wind; an example is what happens during an El Niño. These waves don't spread out and move at a constant phase speed, $c = \sqrt{g'H}$. Kelvin waves only travel in one direction. The Kelvin wave's existence depends on gravity and stable layers of water, which help to maintain a swinging motion caused by gravity. It also requires a strong Coriolis force and either a coastline or the equator. They spin in the counterclockwise direction in the Northern Hemisphere and clockwise in the Southern Hemisphere, as

discussed in [21].

One hypothesis, from [3], suggests that upwelling along the Gulf of Guinea is probably due to Kelvin waves propagating eastward from the Brazillian coast along the equator. To investigate this hypothesis, they set up a mathematical model from the Navier-Stokes equations and solved them analytically to study the propagation of the Kelvin waves. To understand Kelvin waves, we can look at a signal that moves horizontally in a rotating water column, so that $\frac{\mathrm{D}w}{\mathrm{D}t}$ is negligible and the pressure distribution is hydrostatic. A single layer of fluid over a flat bottom is considered for this model. Also, w is the vertical velocity along the z-direction. The fluid particles move horizontally without being affected by their vertical position.The water column has a thickness, H, which is smaller than the width of the fluid. The displacement of the sea surface is represented by η. We assume that the fluid has the same density throughout and has a surface that is restricted by a vertical boundary. This kind of model is described as a shallow-water problem by [21]. At this point, the Kelvin wave energy travels at the same speed as the shallow water gravity wave. The pressure above the bottom being hydrostatic is

$$P = \rho g(H + \eta - z) \implies \frac{\partial P}{\partial x} = \rho g \frac{\partial \eta}{\partial x} \text{ and } \frac{\partial P}{\partial y} = \rho g \frac{\partial \eta}{\partial y}.$$

Under these conditions we have the **Shallow-water wave equations** modified from Equations (4.1), (4.2), (4.3), and (4.4) of the Navier-Stokes equations:

$$\frac{\partial u}{\partial t} + u\frac{\partial u}{\partial x} + v\frac{\partial u}{\partial y} - fv = -g\frac{\partial \eta}{\partial x} + \nu\left[\frac{\partial^2 u}{\partial x^2} + \frac{\partial^2 u}{\partial y^2}\right] \tag{4.30}$$

$$\frac{\partial v}{\partial t} + u\frac{\partial v}{\partial x} + v\frac{\partial v}{\partial y} + fu = -g\frac{\partial \eta}{\partial y} + \nu\left[\frac{\partial^2 v}{\partial x^2} + \frac{\partial^2 v}{\partial y^2}\right] \tag{4.31}$$

$$\frac{\partial \eta}{\partial t} + \frac{\partial}{\partial x}(H + \eta)u + \frac{\partial}{\partial y}(H + \eta)v = 0. \tag{4.32}$$

The shallow water wave equations are hyperbolic partial differential equations that describe the conservation of mass and momentum in a fluid ([28]). We can further assume that the flow is inviscid ($\nu = 0$) and linear, where the advection terms are dropped. Linearization can be done by considering $\eta << H$. Equation (4.30), (4.31),

and (4.32) reduce to the **Kelvin and inertia-gravity wave equations**

$$\frac{\partial u}{\partial t} - fv = -g\frac{\partial \eta}{\partial x} \tag{4.33}$$

$$\frac{\partial v}{\partial t} + fu = -g\frac{\partial \eta}{\partial y} \tag{4.34}$$

$$\frac{\partial \eta}{\partial t} + H\left[\frac{\partial u}{\partial x} + \frac{\partial v}{\partial y}\right] = 0. \tag{4.35}$$

The Coriolis parameter f is constant and assumes the presence of a wall at $x = 0$ so that the zonal velocity must be zero ($u = 0$) everywhere. These assumptions result in a balance between the forces caused by the earth's rotation and the force exerted by the pressure gradient in the x-direction.

From Equation (4.33), (4.34), and (4.35), the Kelvin wave equations simplify to

$$-fv = -g\frac{\partial \eta}{\partial x} \tag{4.36}$$

$$\frac{\partial v}{\partial t} = -g\frac{\partial \eta}{\partial y} \tag{4.37}$$

$$\frac{\partial \eta}{\partial t} + H\frac{\partial v}{\partial y} = 0. \tag{4.38}$$

Consider a solution of the form

$$\begin{pmatrix} u \\ v \\ \eta \end{pmatrix} = \mathrm{Re}\begin{pmatrix} 0 \\ V \\ A(x) \end{pmatrix} e^{\mathrm{i}(ly - \omega t)} \tag{4.39}$$

Equation (4.37) can be written as

$$v = -\mathrm{i}\frac{g}{\omega}\frac{\partial \eta}{\partial y} \tag{4.40}$$

Put Equation (4.40) into (4.38) to get

$$\frac{\partial^2 \eta}{\partial y^2} + \frac{\omega^2}{gH}\eta = 0 \implies l^2 = \frac{\omega^2}{gH} \iff l = \pm\sqrt{\frac{\omega^2}{gH}}. \tag{4.41}$$

The zonal and meridional momentum equation can be combined by putting (4.40) into (4.36) to get

$$-\mathrm{i}\omega\frac{\partial \eta}{\partial x} + f\frac{\partial \eta}{\partial y} = 0 \implies -\mathrm{i}\omega\frac{dA(x)}{\partial x} + \mathrm{i}lfA = 0. \tag{4.42}$$

Using separation of variables, the solution is $A(x) = A_0 e^{\frac{lf}{\omega}x}$. Thus,

$$\eta(x, y, t) = A_0 e^{\frac{lf}{\omega}x} e^{\mathrm{i}(ly - \omega t)}. \tag{4.43}$$

Deductions:

In the northern hemisphere, $f > 0$ and a wave on $x > 0$ side of the boundary exponentially grow infinitely if $l = \sqrt{\frac{\omega^2}{gH}}$ in equation (4.42). So we take $l < 0$ so that the wave propagates in the negative y - direction as it decays exponentially to the right. Thus, if a system is bounded on $x > 0$ (eastern) in the northern hemisphere, the wave propagates in the positive y - direction (northward) as shown in Figure 4.7. Due to the Coriolis effect, Kelvin waves flow with the shore to their right in the northern hemisphere. In the southern hemisphere, the direction of Kelvin waves changes, and they are deflected with the shore or coast to their left.

On the earth's surface, Coriolis force deflects objects to the right when moving in the eastward direction. The geostrophic balance is the result of the balance between the Coriolis force and the pressure gradient force as shown in Equation (4.36). Note that the pressure gradient force is balanced by hydrostatic pressure. This process leads Kelvin waves to go around anticlockwise in the northern hemisphere.

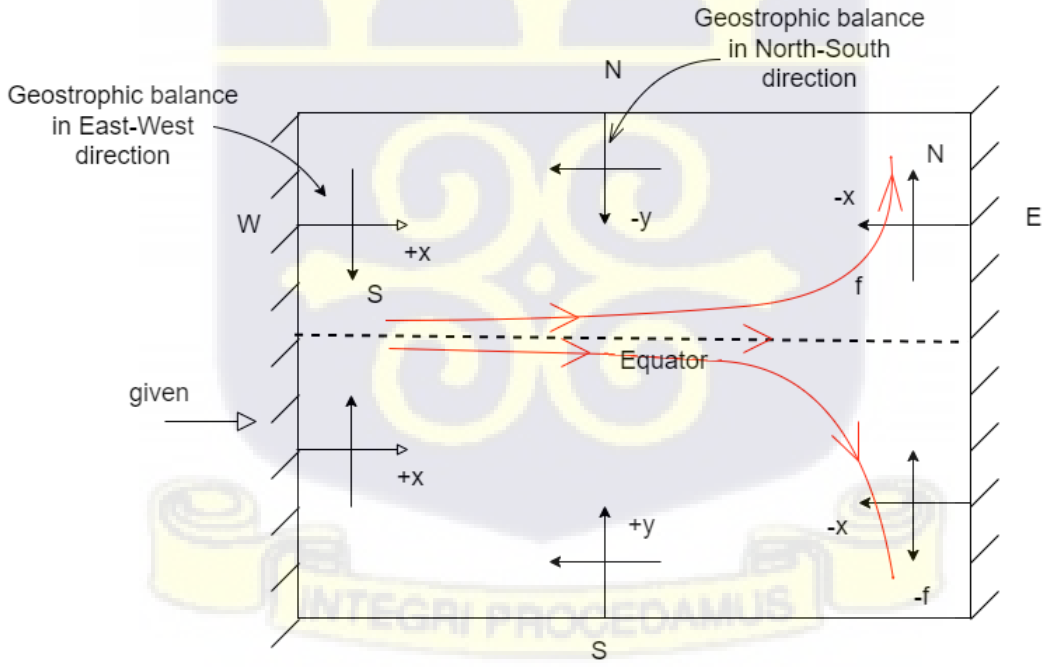

Figure 4.7: Schematic behaviour of the Kelvin waves

In contrast, Kelvin waves in the southern hemisphere move in a clockwise direction, following the path of the red arrow curves as in Figure 4.7. The equator lies between the northern and southern hemispheres, forming a boundary along which the Kelvin waves are triggered, called equatorial Kelvin waves propagating towards the eastern direction.

4.3 Equatorial Kelvin Waves

The theory of equatorial Kelvin waves forms the idea behind EL Niño modelling and prediction. Along the equator, $f = 0$, so we assume an equatorial β-plane approximation such that $f = \beta y$. Recall that the Coriolis force $f = 2\Omega\sin(\phi)$, where ϕ is latitude and $\Omega = 2\pi$ radian per day is the angular rotation of the earth. Consider a signal moving in the meridional direction very close to the equator so that $\phi = \phi_o + y/a$, where y is a point on the signal oriented northward and estimated from an initial position, ϕ_o such that y/a is a small perturbation in the latitude close to the equator and $a = 6371$ km is the radius of the earth. The Coriolis parameter is given by:

$$f = 2\Omega\sin(\phi) = 2\Omega\sin(\phi_o + y/a). \tag{4.44}$$

Using Taylor's expansion gives:

$$\sin(\phi_o + y/a) = \sin(\phi_o) + (y/a)\cos(\phi_o + y/a) + O(y/a)^2. \tag{4.45}$$

Assume y/a is very small, then Equation (4.44) becomes

$$f \approx 2\Omega\sin(\phi_o) + 2\Omega/a\cos(\phi_o)y = f_o + \beta y, \tag{4.46}$$

where $\beta = 2\Omega/a$.
At the equator, $\phi_o = 0$ which implies

$$f \approx \beta y. \tag{4.47}$$

Consider the equator as a wall and seek a solution such that the meridional velocity, $v = 0$ everywhere.

From Equations (4.33), (4.34), (4.35), and (4.47), the equatorial Kelvin wave equa-

tions are given by:

$$\frac{\partial u}{\partial t} = -g\frac{\partial \eta}{\partial x} \tag{4.48}$$

$$\beta y u = -g\frac{\partial \eta}{\partial y} \tag{4.49}$$

$$\frac{\partial \eta}{\partial t} + H\frac{\partial u}{\partial y} = 0 \tag{4.50}$$

Assume a solution of the form $\begin{pmatrix} u \\ v \\ \eta \end{pmatrix} = \text{Re}\begin{pmatrix} U \\ 0 \\ A(y) \end{pmatrix} e^{\mathrm{i}(kx-\omega t)}$.

Equation (4.48) reduces to

$$u = -\mathrm{i}\frac{g}{\omega}\frac{\partial \eta}{\partial x}. \tag{4.51}$$

Put Equation (4.51) into Equation (4.50) to get

$$\frac{\partial^2 \eta}{\partial x^2} + \frac{\omega^2}{gH}\eta = 0 \implies k^2 = \frac{\omega^2}{gH} \iff k = \pm\sqrt{\frac{\omega^2}{gH}}. \tag{4.52}$$

Combine Equation (4.48) and (4.49) to get

$$-\mathrm{i}\beta y\frac{\partial \eta}{\partial x} + \omega\frac{\partial \eta}{\partial y} = 0 \implies \frac{dA(y)}{\partial y} - \frac{\beta k}{\omega}A(y) = 0. \tag{4.53}$$

Using separation of variables, the solution is $A(y) = A_0 e^{-\frac{\beta k}{2\omega}y^2}$ and

$$\eta(x, y, t) = A_0 e^{-\frac{\beta k}{2\omega}y^2} e^{\mathrm{i}(kx-\omega t)}. \tag{4.54}$$

We take $k > 0$, so that the wave propagation is in the eastward direction and decays exponentially with increasing latitude. $\eta(x, y, t) = A_0 e^{-\frac{y^2}{2L_r^2}} e^{\mathrm{i}(kx-\omega t)}$, where $L_r = \sqrt{c/\beta}$ is the equatorial deformation radius and $c = \sqrt{gH}$ is the phase speed. The equatorial deformation radius is a length scale at which the Kelvin waves can be observed which is dependent on latitude.

4.3.1 The effect of Equatorial Kelvin waves at the thermocline level

We derive equations governing Kelvin waves at the interface of two fluid layers following the work of [3]. The mechanism of the Kelvin wave can be illustrated by

considering that $\frac{Dw}{Dt}$ is negligible in the vertical momentum equation so that the pressure distribution is hydrostatic. The fluid particles execute a horizontal motion independent of z. In a double layer, the linear inviscid flow of the fluid over a flat bottom is considered. Let η be the displacement or perturbation of the sea surface, and H be the resting water column thickness. Assume the fluid is homo-

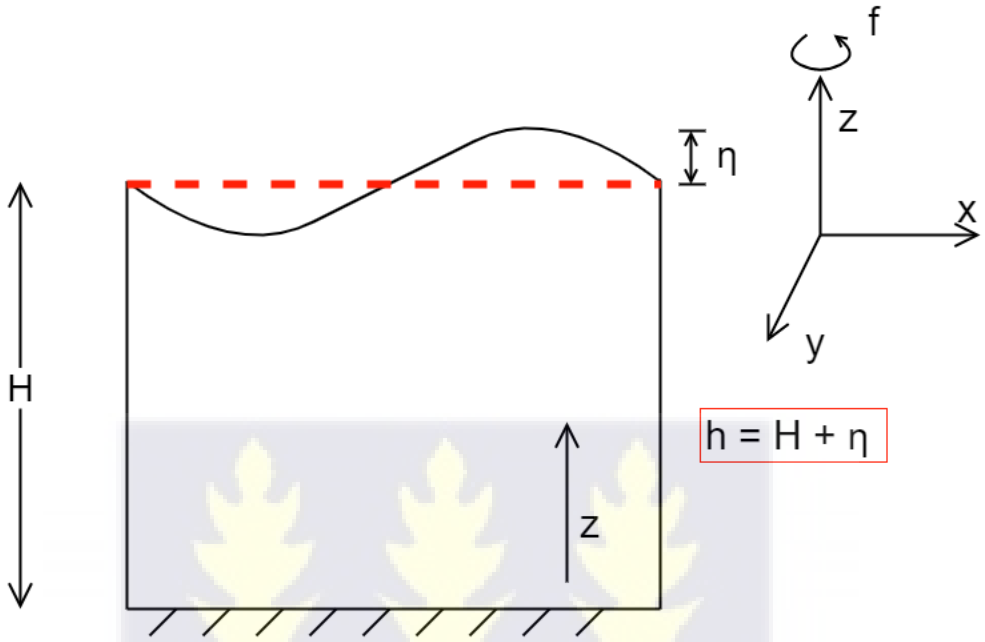

Figure 4.8: Schematic illustration of the Kelvin wave

geneous (constant density). The pressure above the bottom being hydrostatic is $P = \rho g(H + \eta - z) \implies \frac{\partial P}{\partial x} = \rho g \frac{\partial \eta}{\partial x}$ and $\frac{\partial P}{\partial y} = \rho g \frac{\partial \eta}{\partial y}$. Since the horizontal pressure gradient is proportional to the sea surface slope (hydrostatic pressure), we integrate the continuity equation for a flat bottom ocean. The fact that $\frac{\partial u}{\partial z} = \frac{\partial v}{\partial z} = 0$ in a barotropic fluid (constant density), it is possible to write a vertically integrated form of the continuity equation with the total water column, $h = H + \eta$ as seen in Figure 4.8. That is,

$$\int_0^h \left(\frac{\partial u}{\partial x} + \frac{\partial v}{\partial y} + \frac{\partial w}{\partial z}\right) dz = \left(\frac{\partial u}{\partial x} + \frac{\partial v}{\partial y}\right) z\Big|_0^h + \int_0^h \partial w \tag{4.55}$$

$$= \left(\frac{\partial u}{\partial x} + \frac{\partial v}{\partial y}\right)(h) + w(h) - w(0) = 0 \tag{4.56}$$

For simplicity, assume the bottom is flat and that there is no vertical velocity at the

bottom, that is, $w(0) = 0$. This implies that

$$\left(\frac{\partial u}{\partial x} + \frac{\partial v}{\partial y}\right)(h) + w(h) = 0 \tag{4.57}$$

Also the vertical velocity at the surface is equal to the rate of change of the free surface, that is,

$$w(h) = \frac{\partial h}{\partial t} + u\frac{\partial h}{\partial x} + v\frac{\partial h}{\partial y}. \tag{4.58}$$

From Equation (4.57) and (4.58), we get

$$\left(\frac{\partial u}{\partial x} + \frac{\partial v}{\partial y}\right) h + \frac{\partial h}{\partial t} + u\frac{\partial h}{\partial x} + v\frac{\partial h}{\partial y} = 0. \tag{4.59}$$

Since $\dfrac{\partial u}{\partial x} + \dfrac{\partial v}{\partial y} = 0$ for an incompressible fluid, equation (4.59) reduces

$$\frac{\partial h}{\partial t} + \frac{\partial (hu)}{\partial x} + \frac{\partial (hv)}{\partial y} = 0 \tag{4.60}$$

$$\implies \frac{\partial}{\partial t}(H+\eta) + \frac{\partial}{\partial x}(H+\eta)u + \frac{\partial}{\partial y}(H+\eta)v = 0. \tag{4.61}$$

Under these conditions we have the Shallow-water wave equations given by:

$$\frac{\partial u}{\partial t} + u\frac{\partial u}{\partial x} + v\frac{\partial u}{\partial y} - fv = -g\frac{\partial \eta}{\partial x} + \nu\left[\frac{\partial^2 u}{\partial x^2} + \frac{\partial^2 u}{\partial y^2}\right] \tag{4.62}$$

$$\frac{\partial v}{\partial t} + u\frac{\partial v}{\partial x} + v\frac{\partial v}{\partial y} + fu = -g\frac{\partial \eta}{\partial y} + \nu\left[\frac{\partial^2 v}{\partial x^2} + \frac{\partial^2 v}{\partial y^2}\right] \tag{4.63}$$

$$\frac{\partial \eta}{\partial t} + \frac{\partial}{\partial x}(H+\eta)u + \frac{\partial}{\partial y}(H+\eta)v = 0, \text{ where } \nu = \mu/\rho. \tag{4.64}$$

Assume the flow is linear so that advection terms are dropped. Along the equator, $f = 0$, so we assume a baroclinic mode of an equatorial β-plane approximation such that $f = \beta y$. The equatorial Kelvin wave equations for a 2-layer flow as seen in Figure 4.9 with an increase in westward wind stress integrated over the tropical

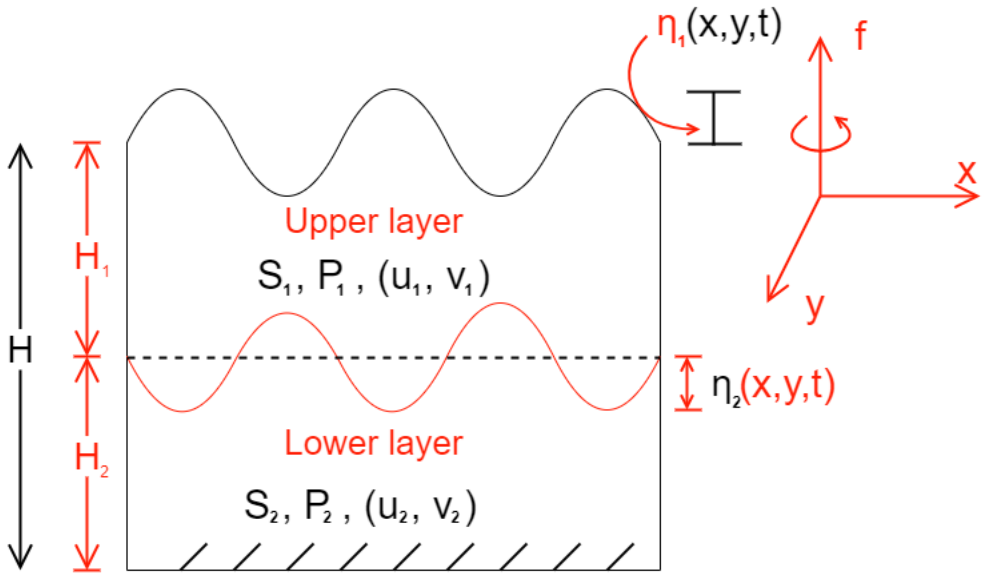

Figure 4.9: Sketch of the 2-layer flow

Atlantic ocean are given by:

$$\frac{\partial u_1}{\partial t} - \beta y v_1 + P_{1x}/\rho_1 = \tau_x/\rho_1 H_1 \tag{4.65}$$

$$\frac{\partial v_1}{\partial t} + \beta y u_1 + P_{1y}/\rho_1 = \tau_y/\rho_1 H_1 \tag{4.66}$$

$$\frac{\partial \eta_1}{\partial t} + H_1\left(\frac{\partial u_1}{\partial x} + \frac{\partial v_1}{\partial y}\right) = 0 \tag{4.67}$$

for the upper or first layer and

$$\frac{\partial u_2}{\partial t} - \beta y v_2 + P_{2x}/\rho_2 = 0 \tag{4.68}$$

$$\frac{\partial v_2}{\partial t} + \beta y u_2 + P_{2y}/\rho_2 = 0 \tag{4.69}$$

$$\frac{\partial \eta_2}{\partial t} + H_2\left(\frac{\partial u_2}{\partial x} + \frac{\partial v_2}{\partial y}\right) = 0 \tag{4.70}$$

for the lower layer.

ρ_1, ρ_2, ρ is the density of sea water, P_1, P_2, P is the local pressure, t is the time, H, H_1, H_2 is the undisturbed thickness of the layers, u_1, u_2, u is the x-directed component of the velocity, v_1, v_2, v is the y-directed component of the velocity, and τ_x, τ_y is the x, y-directional wind stress on the surface of the ocean.Recall hydrostatic pressure is the pressure exerted by a fluid at equilibrium at a given point within the fluid due to the force of gravity. If the fluid is hydrostatic and the lower layer is assumed to

adjust so that $P_{2x} = P_{2y} = 0$. The system reduces to

$$\frac{\partial u}{\partial t} - \beta y v + g'\eta_x = \tau_x/\rho H \tag{4.71}$$

$$\frac{\partial v}{\partial t} + \beta y u + g'\eta_y = \tau_y/\rho H \tag{4.72}$$

$$\frac{\partial \eta}{\partial t} + H\left(\frac{\partial u}{\partial x} + \frac{\partial v}{\partial y}\right) = 0, \tag{4.73}$$

where $g' = \left(\frac{\rho_2 - \rho_1}{\rho_2}\right)g$ is the reduced gravity, u is the average velocity of u_1 and u_2, v is the average velocity of v_1 and v_2, and η is the average perturbation from η_1 and η_2. The Equations (4.71), (4.72), and (4.73) are free modal responses which are referred to as the reduced gravity formulation used by [23] to effectively simulate many of the features of the Somali current. Another free modal response is the flow on a β-plane when the value of the meridional velocity, $v = 0$. This further reduces the system to

$$\frac{\partial u}{\partial t} + g'\eta_x = \tau_x/\rho H \tag{4.74}$$

$$\beta y u + g'\eta_y = \tau_y/\rho H \tag{4.75}$$

$$\frac{\partial \eta}{\partial t} + H\frac{\partial u}{\partial x} = 0. \tag{4.76}$$

To solve Equation (4.74), (4.75), and (4.76), we assume a wave solution of form $\begin{pmatrix} u \\ v \\ \eta \end{pmatrix} = \mathrm{Re}\begin{pmatrix} U \\ 0 \\ A(y) \end{pmatrix} e^{\mathrm{i}(kx-\omega t)}$. $\frac{\partial \star}{\partial t} = -\mathrm{i}\omega\star$ and Equation (4.74) reduces to

$$u = \frac{\mathrm{i}}{\omega}\left(-g'\frac{\partial \eta}{\partial x} + \tau_x/\rho H\right). \tag{4.77}$$

Put Equation (4.77) into Equation (4.76) to get

$$\frac{\partial^2 \eta}{\partial x^2} + \frac{\omega^2}{g'H}\eta = 0 \implies k^2 = \frac{\omega^2}{g'H} \iff k = \pm\sqrt{\frac{\omega^2}{g'H}}. \tag{4.78}$$

Combine Equation (4.74) and (4.75) to get

$$\frac{dA(y)}{\partial y} + \frac{\beta k y}{\omega} A(y) = \left(-\mathrm{i}\frac{\beta y}{\omega g'} \tau_x/\rho H + \frac{1}{g'} \tau_y/\rho H \right) e^{-\mathrm{i}(kx-\omega t)}. \tag{4.79}$$

Assume there is no wind stress in the meridional (y-direction), that is, $\tau_y = 0$, the solution becomes

$$A(y) = \frac{a\omega}{\beta k} + \left(A_0 - \frac{a\omega}{\beta k} \right) e^{-\frac{\beta k}{2\omega} y^2}, \tag{4.80}$$

where $a = -\mathrm{i}\dfrac{\beta}{\omega g'} \tau_x/\rho H \, e^{-\mathrm{i}(kx-\omega t)}$.

The displacement of the ocean surface is

$$\eta(x, y, t) = \left[\frac{a\omega}{\beta k} + \left(A_0 - \frac{a\omega}{\beta k} \right) e^{-\frac{\beta k}{2\omega} y^2} \right] e^{\mathrm{i}(kx-\omega t)} \tag{4.81}$$

$$= \left[\frac{a\omega}{\beta k} + \left(A_0 - \frac{a\omega}{\beta k} \right) e^{-\frac{y^2}{2L_r^2}} \right] e^{\mathrm{i}(kx-\omega t)}, \tag{4.82}$$

where $L_r = \sqrt{c/\beta}$ is the equatorial deformation radius, $k = \pm\sqrt{\dfrac{\omega^2}{g'H}}$ is the wave number in the x-direction, and $c = \sqrt{g'H}$ is the phase speed. We take $k > 0$, so that the wave propagation is in the eastward direction. The wave reaches its maximum magnitude at the equator and decays exponentially with increasing latitude.

[3] concluded that increasing westward wind stress along the equatorial Atlantic ocean causes the accumulation of surface water to pile up along the Brazilian coast. This initiates a zonal pressure gradient balanced by the wind stress. The Kelvin waves propagate eastward at a speed of $c = \sqrt{g'H}$. The Kelvin waves split at the eastern boundary, with waves going poleward along the coast in both the northern and southern hemispheres. This hypothesis is supported by [14], [2], and [7].

As mentioned in the introduction, the main goal of this thesis is to test the hypothesis of [3] concerning the Kelvin wave theory of upwelling in the Gulf of Guinea. In the rest of the chapters, we present the analysis of results from observations and output from a state-of-the-art realistic ocean model. [14] indicated that the explanation given for the annual upwelling in the Gulf of Guinea is similar to the theories of El Niño in the Pacific ocean. Trade winds push warm surface water from east to west during normal conditions in the central tropical Pacific. By conservation of mass, cold water from the bottom upwells to the surface. The warm water on the western side rises to form clouds through convection, resulting in rainfall. When the westward trade

winds weaken, less surface warm water is pushed from east to west. As the warm water in the western part slows down, it starts to move towards the east as a wave towards the middle of the ocean. As the situation worsens, a pool of warm water forms near Peru's coast, causing a phenomenon known as El Niño.

Chapter 5

Upwelling in the Gulf of Guinea

The Prediction and Research Moored Array in the Atlantic (PIRATA) is a system designed to study the interactions between the ocean and atmosphere in the tropical Atlantic region, which affect the regional climate variability on seasonal, interannual and longer time scales. Instrumented moorings are deployed in depths up to 6000 meters. However, measurements from the instrument include surface variables like temperature down to a depth of 500 meters, as discussed in [71]. The data collected

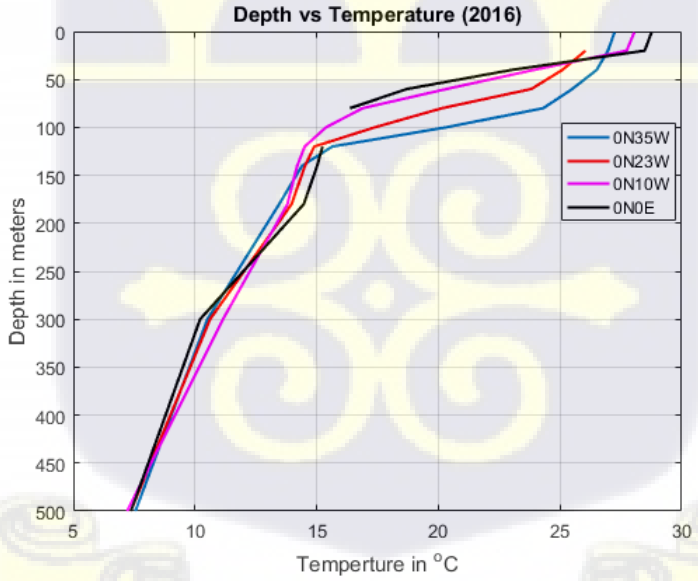

Figure 5.1: Vertical Structure of Temperature

by the Pirata array will help in understanding the oceanic and climate events in the tropical Atlantic region. The question of when upwelling events occur in the western tropical Atlantic before propagating eastward to the west coast of Africa (Gulf of

Guinea) has not been utilised thoroughly in past research. With the help of the tropical Atlantic observing system (TAOS), in particular, the Pirata data, issues of coastal upwelling with large-scale atmospheric forcing and oceanic wave responses can fully be analysed. Consider four points along the equator at the tropical Atlantic region in the year 2016 from the Pirata data. The four locations are (0°N 35°W), (0°N 23°W), (0°N 10°W), and (0°N 10°E). From Figure 5.1, the ocean temperature

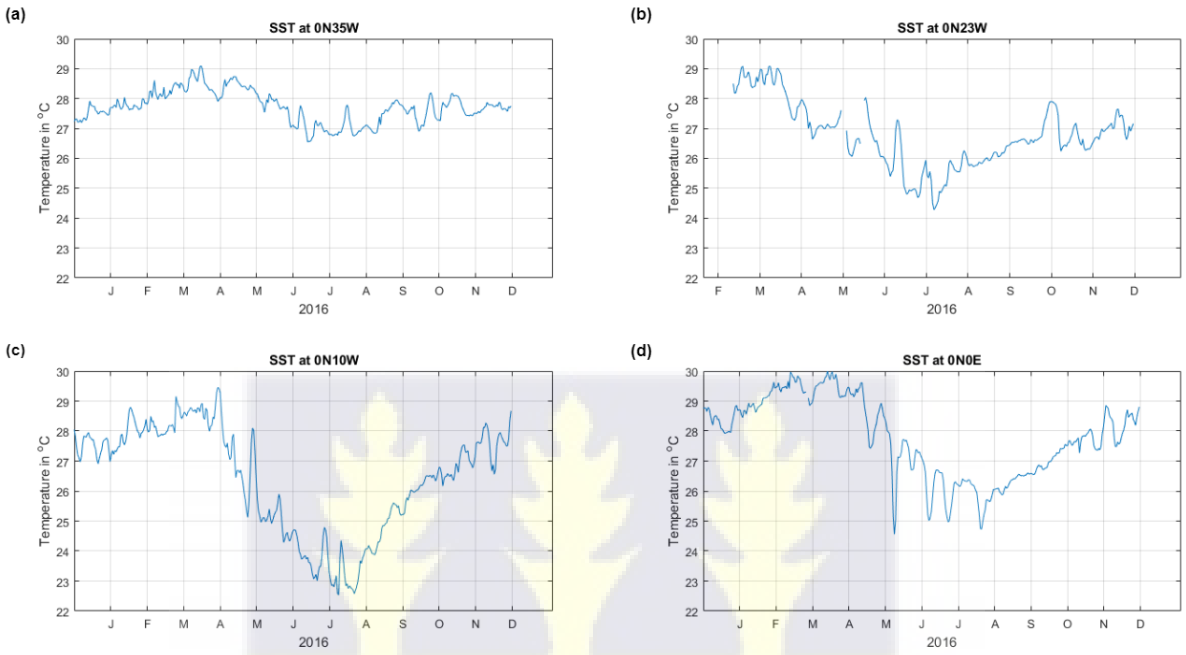

Figure 5.2: SST at different location

range from about 7°C to 30°C. It can be observed from Figure 5.1 that the surface ocean is warm, with the deeper part of the ocean being cold. The ocean's surface is generally warm as the sun's rays warm it, and below a depth of about 250 meters, the sun's rays are ineffective in the deep part of the ocean. Since warm water is less dense than cold water, surface water that is warmer remains at the surface.

At the equator or latitude 0°, on average, the water on the eastern part of the ocean is cooler than the water on the western part of the ocean as observed in the pattern from (0°N 35°W) to (0°N 10°E) in Figure 5.2. In May, June, July, August, and September, the temperature is generally low as it coincides with the upwelling season in the Gulf of Guinea. However, this observation does not reveal what causes upwelling in the Gulf of Guinea, but it helps in understanding the cold seasonal behaviours along the equator.

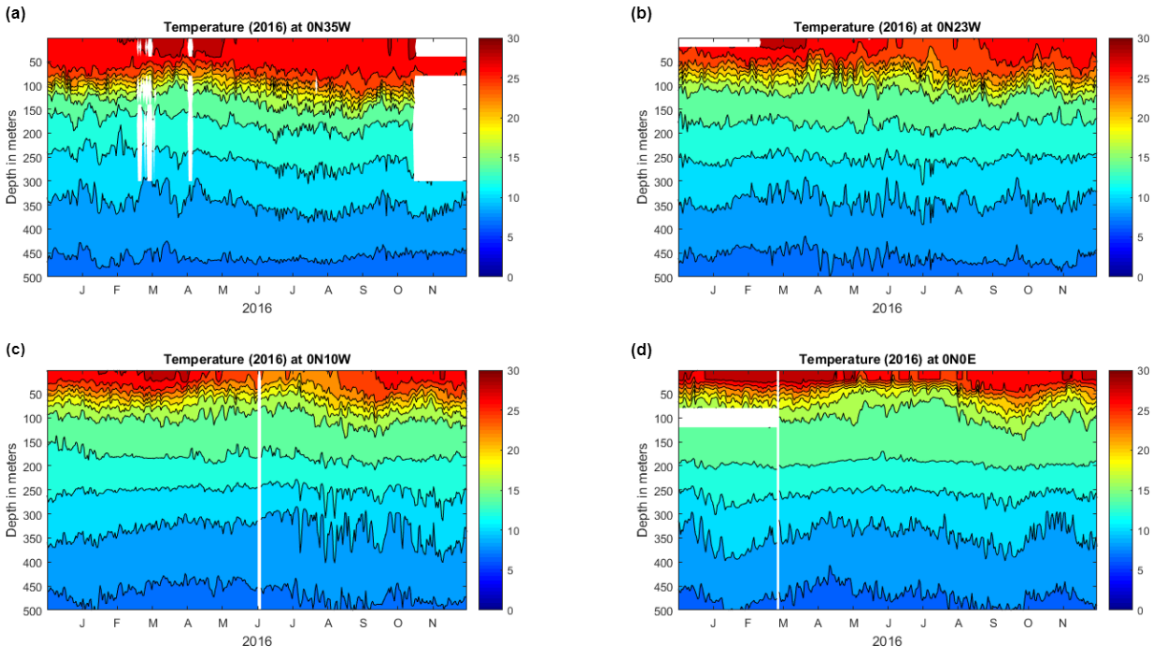

Figure 5.3: Temperature as a function of depth and time from observed data along the equator.

Figure 5.3 shows typical temperature profiles of the ocean from the PIRATA data in which temperature is a function of depth and time. The white spaces are missing data. The temperature remains unchanged in the upper 50 meters region, termed the mixed layer ([36]). The mixed layer occurs due to the interactions between the surface winds, waves, and surface currents that mix the upper ocean to generate heat distribution throughout the mixed layer. Between 50 to 100 meters region below the mixed layer is the thermocline, where there is a rapid decline in temperature. Below 100 meters, the temperature of the deep ocean is slightly constant at about 2 °C, which continues down to the bottom of the ocean. Below 250 meters, there is little temperature change as the sun's heat source is removed, making it one of the most thermally stable regions.

The warm climate found near the equator and in the Gulf of Guinea is causing an increase in the size of the thermocline, which is responsible for causing coastal upwelling ([2]; [3]).

Consider the monthly averages of sea surface temperature (SST) from west of (0°N 35°W) to the east of (0°N 10°E) from observations in Figure 5.4a. It is clear that June, July, August, and September are associated with low SST. [22] used daily times series of NOAA Optimally Interpolated SST and ERA5 reanalysis wind products to

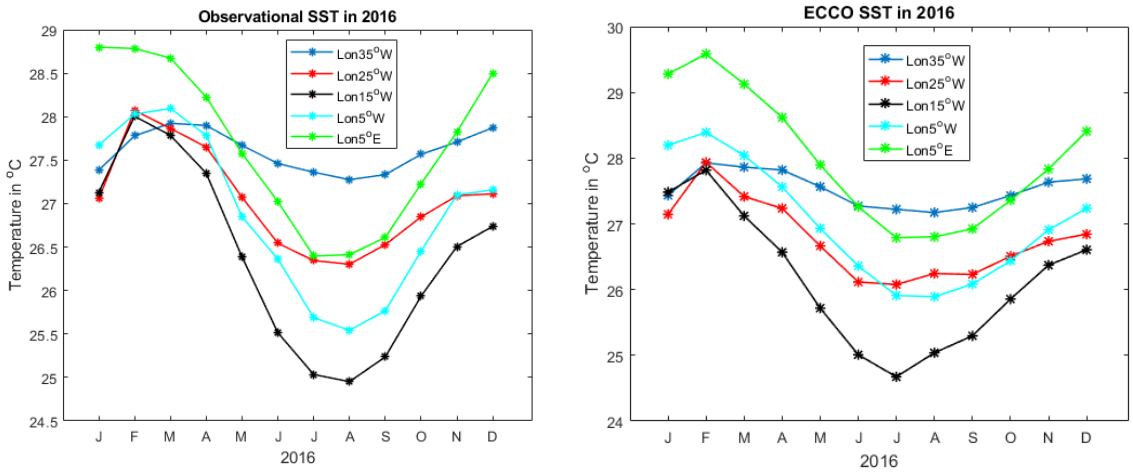

(a) **(b)**

Figure 5.4: Temperature distribution in 2016 from observation and model data

describe upwelling signals in the four Eastern Boundary Upwelling Systems. Their results indicated that a decrease in SST was associated with an increased number of upwelling events. However, low SST alone does not give enough evidence of what causes upwelling in general. Here, we want to test the hypothesis that there is a propagation of Kelvin waves from west of (0°N 35°W) to east of (0°N 10°E) which causes upwelling. From ECCO output model data in Figure 5.4b, there is low SST from June, July, August, and September, but the temperature distributions compared to observations are not similar for the year 2016. There are some years, as discussed in chapter 7 in which the observation from the satellite and the model output from ECCO show similar characteristics.

Consider the monthly averages of sea surface height (SSH) from west of (0°N 35°W) to the east of (0°N 10°E) from observation in Figure 5.5a and ECCO output model data in Figure 5.5b. Note that the vertical scales on the two plots are different, with the model having larger SSH, in general, than the observations. These two figures show a general linear increase in SSH between June and September. There is no clear connection between SSH and upwelling events along the equator. However, [7] indicates the remote forcing effect of Kelvin waves extracted from SSH with 25 to 95 days bandpass was evident over the coastal upwelling regions.

From the plots, it is clear that using one year, for example, the year 2016, to explain upwelling events in the Gulf of Guinea is not enough; instead, a more extended time series would help us explore and understand the cause of the Gulf of Guinea's upwelling. Another way of exploring upwelling events in the Gulf of Guinea is to

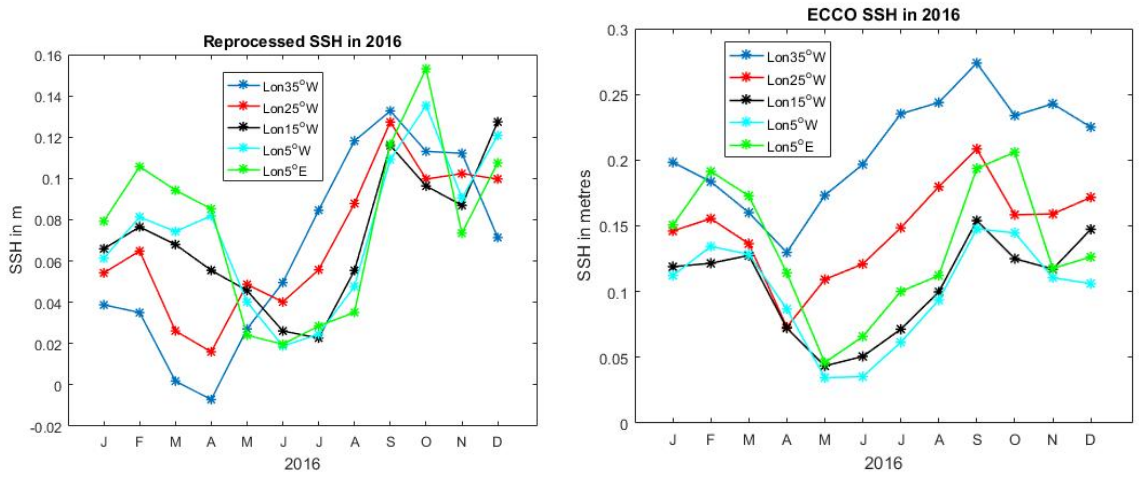

(a) **(b)**

Figure 5.5: SSH in 2016 from observation and model data

determine the most significant upwelling events by computing interannual anomalies, say, from 1993 to 2016.

An interannual anomaly is the process whereby the monthly mean (also known as monthly climatology) is subtracted from the data for that month. It is imperative to use average values distributed globally to obtain a climatology. The mean values can be constructed daily, monthly or seasonally, which can be referred to as daily, monthly or seasonal climatologies. Monthly climatology is the mean of that month. So, for example, January climatology is the mean of all the Januarys in your record. For instance, finding the anomaly for January 1999 will be

$$\text{January 1999 SST anomaly} = \text{January 1999 SST} - \text{January SST climatology}.$$

One way to classify significant events in the Gulf of Guinea is to use standard deviations (STD). Since upwelling is manifested in low SST, here, the lower SSTs are the coldest relative to their monthly means (that is, climatologies).

Now consider the most significant upwelling events from satellite observations, ECCO 1-degree and ECCO 1/3-degree simulations. The version of the ECCO product used was ECCO LLC270 (1/3-degree) which was interpolated to a 1/4-degree latitude-longitude (lat–lon) grids, and the ECCO product ECCO LLC90 (1-degree) interpolated to a 1-degree latitude-longitude (lat–lon) grids.

Figure 5.6, shows that the SST anomalies from 1993 to 2016 for Lat 3°N – 7°N and Lon 10°W – 4°E for the observed SST anomalies, ECCO SST 1-degree, and ECCO

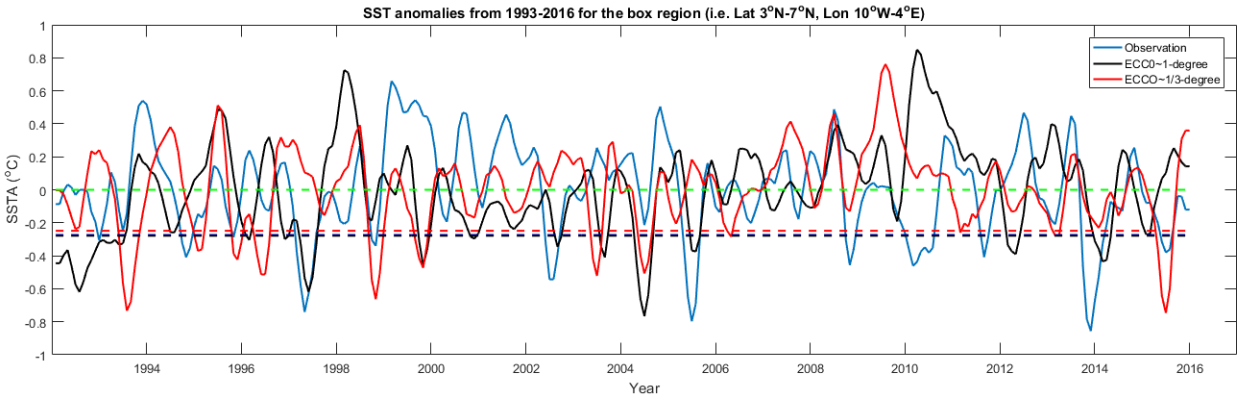

Figure 5.6: SST anomalies from 1993 to 2016

SST 1/3-degree anomalies. The short green dashes indicate the approximate average for observed SST anomalies, ECCO SST 1-degree anomalies, and ECCO SST 1/3-degree anomalies, whiles the red and black short dashes indicate their standard deviations from the means. Thus, the sea surface temperature anomalies (SSTA) for the observation greater than the standard deviation (STD) are thus considered significant upwelling years regarding the drop in SST and are considered the biggest upwelling years. These are 1997, 2005, 2006, and 2016. Also, the sea surface tem-

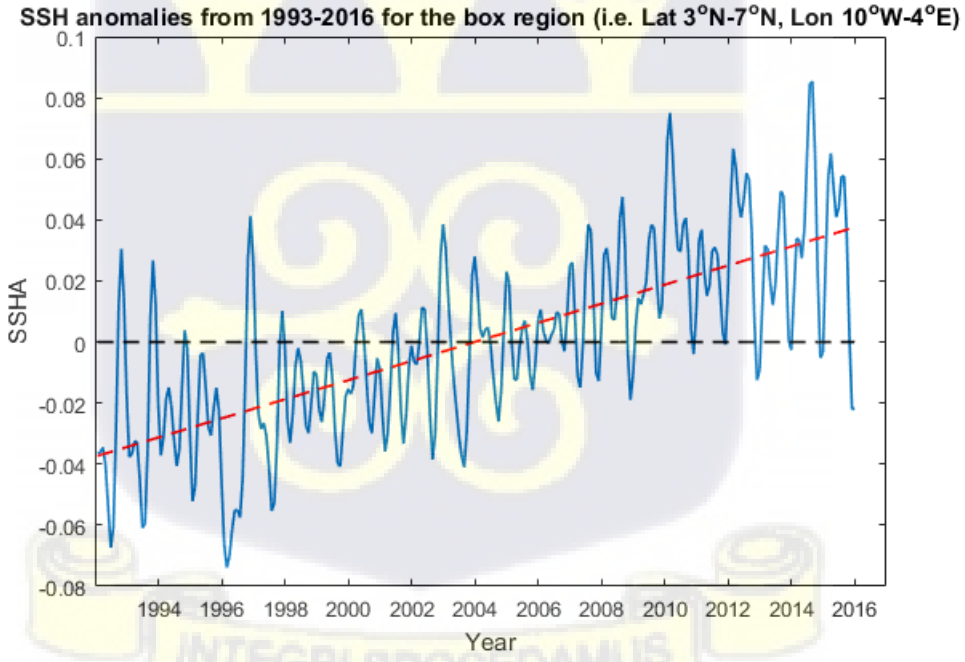

Figure 5.7: SSH anomalies from 1993 to 2016 in centimeters.

perature anomalies (SSTA) for the ECCO 1 - degree model greater than STD are thus considered upwelling years regarding the drop in SST. These upwelling years are

1993, 1997, 2005, and 2006. Similarly, the sea surface temperature anomalies (SSTA) for the ECCO 1/3-degree model greater than STD are 1994, 1997, 2004, 2005, 2006, and 2016. In 1998, 2003, and 2006 of the "bigger" upwelling years, the ECCO 1-degree model matched with observation, whiles in 2016, the ECCO 1/3-degree model matched with the observation. However, the model did not match the observation from 1995, 2008, 2011, and 2012.

In Figure 5.7, we observe sea level rise from satellite data. Here, the SSH anomalies from the observations is also computed from the year 1993 to 2016 for Lat 3°N – 7°N and Lon 10°W – 4°E. Though the average of the sea surface height anomaly (SSHA) is around zero, the SSHA is increasing. We can use this to predict the sea level rise by estimating the line of best fit. Consider the points $(1993, -0.038)$ and $(2016, 0.0389)$ from Figure 5.7. The line of best fit can be computed as

$$\mathbf{SSHA} = 0.0033043 \times \mathbf{Year} - 6.623565, \tag{5.1}$$

using a simple linear regression approach. Equation (5.1), shows that the SSH is rising by 3.3 mm per year and this is consistent with [72].

Chapter 6

Equatorial Kelvin Waves Signatures from Observations and Model Data

6.1 Introduction

It is not easy to identify waves on the sea surface as sinusoids. The ocean surface is a combination of random signals or waves of different wavelengths and periods. It is not straightforward to describe the waves. One can describe the ocean's surface by using the idea of wave energy distribution among various wave frequencies and wavelengths. These waves, in general, can be characterized by their period, wavelength, speed, and amplitude.

Recall that upwelling in the Gulf of Guinea is different from the classical theoretical wind versus the direction of transport. One hypothesis from papers like [14], [2], [3] and [4] suggests upwelling along the Gulf of Guinea is probably due to Kelvin waves propagating eastward from the Brazilian coast along the equator. Thus, there is a need to extract Kelvin waves from observational sea surface height (SSH) or sea level anomaly (SLA) in testing this hypothesis. Once the Kelvin waves have been extracted, the next step is to determine how to characterize them. We will determine Kelvin waves' phase speeds, wavelengths, and spatial structure and possibly link them to upwelling.

6.2 Filtering signal from Synthetic signal

To extract the Kelvin waves from observational ocean data, a synthetic signal was first created from the modified Kelvin waves solution obtained from Equation (4.81) and (4.82) of Chapter 4, given by

$$\begin{aligned}\eta(x,y,t(i)) &= \left[\frac{a\omega}{\beta k}+\left(A_0-\frac{a\omega}{\beta k}\right)e^{-\frac{\beta k}{2\omega}y^2}\right]e^{\mathrm{i}(kx-\omega t(i))}\\ &= \left[\frac{a\omega}{\beta k}+\left(A_0-\frac{a\omega}{\beta k}\right)e^{-\frac{y^2}{2L_r^2}}\right]e^{\mathrm{i}(kx-\omega t(i))},\end{aligned}$$

where $L_r = \sqrt{c/\beta}$ is the equatorial deformation radius and $c = \sqrt{g'H}$ is the phase speed. We take $k > 0$, where k is the wavenumber in the x-direction so that the wave propagation is in the eastward direction. Knowledge of Fourier analysis is needed to understand the extraction of the wanted signal. Some theoretical background on Fourier analysis is available in the Section A.1.

The synthetic signals contain different signals whose periods are 5, 10, 20, and 40 days with their frequencies ω given by $\frac{2\pi}{5}$, $\frac{2\pi}{10}$, $\frac{2\pi}{20}$, and $\frac{2\pi}{40}$ respectively. The amplitude is given as $A = 1$, $L = 25/11$. The displacement of the Kelvin waves is given by

$$\begin{aligned}E(:,:,i) = A\exp(-0.5(Y+8)^2/L^2)\cos(kX-\omega(1)t(i))+\\ A\exp(-0.5(Y+16)^2/L^2)\cos(kX+\omega(2)t(i))+\\ A\exp(-0.5Y^2/L^2)\cos(kX-\omega(3)t(i))+\\ A\exp(-0.5(Y-8)^2/L^2)\cos(kX+\omega(4)t(i)),\end{aligned}$$

where $i = 1, 2, \cdots, 365$. The 3-dimensional surface contains the longitude in the x-direction, latitude in the y-direction, and the displacement of the Kelvin waves sampled daily for 365 days. The longitude ranges from -40 degrees from the west to 10 degrees in the east. The latitude ranges from -20 degrees from the south to 20 degrees north. The longitude and latitude spatial coordinates are chosen to depict the eastern Atlantic region containing the Gulf of Guinea. The latitude and longitude coordinates create a 2-dimensional mesh grid with 100 points. For all the latitude and longitude coordinates given, the displacement of Kelvin waves $E(:,:,i)$ can be computed daily for 365 days.

In the first subplot of Figure 6.1, all the signals are shown and are composed of

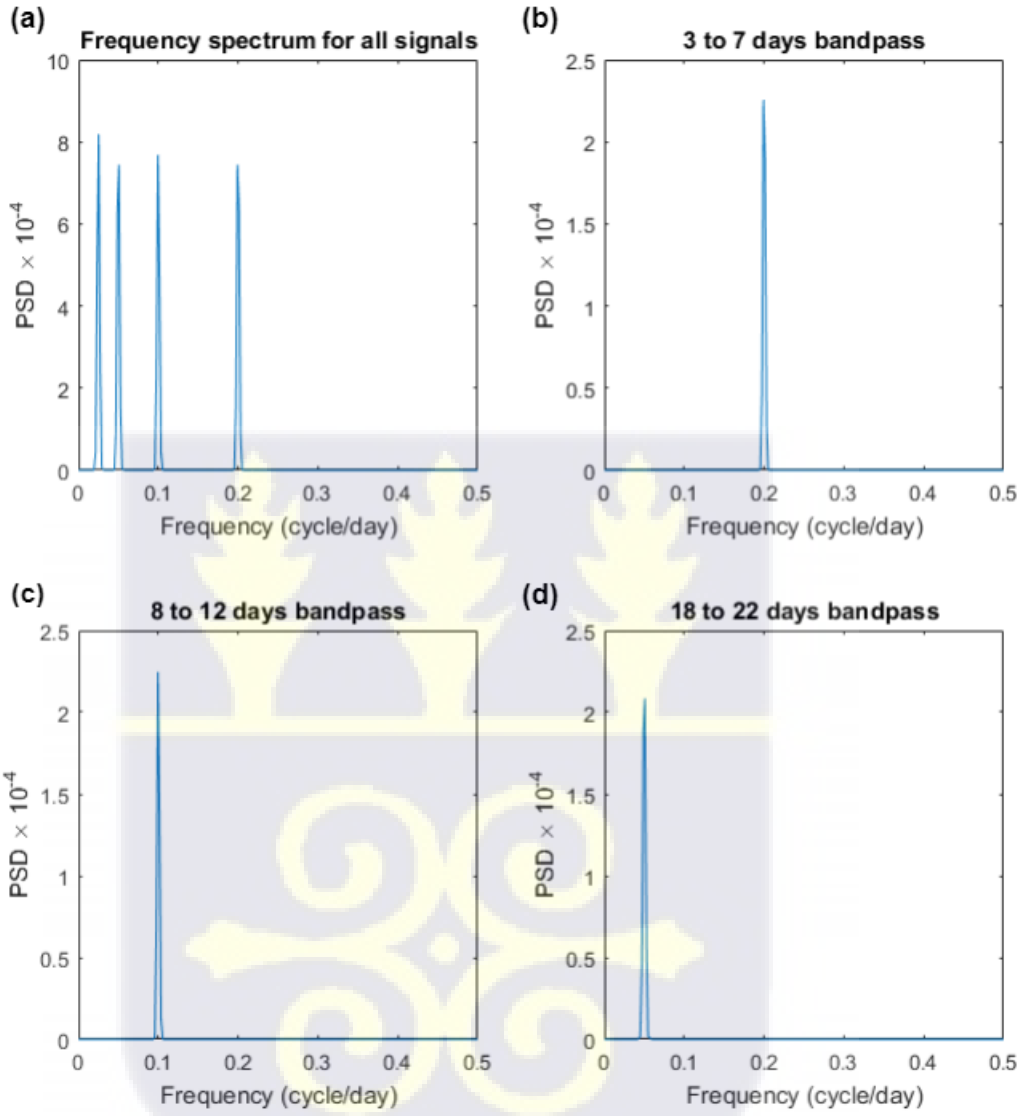

Figure 6.1: Bandbass filtering at different frequencies

the various frequencies in cycles per day and power spectral density (PSD). Detail reading of the bandpass filtering is found in the appendix Section A.2. With spectral analysis, the waves are decomposed to extract their different frequencies by setting the bandpass. The bandpass filter sets a bandwidth, allowing specified frequencies to pass as observed in the second, third, and fourth subplots of Figure 6.1. Recall the various frequencies of the signals have approximately the same energies since the amplitude was set the same for all frequencies.

6.2.1 25 to 95 days filtering from SSH along the equator

The idea built on filtering data by extracting the time series frequency was applied to 24 years of data from 1993 to 2016 of the sea surface height (SSH) along the equator. The seasonal upwelling in the West Africa subregion, according to the literature, is caused by Kelvin waves travelling eastward along the equator. We first set a bandpass between 25 and 95 days to extract Kelvin waves in the ocean. However, as shown in Figure 6.2, it is not easy to observe the Kelvin waves.

In the middle subplot (Figure 6.2b), the 25 to 95 days bandpass filter removes the linear trend, mean, and the seasonal cycle that is the dominant variability. Nevertheless, the filter does not show the Kelvin waves as the filtered data shows other unknown signals like the dominant tropical instability waves (see the Hovmöller diagram in Figure 6.3). The Hovmöller diagram of Figure 6.3 is a function of time and longitude. The Figure shows other signals instead of the Kelvin waves. These signals may be dominated by tropical instability waves and other non-propagating waves, indicating that the Kelvin waves signals haven't been filtered or captured using the 25 to 95 days bandpass filter.

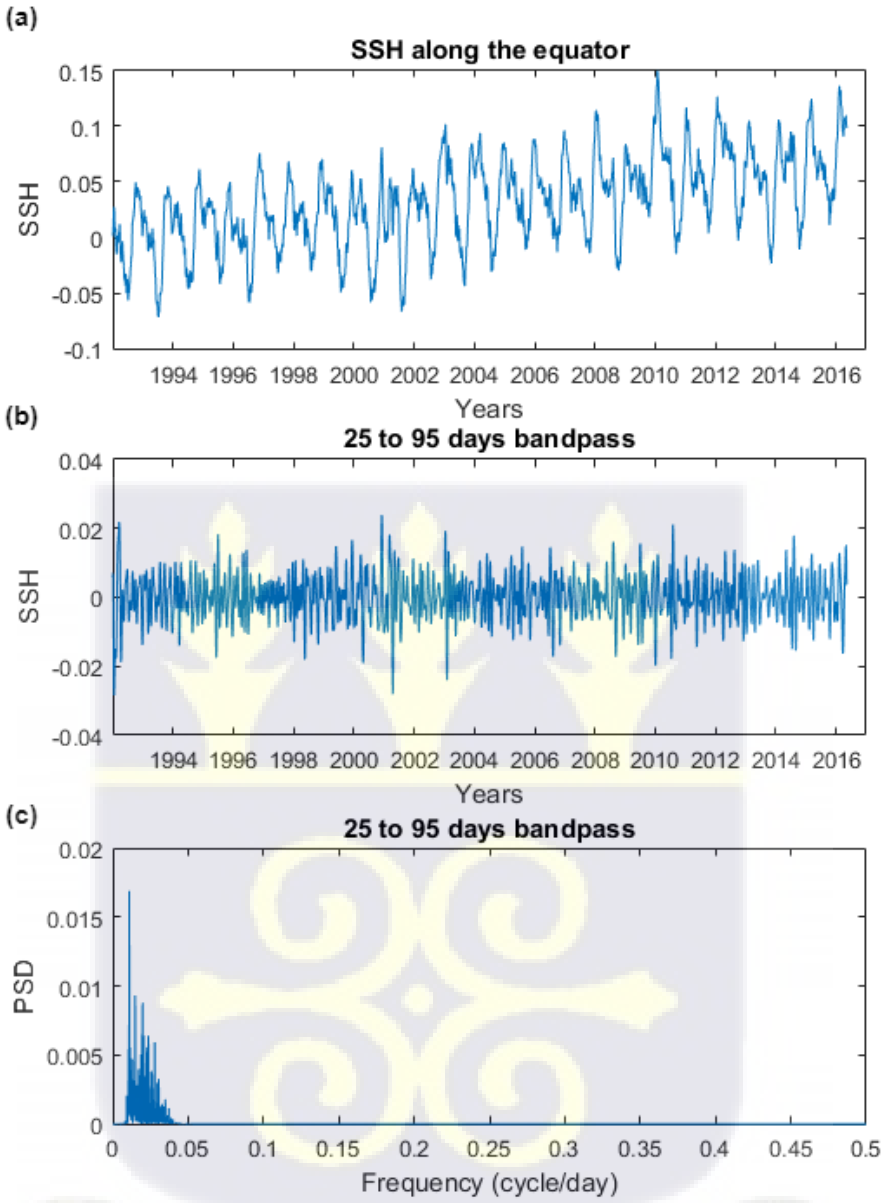

Figure 6.2: 25 to 95 days bandpass filtering from SSH

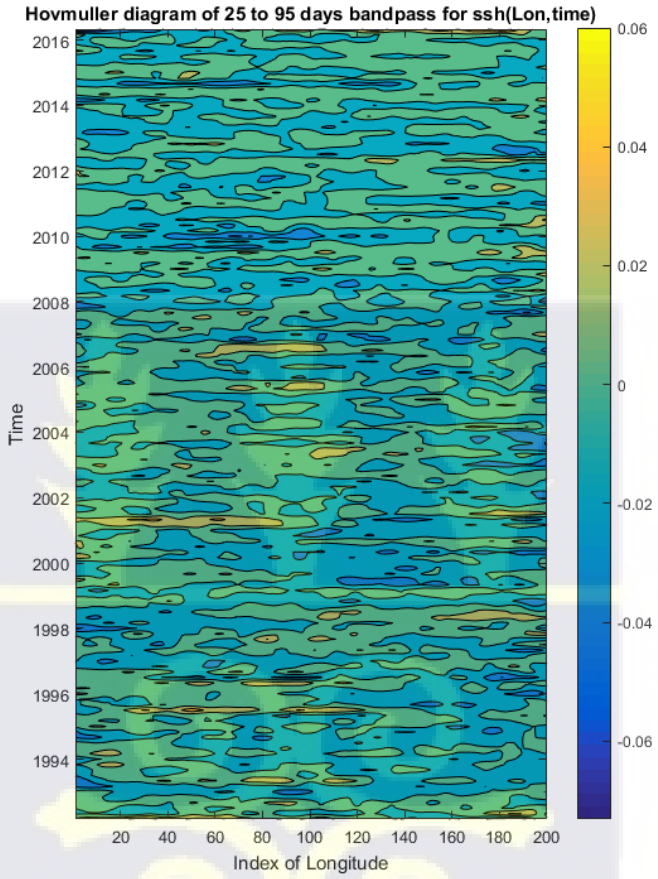

Figure 6.3: Hovmöller diagram of SSH as a function of time and longitude

6.2.2 Characterization of Kelvin waves from Observations and ECCO $\sim 1/3^{o}$ (1997)

Using real satellite observations from Copernicus (formerly Aviso), we denote the Sea Surface Height (SSH) or Sea Level Anomaly (SLA) as η. The SLA signals are composed of different signals whose characteristics or signatures are different in terms of their period, wavelength, frequency, amplitude, and phase speed. The SSH, η, as discussed by [9] can be decomposed or filtered into :

$$\eta = \eta_R + \eta_T + \eta_K + \eta_E + \eta_N. \tag{6.1}$$

The Rossby waves (η_R) are westward propagating waves which are about 1,000 to 10,000 km long. They have a period of months to years and cause a surface displacement of about 1 to 10 cm. The Rossby waves are long, non-dispersive, and transport energy westward to help intensify the currents at the western boundary. The energy and the phase speed travel at the same speed with a typical magnitude of 1 to 100 km/day. For instance, along latitude 0.125°N on the eastern equatorial Atlantic ocean, the Rossby waves at period $T = 44$ days with amplitude of 7 mm and wavelength of 2625 km produces a phase speed of 0.693 m/s. Similarly, along latitude 0.125°N on the Atlantic ocean, the Rossby waves with period $T_3 = 70$ days with amplitude of 4 mm and wavelength of 12678 km produces a phase speed of 2.096 m/s. Also, along latitude 0.125°N on the Atlantic ocean, the Rossby waves (η_6) at period $T_6 = 207$ days with amplitude at 4 mm and wavelength at 11032 km produces a phase speed of 0.6155 m/s.

Tropical instability waves (η_T) are signals that occur in the ocean between regions of colder and hotter surface temperatures. They create a consistent pattern of moving signals towards the west in the Atlantic ocean along the equator. Tropical instability waves mostly occur in the Atlantic region. They spread from the African coast towards the western direction. These waves usually last for about 1 to 1.5 days and have a wavelength of around 1100 kilometers.

Kelvin waves (η_K) are present as an eastward propagating signal along the equator in which some of its characteristics, structure or signatures have been described in Chapter 4 of Section 4.2.

Mesoscale eddies (η_E) are time-dependent circulations or swirlings about 100 km long and have a period of about a month. They are visible in the satellite images of sea

surface height or temperatures.

Non propagating waves or signals (η_N) which are dominated by seasonality as well as other features cannot be identified as any of the above.

[9], [10] and [16] used a filtering code to extract and characterize the westward propagating signals (Rossby waves) at several spectral bands. Their filtering code filters a series of Hovmoller diagrams of SLA from Topex Poseidon. For each latitude, the code converts SLA to Hovmoller diagrams of the filtered SLA. A module within the code filters the westward propagating signals (Rossby waves) and other signals as defined by Equation 6.1.

In the previous section, we found that the 25 to 95 days bandpass filter could not extract the Kelvin waves. Therefore, there is a need to modify the filtering code used by [9] in characterizing Rossby waves at several spectral bands.

The modified filtering code filters a series of Hovmoller diagrams of SLA from AVISO or CMEMS. For each latitude, the code converts SLA to Hovmoller diagrams of the filtered SLA, which are functions of longitude and time. The code contains an ocean basin represented by numbers 1 to 7, where we choose 1, which is the Atlantic ocean. A module within the code filters the eastward propagating signals (Kelvin waves) and measures the phase speed, wavelength, period, and amplitude. This code considers time domain and spatial domain.

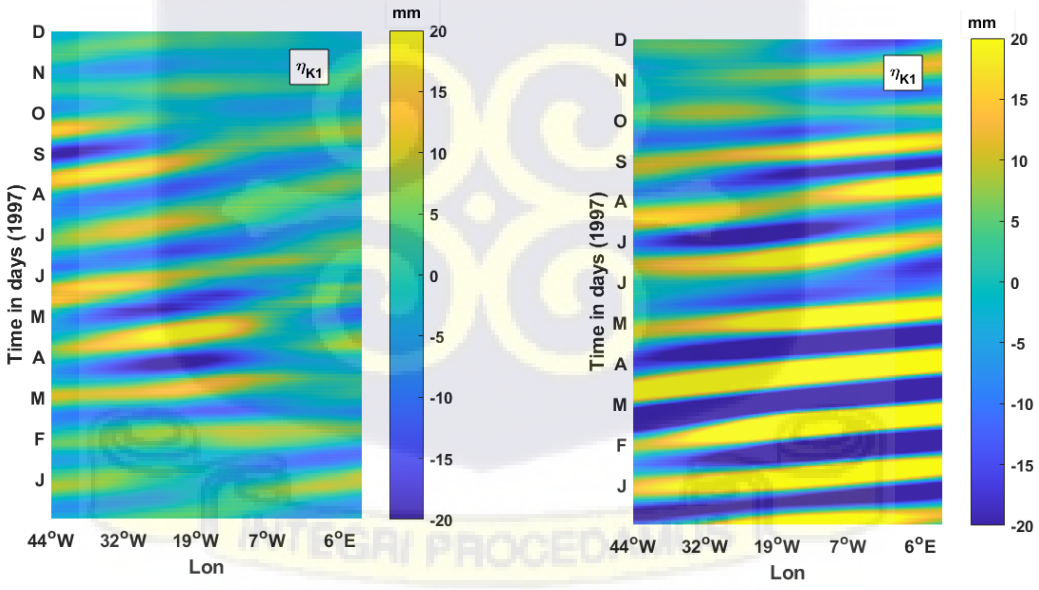

Figure 6.4: Kelvin waves from satellite observations (left panel) and ECCO (right panel) for the year 1997 using 1.5 months bandpass filtering.

A series of finite impulse response (FIR) filters from the filtering code is applied to SLA to extract the Kelvin waves for the Atlantic basin at each latitude. With the global Sea Level Anomaly (SLA) data, the code can extract Kelvin waves, construct Hovmöller diagrams, and compute the phase speeds, amplitude and wavelengths at different periods. Kelvin waves are typically about 1,000–10,000 km long and have a period of 25–95 days as discussed in [7].

The structure of Kelvin waves can be characterized at different bands, for example, from the 1997 SSH data from observations and ECCO. The η_{K1} on the left side of Figure 6.4 refer to Kelvin waves extracted with a one month period, η_{K3} is Kelvin waves extracted with a three months period, and η_{K6} is Kelvin waves extracted with a six months period. The filtered Kelvin waves can be analyzed for each latitude. For example, along latitude 0.125°N in the Atlantic ocean, from observation, Kelvin waves (η_{K1}) at period $T_{K1} = 44$ days with amplitude of 14 mm and wavelength of 6726 km produces a phase speed of 1.834 m/s as observed in Figure 6.4, which is consistent with the result of [7]. On the same latitude, Kelvin waves (η_{K3}) (Figure 6.5) were extracted from observation at period $T_{K3} = 85$ days with an amplitude of 12 mm and wavelength of 12336 km, producing a phase speed of 1.825 m/s which is also consistent with the result of [7].

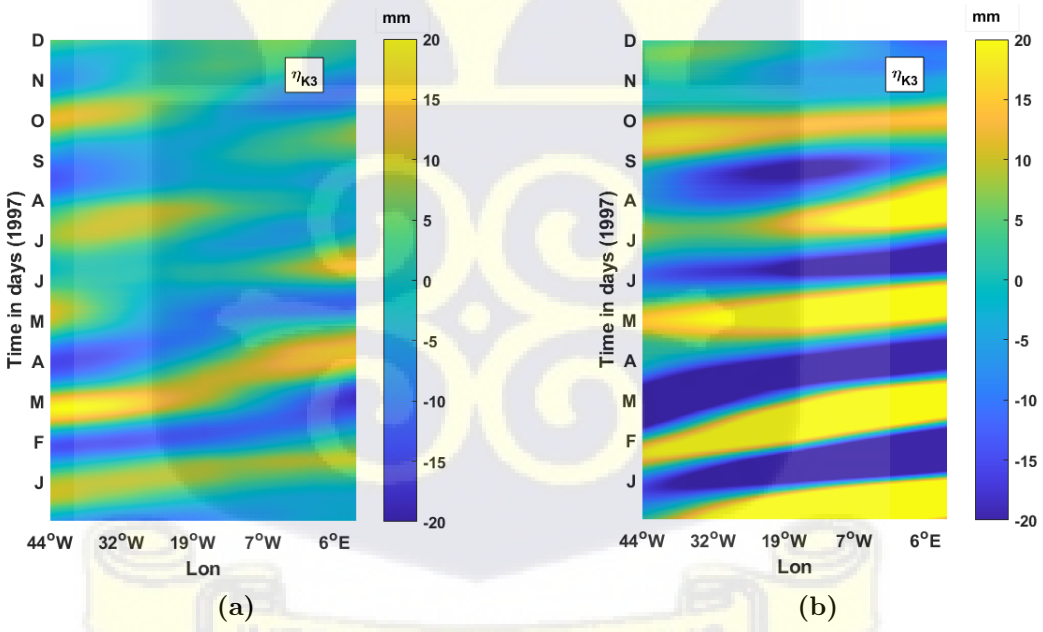

Figure 6.5: Kelvin waves from satellite observations (left panel) and ECCO (right panel) for the year 1997 using 3 months bandpass filtering.

Figure 6.4 (right panel) shows the structure of Kelvin waves from 1997 SSH data from ECCO output. Kelvin waves (η_{K1}) were extracted from ECCO output along

latitude 0.125°N in the Atlantic ocean at period $T_{K1} = 40$ days with an amplitude of 34 mm and wavelength of 9798 km and produces a phase speed of 2.82 m/s. This is consistent with the result of [7]. Similarly on the same latitude of the Atlantic ocean, Kelvin waves (η_{K3}) from ECCO at period $T_{K3} = 74$ days with amplitude of 38 mm and wavelength of 12893 km produces a phase speed of 2.013 m/s, consistent with the result of [7].

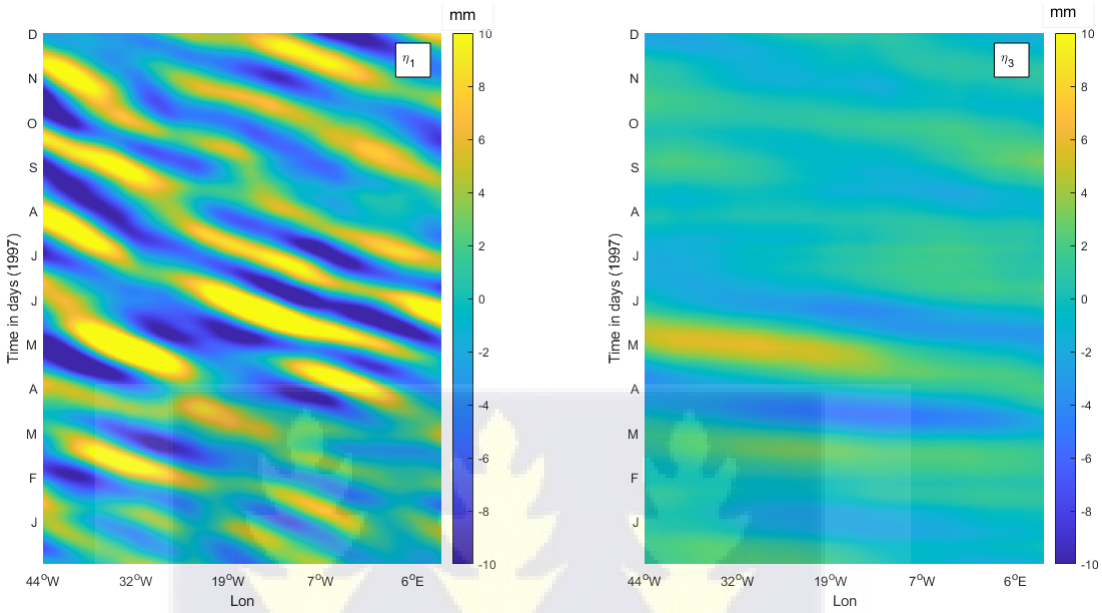

Figure 6.6: Hovmöller diagram of Rossby Waves from observation (1997) at lat0.125N along the Atlantic at different spectral bands

Note that other signals like the Rossby waves, which are dominant in the Atlantic ocean as westward propagating signals, can also be characterized in different bands. Along latitude 0.125°N in the Atlantic ocean, Rossby waves (η_1) from observation at period $T_1 = 45$ days with amplitude at 8 mm and wavelength at 2425 km produces a phase speed of 0.693 m/s as observed in Figure 6.6. Along the same latitude on the Atlantic ocean, Rossby waves (η_3) at period $T_3 = 70$ days with amplitude of 4 mm and wavelength of 12678 km produces a phase speed of 2.096 m/s.

Chapter 7

Relationship between Upwelling and Kelvin waves

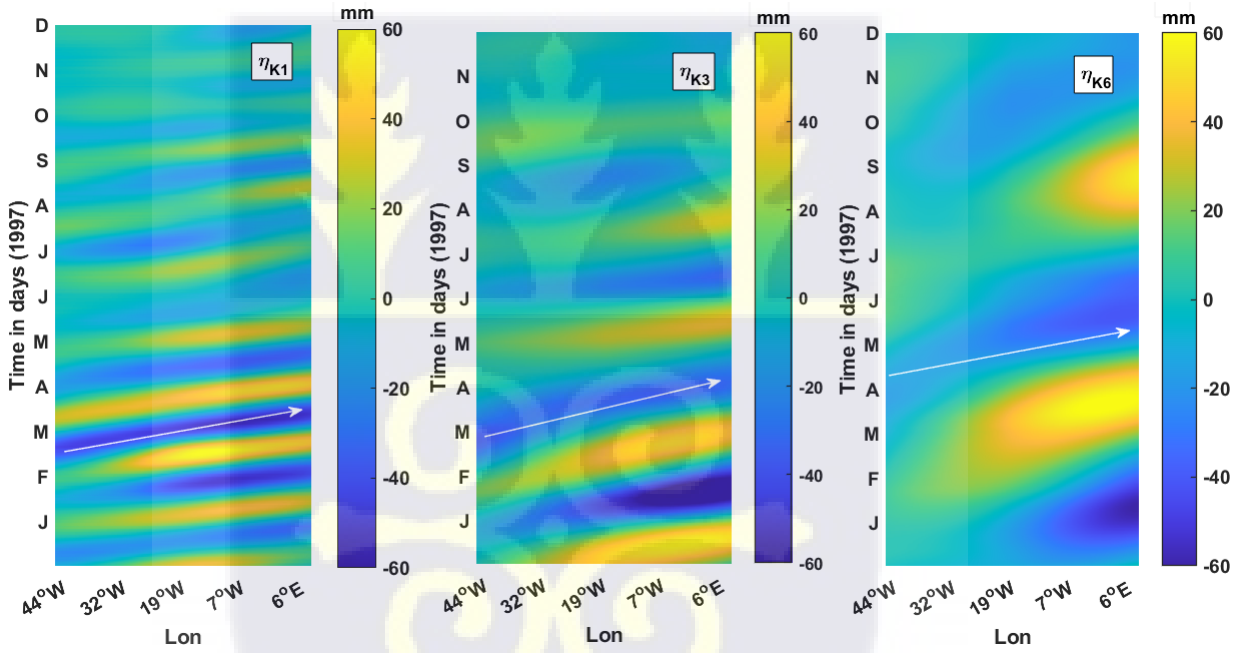

Figure 7.1: Kelvin waves from ECCO $\sim 1/3$ degree at latitude 0.125°N along the Atlantic ocean for 1997 period, where η_{K1}, η_{K3} (η_3), and η_{K6} (η_6) correspond to Kelvin waves at one month, three months, and six months period respecteively.

Kelvin waves propagating eastward along the equatorial Atlantic region to the West African coast are obtained from filtered ECCO (Estimating the Circulation and Climate of the Ocean) SSH signals after applying a 25–95 days bandpass filter. Most figures in this chapter have the following symbols: η_{K1} (η_1), η_{K3} (η_3), and η_{K6} (η_6) represent Kelvin waves extracted with a period of one month, three months, and

six months respectively. Figure 7.1 shows a Hovmöller diagram of Kelvin waves filtered from ECCO at latitude 0.125°N and longitude about 45 °W to 12 °E on the equatorial Atlantic region. The eastward propagating signals are shown for 1997. A visual estimation of the slopes for the Kelvin waves suggests a uniform phase speed of 1.92 m/s, illustrated with white arrows on the left panel of Figure 7.1. From left to right of Figure 7.1, the Kelvin waves become less visible as the period increases from 30 to 100 days. These results of the Kelvin wave's phase speeds are consistent with the phase speed obtained by Polo et al., 2008. Polo et al., 2008 analyzed the oceanic Kelvin waves propagating eastward in the tropical Atlantic region. The Kelvin waves showed continuous propagations, which were detectable between 1000–10000 Kilometers (Km) at longitude 45 ° W to 12 ° E along the equatorial region towards Equatorial Guinea. The mean value of the Kelvin waves amplitude is 12–22 mm (1.2–2.2 cm) at the equator and the coast of the Gulf of Guinea. We can deduce that the eastward propagating Kelvin waves are significant with SSH signals at the equatorial basin.

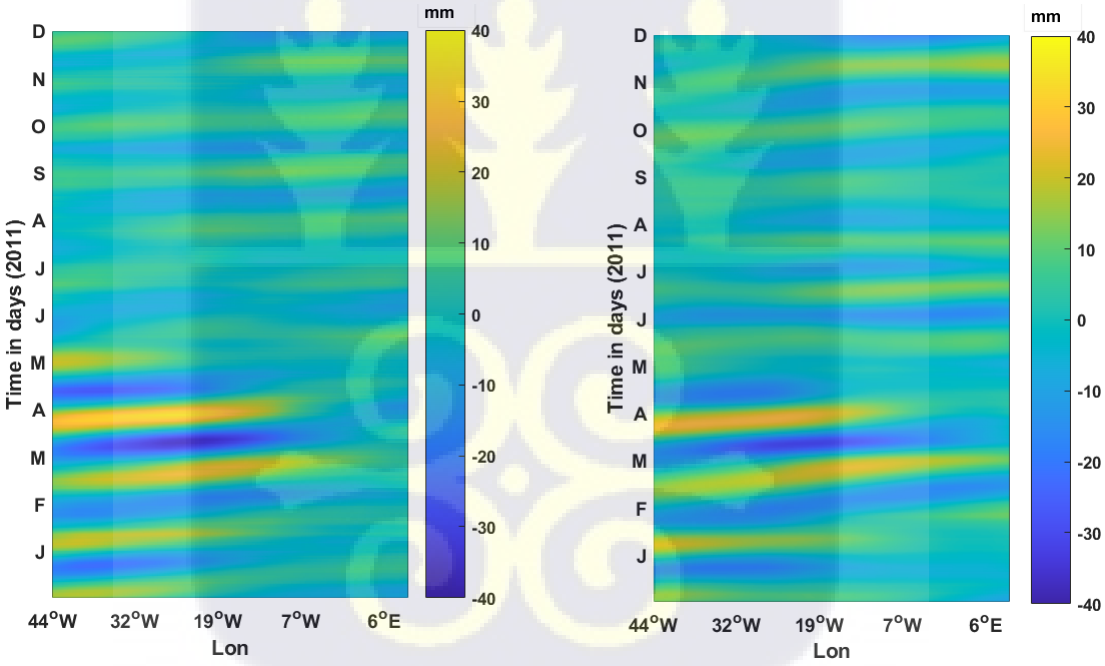

Figure 7.2: The Hovmöller diagram on the left panel shows Kelvin waves (η_1) from observation compared with Kelvin waves (η_1) from ECCO $\sim 1/3$ (rigth panel) in the year 2011, constructed along latitude 0.125°N.

SSH was obtained from the ECCO LLC270 output product to compare with observations and to determine the extent it could be used to predict upwelling events in the Gulf of Guinea. The Kelvin waves were extracted from observations and model

data at about one month, three months, and six months respectively.

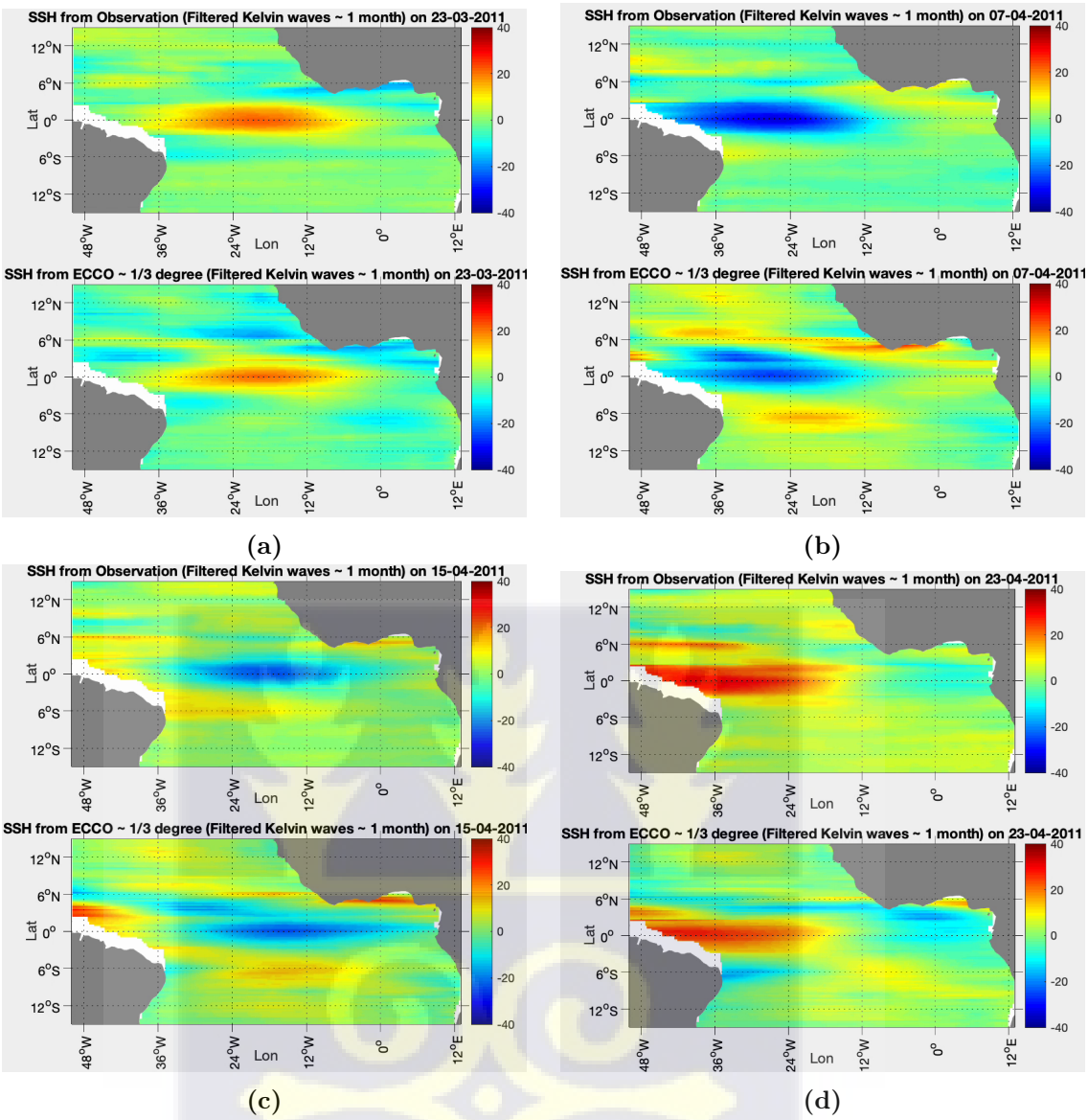

Figure 7.3: (a) Snapshots of Kelvin wave SSH from satellite observations (upper panels) and ECCO (lower panels) on March 25, 2011. Panels (b), (c) and (d) are the same as in (a) but at two week intervals. Waves are propagating from west to east in each panel.

Comparing Kelvin waves extracted from observation and model data from 1993 to 2016, it can be observed that there are some years when Kelvin waves from observations and ECCO agree quite well. For example, in the year 2011, Kelvin waves from observations match well with ECCO (Figure 7.3). Figure 7.3 a shows an almost symmetric height field of Kelvin waves around the equator with a latitudinal extent of about 300 km on either side of the equator, comparable to the e-folding length in [3]. The wave propagates eastward, and about two weeks later (Figure 7.3 b) we find

that the observational signal appears more symmetric about the equator than the signal in ECCO.

The Hovmöller diagram in Figure 7.2 shows that the modeled Kelvin waves match very well to those from the satellite observations as seen in Figure 7.3. In both data sets, the waves have larger amplitudes between January and May and become less energetic from June to the end of the year. Lag correlation analysis will be used later to quantify the similarities and differences between the model and observations.

The spatial pattern and amplitude of Kelvin waves in ECCO do not always match well to those in the satellite observations (e.g. Figure 7.4) for some years. The wave signals are not as symmetric about the equator as in Figure 7.3 for both data sets. However, the amplitudes appear larger in ECCO (e.g., Figures 7.4 b,c,d). This is more visible in Figure 6.4, constructed along latitude 0.125°N with wave period $T_{K1} = 44$ days and wavelength of 6726 km. The phase speed is about 1.834 m/s, which is consistent with the result of [7]. Similarly, Kelvin waves extracted along the same latitude with period of $T_{K3} = 85$ days and wavelength of 12336 km have comparable phase speeds (1.825 m/s) in both data sets but the amplitudes in ECCO are larger than in the observations (Figure 6.5).

The comparison can be done using correlation analysis as outlined in Subsection A.2.2. In Figure 7.2, both Kelvin waves (η_3) from the observation and model were taken along the equator at latitude 0.125°N from longitude about 45 °W to 12 °E on the Atlantic region. The Hovmöller diagram from Figure 7.2 shows the model captures the results of Kelvin waves from observation very well. Similarly, the model data can reproduce the Kelvin waves from observation by 58.44 % at a phase lag of 0 days, as observed in Figure 7.5. This means in the year 2011, Kelvin waves from ECCO lag behind the observation by 0 days and their signals are in-phase.

The lag correlations between observation and ECCO have similar characteristics or signatures for different regions and years. The model data (ECCO) can capture the Kelvin waves from observation by 74.82 % at a phase lag of 5 days, as observed in Figure 7.6. This means in 2002, Kelvin waves from ECCO lag behind the observation by 5 days.

In Figure 7.7, both Kelvin waves (η_3) from the observation and model were taken along the equator at latitude 0.125°N and longitude about 45 °W to 12 °E on the Atlantic region. The Hovmöller diagram in Figure 7.7 shows the model matches the results of Kelvin waves from observation very well. However, a lag correlation analysis indicates

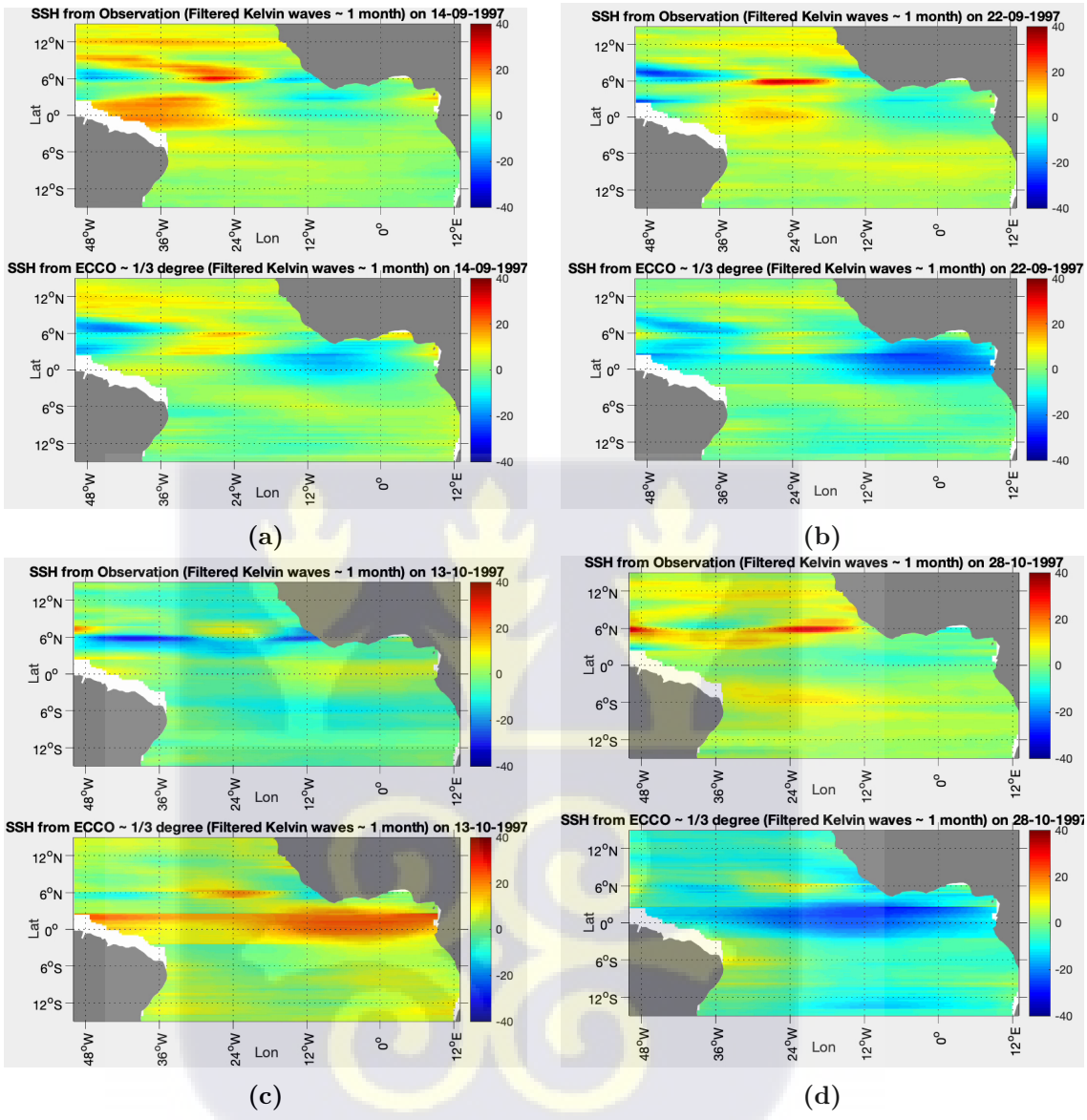

Figure 7.4: (a) Snapshots of Kelvin wave SSH from satellite observations (upper panels) and ECCO (lower panels) on September 14, 1997. Panels (b), (c) and (d) are the same as in (a) but at two week intervals. Waves are propagating from west to east in each panel.

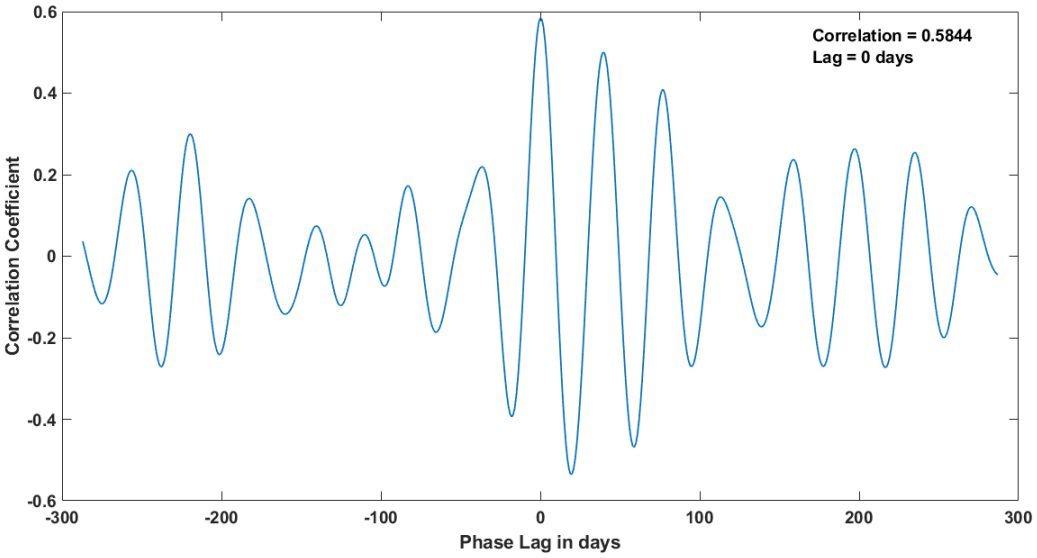

Figure 7.5: Correlation between Kelvin waves (η_1) from observation compared with Kelvin waves (η_1) from ECCO in the year 2011 from the Brazilian region.

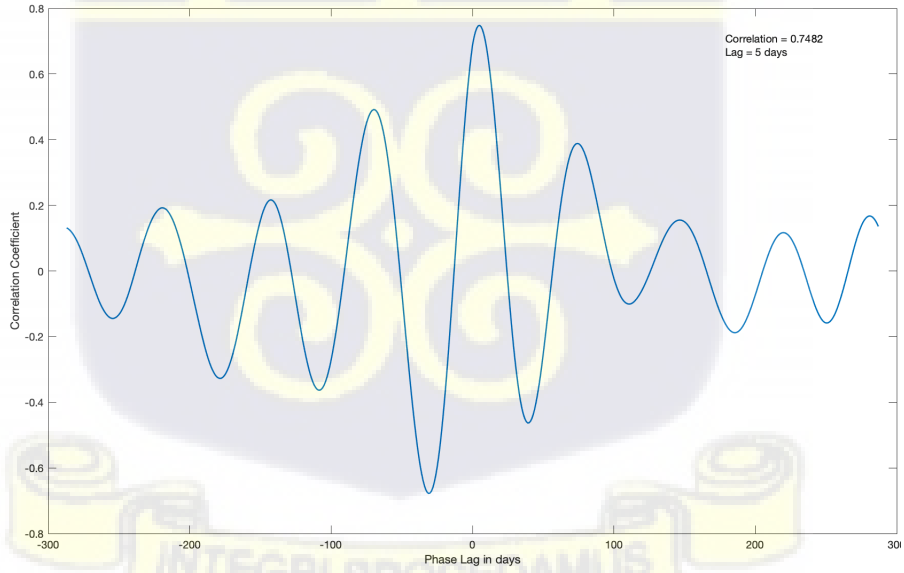

Figure 7.6: Correlation between Kelvin waves (η_3) from observation compared with Kelvin waves (η_3) from ECCO in the year 2002 from the Brazilian region.

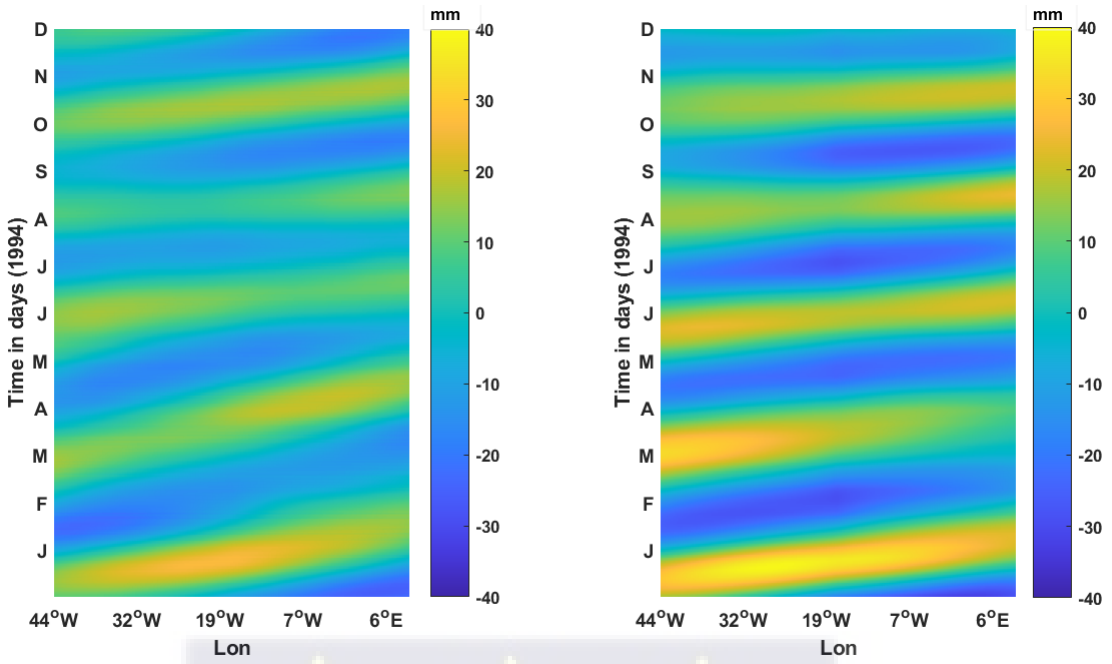

Figure 7.7: The Hovmöller diagram on the left shows Kelvin waves (η_3) from observation compared with Kelvin waves (η_3) from ECCO∼1/3 (right panel) in the year 1994.

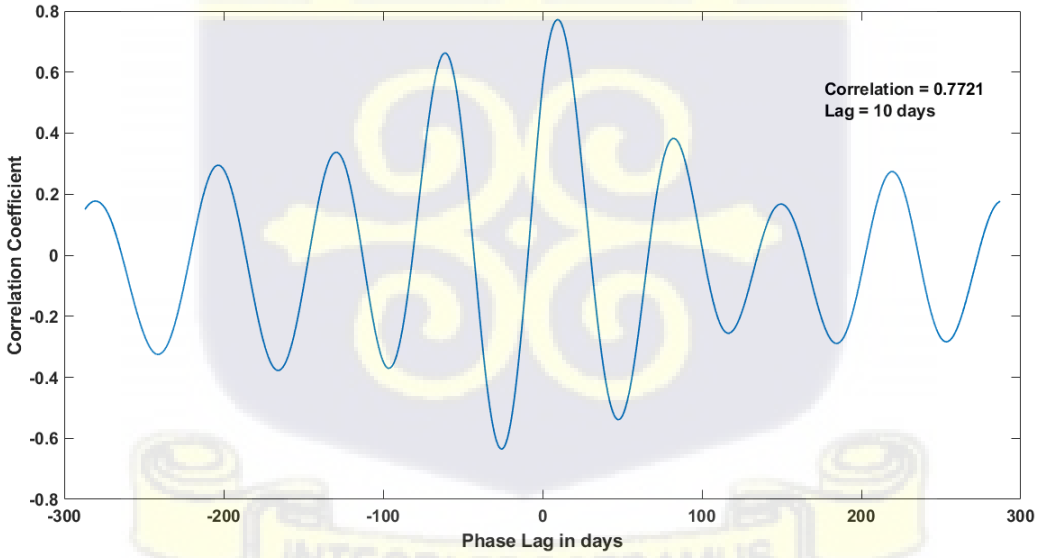

Figure 7.8: Lag Correlation between Kelvin waves (η_3) from observation compared with Kelvin waves (η_3) from ECCO in the year 1994 from the Guinea West of West Africa sub-region.

that in 1994, the model data captures the Kelvin waves from observation by 77.21 % at a phase lag of 10 days, as observed in Figure 7.8. The Hovmöller diagram for the Kelvin waves extracted from the model data presents a clearer anomaly propagation of about three months than the Kelvin waves extracted from observations. This means that in 1994, results from the model data will lag behind the observation by 10 days.

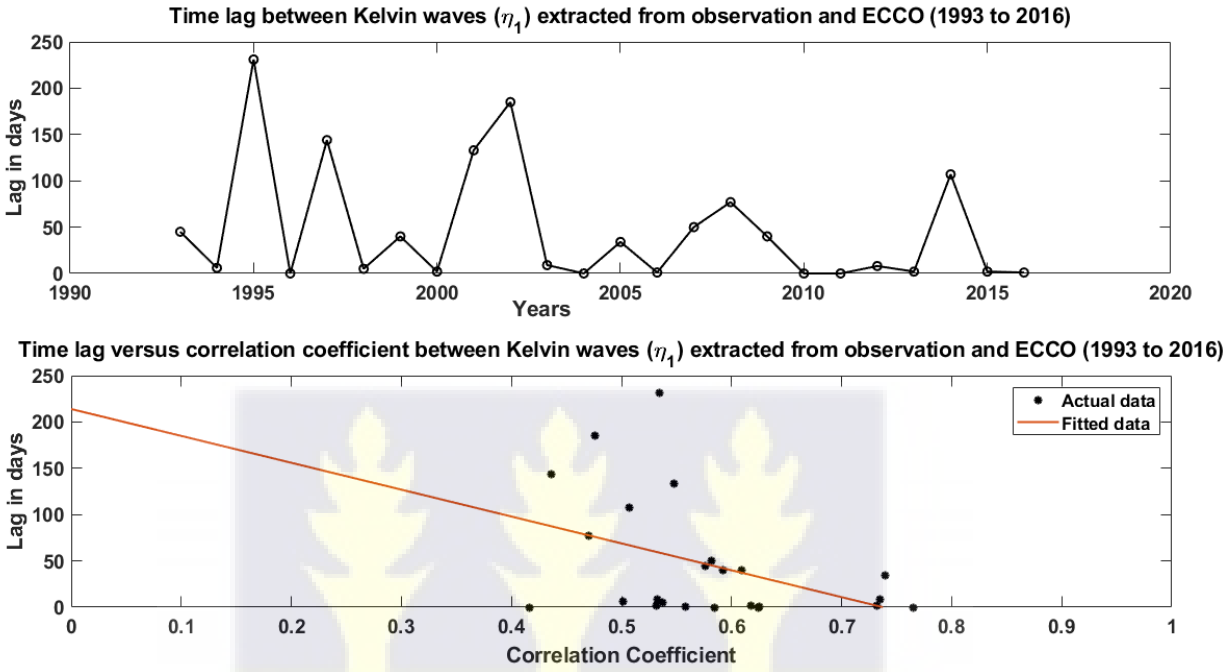

Figure 7.9: Lag correlation between Kelvin waves about one month (η_1) extracted from observation and ECCO (1993 to 2016).

In Figure 7.9, we noticed that the lag between the Kelvin waves extracted from observations and ECCO at one month appears to be getting smaller in recent years. However, the lag correlation trend between the Kelvin waves at three months extracted from observations and ECCO is not as clear as the one month case. The decreasing trend in the Figure 7.9 shows an improvement in the model.

We now consider some selected areas of relevance in the Atlantic region as shown in Figure 7.10. These areas include Brazilian region (BR) 5°N–5°S, 35°W–25°W, Guinea North region (GN) 0°N–5°N, 10°W–10°E, Guinea West region (GW) 5°N-5°S, 10°W-5°W, Northeastern region (NE), and southeastern region (SE) as was done in [6].

$\Delta\tau_x$ is the anomaly of the wind stress in the zonal direction, $\Delta\tau_y$ is the wind stress in the meridional direction, and ΔSST is sea surface temperature anomaly.

In Figure 7.11, we observe that the zonal wind stress anomaly in the Brazilian region

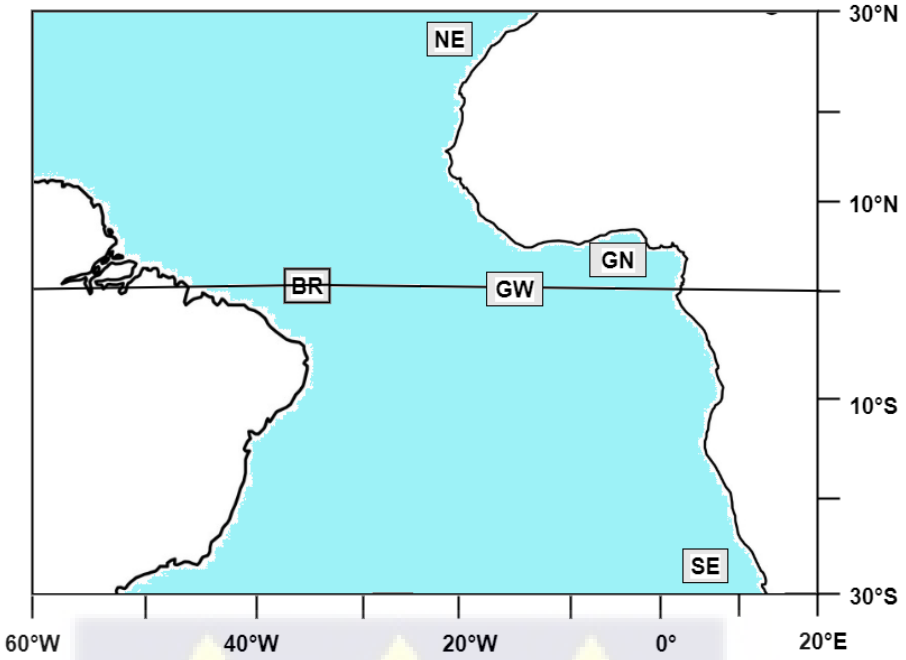

Figure 7.10: Selected areas of relevance in the Atlantic region as in [6].

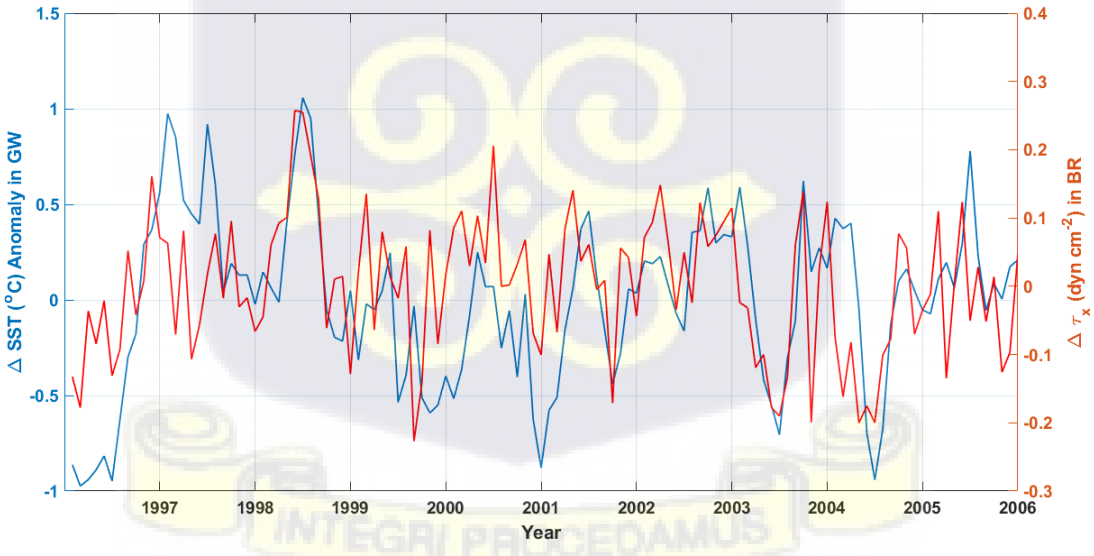

Figure 7.11: SST anomaly in Guinea West (GW) and zonal wind stress anomaly in Brazilian region (BR) from observations (1997 to 2016).

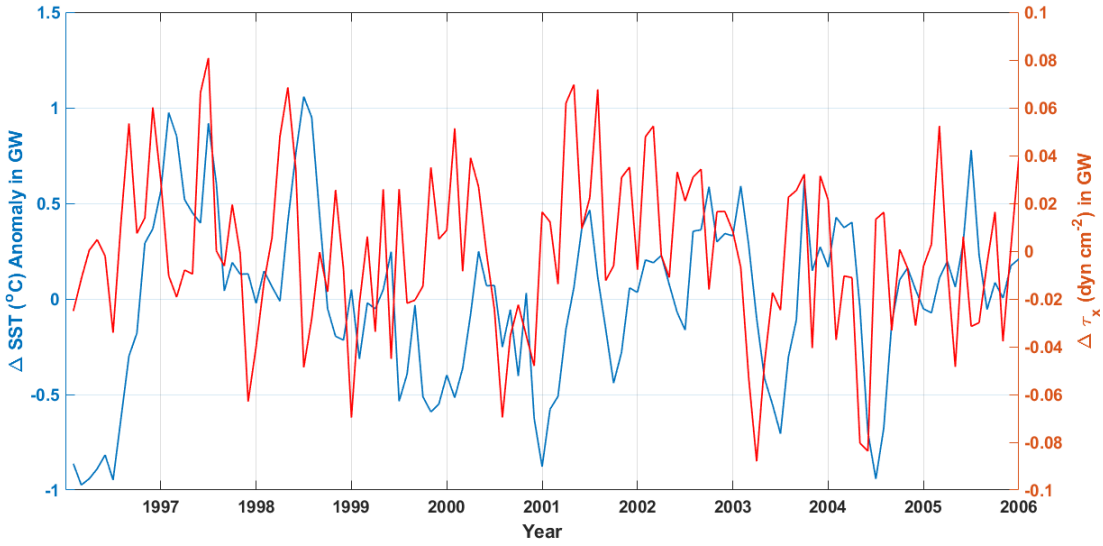

Figure 7.12: SST Anomaly in Guinea West region (GW) and zonal wind stress anomaly in Guinea West region (GW) from observations (1997 to 2016).

(BR) correlates well with the SST anomaly in the Guinea West (GW) region (Figure 7.10). However, the correlation between the zonal wind stress and SST anomaly in the Guinea West region is poor (Figure 7.12). This indicates that the local zonal winds in the Guinea West region have little or no effect on low SST in the Gulf of Guinea. This points to the reason behind the hypothesis that upwelling in the Gulf of Guinea is not connected in any obvious way to the local winds, as indicated by [1] and [6]. Further, we performed correlation analysis with current observational data and model output from ECCO was done to test the hypothesis that the upwelling event in the Gulf of Guinea was remotely influenced by the westward wind stress in the Brazilian region. Observational wind product and sea surface temperature (SST) data were obtained from ECMWF ERA5. The nonseasonal variations of SST and wind stress from zonal ($\Delta\tau_x$) and meridional ($\Delta\tau_y$) components were computed by subtracting the monthly mean values from the actual data. These monthly means were obtained by calculating monthly climatology from 1981 to 2016 to produce a 36-year time series. Similarly, for ECCO, the SST monthly averages were obtained by calculating monthly climatology from 1993 to 2016 to produce a 24-year time series.

The lag correlations from observations for the selected regions are displayed in Figure 7.13 and look similar to the lag correlation obtained by [6], who used 60-year time series from 1911 to 1972. The fact that the highest correlation occurs between $\Delta\tau_x$ from the Brazilian region and SST from the Gulf of Guinea region (GW) suggests the plausibility that the SST signals during upwelling are influenced by a remote source

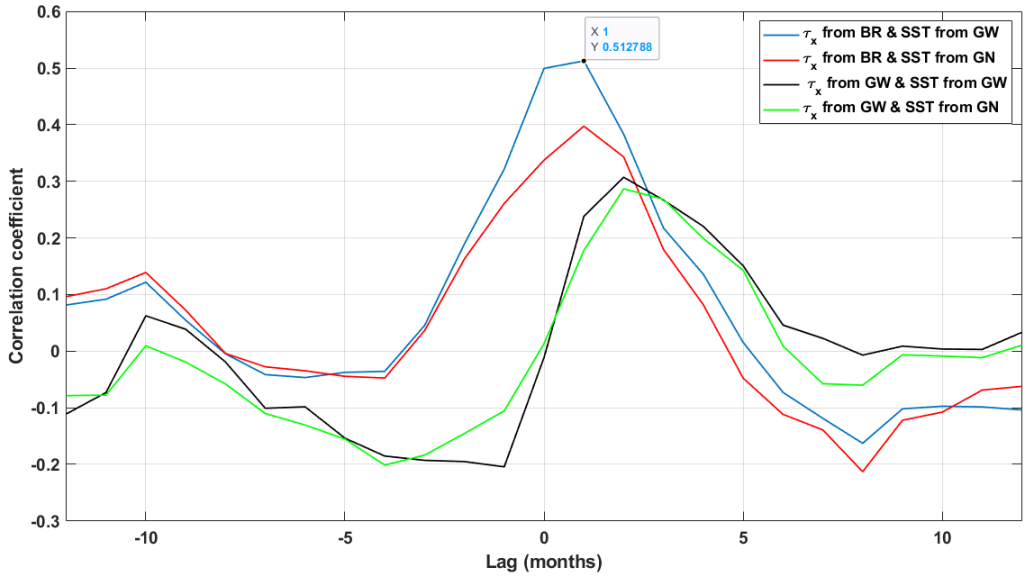

Figure 7.13: Lag correlation between τ_x and SST from satellite observations for the different regions (see legend).

around the Brazilian region. A similar lag correlation analysis using data from ECCO is shown in Figure 7.14, and looks very much like those obtained from the satellite observations. By comparing Figures 7.13 and 7.14, and the results of [6], we see that increasing the duration of the time series provides a better representation of lag correlations. Furthermore, additional data from the model (Figure 7.14) has been used to produce similar results with a marginal improvement to [6].

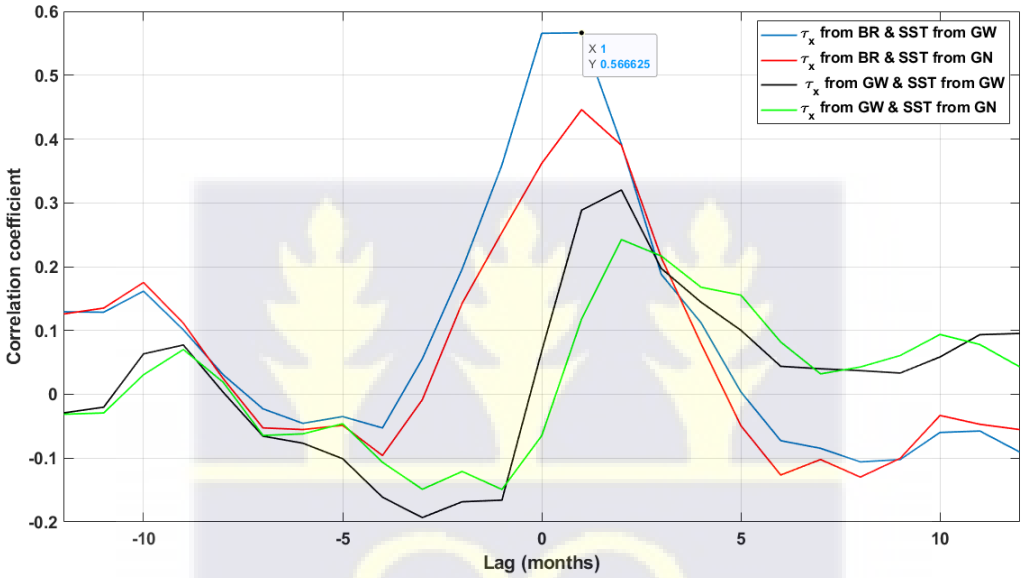

Figure 7.14: Lag correlation between τ_x and SST from ECCO for different regions (see legend).

Chapter 8

Conclusion

In this thesis, we analyzed upwelling events from time series of about 20 to 36 years long in the Gulf of Guinea using satellite data and ECCO model output.

Our analysis helps to zero in on the causes of upwelling in the Gulf of Guinea. Early historical discussions of the possible causes of upwelling events in the eastern Atlantic region and the Gulf of Guinea used limited observational data and simple numerical model outputs to analyze and study upwelling events (example, [14], [2], [6], [4], and [3]). [3] had issues with the irregular geometry of the equatorial Atlantic basin, which approximately extends 5000 km zonally, and 1500 km on either side of the equator, leading to some errors in the numerical model. Such errors are minimized in the ECCO model, making the model more realistic than previous models.

[14], [2], [3], and [4] suggested that upwelling events in the Gulf of Guinea is not associated with the local winds. This is because upwelling in the Gulf of Guinea is different from the theoretical wind versus water flow direction. They hypothesized that upwelling in the Gulf of Guinea results from Kelvin waves propagating eastward from the Brazilian coast along the equator. The equatorially trapped Kelvin waves reach the eastern coast of Africa and then propagate along the coastal boundary of West Africa as coastally trapped Kelvin waves. This research uses SSH (SLA), SST, and Wind data from the satellite (observations) and ECCO (model data). One of the research questions was to determine how well Kelvin waves in the Gulf of Guinea region are reproduced from the output of the ECCO model. We found that, there were some years where the observational results correlated very well with model data for the extracted Kelvin waves, as discussed in Chapter 7. This research also helps to provide some documentation of the signatures of Kelvin waves in the satellite

observations and ECCO output in the Gulf of Guinea region.

[6] discussed the relationship between the wind stress from the Brazilian region and SST anomalies from the Gulf of Guinea region. Their results indicated that the upwelling is due to events closer to the Brazilian coast. In this thesis, a similar analysis was done using relatively recent data from 1981 to 2016 to obtain a 36-year time series for the wind stress anomaly in the Brazilian region and the SST anomaly from the Guinea-west region. We also use output from a state-of-the-art global ocean model to study this phenomenon, in contrast to [6] who used data collected from ship. The lag correlation is similar to the lag correlation obtained in [6] which used 60-year time series. ECCO data from 1993 to 2016 produced a 24-year time series. We find that the lag correlations from ECCO are also similar to those from observations, with the highest correlations occurring between the zonal wind stress from the Brazilian region and the SST signals from the Gulf of Guinea region. This provides some hope that ECCO could be used to make predictions of upwelling in the Gulf of Guinea.

Further work is still needed in the future to properly link the equatorial Kelvin waves that reach the eastern part of Equatorial Guinea and propagate west to the Gulf of Guinea to cause upwelling. Once the connection between the equatorial Kelvin waves and upwelling events in the Gulf of Guinea has been bridged, the results could be used to predict upwelling events on the West African coast. This will help measure, if possible, the strength of upwelling events over time and will help fully understand the causes of the minor and major upwelling seasons in the region.

Other studies suggest some contribution of local winds to the Gulf of Guinea upwelling. Another future endeavour would be to determine the fraction of upwelling caused by these local winds versus those attributed to remote forcing by Kelvin waves.

Appendix A

Tools used in analyzing Upwelling events in the Gulf of Guinea

A.1 Fourier Analysis

Fourier Analysis is a method of identifying cycles or patterns within a data. This method quickly gathers more details from a signal. Any changing process in the ocean can be represented as a combination of many basic elements added together in a continuous way. These basic functions can be adjusted to specific functions using least squares. Fourier analysis helps us analyze data about waves and tells us about their sizes (wavelengths) and time durations (periods). These cycles may have periodic or non-periodic waveforms. A periodic function can be expressed in the form $f(t) = f(t+T)$, where T is a constant called the **period**, that is, the function repeats itself after a period, T. $f(t)$ can be approximated as

$$f(t) = a_0/2 + \sum_{k=1}^{\infty}[a_k \cos(kw_0 t) + b_k \sin(kw_0 t)],$$

$$a_0 = 2/T \int_{-T/2}^{T/2} f(t)\, dt, \quad a_k = 2/T \int_{-T/2}^{T/2} \cos(kw_0 t) f(t)\, dt$$

$$b_k = 2/T \int_{-T/2}^{T/2} \sin(kw_0 t) f(t)\, dt,$$

This is called the Fourier series, where $w_0 = 2\pi/T$ is the fundamental frequency. The space for $f(t)$ can be spanned and described by the basis functions $1, \cos(w_0 t), \sin(w_0 t), \cos(2w_0 t), \sin$ The purpose of the Fourier Series is to examine functions that display recurring pat-

terns and decompose them into sums of **sines** and **cosines**.

Complex notation offers a shorter alternative for expressing the Fourier series. This is based on *Euler's formula*, where $\cos(kw_0t) = \dfrac{e^{ikw_0t} + e^{-ikw_0t}}{2}$ and $\sin(kw_0t) = \dfrac{e^{ikw_0t} - e^{-ikw_0t}}{2i}$. These can be substituted into $f(t)$ and simplified to get

$$f(t) = \sum_{k=-\infty}^{\infty} \tilde{c}_k e^{ikw_0t}, \text{ where } \tilde{c}_k = \frac{a_k - ib_k}{2} \text{ and } \tilde{c}_0 = \frac{a_0}{2}.$$

$\tilde{c}_k$ are complex coefficients and $\tilde{c}_k^* = \tilde{c}_{-k}$ are complex conjugate.
Also

$$\tilde{c}_k = 1/T \int_{-T/2}^{T/2} e^{-ikw_0t} f(t)\, dt$$

after replacing expressions for a_k and b_k.

The Fourier series can be written as the sum of an infinite number of sine and cosine functions, which are oriented and directed in different ways, on any surface. The Fourier transformation is a way to show the ocean surface picture using a combination of different waves moving in different directions. Imagine that you gather pictures of the ocean surface at different moments to see a complete view of it. We can show the surface of the ocean as a combination of different wave patterns using sine and cosine functions. These wave patterns can have different lengths and directions. Remember that the lengths of the waves are connected to the numbers and frequencies of the waves. This connection is called the dispersion relation. The ocean surface can also be thought of as a combination of different sine and cosine functions at various frequencies and directions. The top layer of the ocean has a complex mix of signals that vary in their length, speed, and direction.

A.1.1 Fourier Transform (FT), Discrete Fourier Transform (DFT) and Fast Fourier Transforms (FFT)

Signals or waves that do not happen in a regular pattern are called non-periodic, for example. A thunderbolt makes it hard for devices like TVs and radios to work properly. It affects a lot of different frequencies and causes them to have a constant mix of signals. The Fourier Transform can be used to study signals that do not repeat in a regular pattern. The Fourier transform comes from the way we can write the Fourier series using exponentials. The transition from a periodic to a non-periodic

function can be effected by allowing the period approach **infinity**. That is, as T becomes infinite, the function never repeats itself and thus becomes non-periodic. If this is allowed to occur, it can be demonstrated that the Fourier series reduces to $f(t) = 1/(2\pi)\int_{-\infty}^{\infty} F(w)e^{iwt}\,dw$ and the coefficients become a continuous function of the frequency variable w, as $F(w) = \int_{-\infty}^{\infty} f(t)e^{-iwt}\,dt$.

Thus, the pair lets us change from time to frequency and back again for a signal that doesn't repeat. The Fourier series changes a function that repeats over time into different levels at specific frequencies. On the other hand, the Fourier transform changes a function that changes over time into a function that changes over different frequencies. The set of individual frequencies produced by the Fourier series is similar to the range of frequencies produced by the Fourier transform. Both the Fourier transform and Fourier series can be thought of as mathematical tools that have certain properties. They are both linear operators, meaning that they can perform calculations on mathematical functions in a linear manner. Additionally, they are symmetric, which suggests that they have a balanced or equal nature. Why do we use the Fourier Transform (FT)? It helps to shrink audio files and get rid of unwanted sounds or interference from information. The highest number of times something can happen in a signal is called the Nyquist frequency. It is equal to half the rate at which the signal is being measured.

Data are generally given in discrete forms, and **Discrete Fourier Transform (DFT)** is a tool used to compute the Fourier transform of discrete data. For discrete signals, FT is computed to get the Fourier coefficient at each kth frequency, that is

$$F_k = \sum_{j=0}^{n-1} f_j e^{-\mathrm{i}kwj} \text{ and the inverse transform is } f_j = \frac{1}{n}\sum_{k=0}^{n-1} F_k e^{\mathrm{i}kwj}.$$

Let $m = e^{-\mathrm{i}w}$ and $w = 2\pi/n$. Then $F_k = \sum_{j=0}^{n-1} f_j m^{kj}$.

$$\begin{aligned}
F_0 &= f_0 + f_1 + f_2 + \cdots + f_{n-1} \\
F_1 &= f_0 + f_1 m + f_2 m^2 + \cdots + f_{n-1} m^{n-1} \\
\vdots &= \vdots \ + \ \vdots \ + \ \vdots \ + \cdots + \ \vdots \\
F_{n-1} &= f_0 + f_1 m^{n-1} + f_2 m^{2(n-1)} + \cdots + f_{n-1} m^{(n-1)^2}
\end{aligned}$$

$$\Longrightarrow \begin{pmatrix} F_0 \\ F_1 \\ \vdots \\ F_{n-1} \end{pmatrix} = \begin{pmatrix} 1 & 1 & 1 & \dots & 1 \\ 1 & m & m^2 & \dots & m^{n-1} \\ \vdots & \vdots & \vdots & \ddots & \vdots \\ 1 & m^{n-1} & m^{2(n-1)} & \dots & m^{(n-1)^2} \end{pmatrix} \begin{pmatrix} f_0 \\ f_1 \\ \vdots \\ f_{n-1} \end{pmatrix}$$

With the Discrete Fourier Transform, we are interested in extracting frequencies from data or signals. The basic idea here is that you have some discrete data $\{f_o, f_1, \cdots, f_{n-1}\}$ and want to break them down into sums of sine and cosine waves at different frequencies. And you want to know how much energy or amplitude is at each wave frequency. These amplitudes (Fourier coefficients) are $\{F_o, F_1, \cdots, F_{n-1}\}$ and you can achieve this by using a Discrete Fourier Transform matrix (Vandermonde matrix). A total of n^2 operations are needed to compute the Discrete Fourier Transform, which is computationally expensive and very slow in processing results. The Fourier Transform is a numerically efficient method to calculate the Discrete Fourier Transform. Utilizing the Fast Fourier Transform allows for the computation of the Discrete Fourier Transform, which is much quicker of order $O(n\log_2 n)$. It is one of the most important algorithms ever developed.

The Discrete Fourier Transform may be implemented more efficiently if the number of samples, n is a power of 2, example, $\{f_o, f_1, \cdots, f_{511}\}$ which is $512 = 2^9$ samples. Consider a two (2) sample Discrete Fourier Transform and let

$$F_k = \sum_{j=0}^{n-1} f_j m_n^{kj}, \quad \text{where} \quad m_n = e^{-\mathrm{i}2\pi/n}.$$

For $n = 2$ implies that

$$\begin{aligned} F_0 &= f_0 + e^{-\mathrm{i}2\pi/2(0)} f_1 + f_2 + \cdots + f_{n-1} \\ F_1 &= f_0 - e^{-\mathrm{i}2\pi/2(1)} f_1 + f_2 m^2 + \cdots + f_{n-1} m^{n-1}, \end{aligned}$$

where $m_2^0 = e^{-\mathrm{i}2\pi/2(0)} = 1$ and $m_2^1 = e^{-\mathrm{i}2\pi/2(1)} = -1$ which is summarized as

$$\begin{aligned} F_0 &= f_0 + f_1 \\ F_1 &= f_0 - f_1. \end{aligned}$$

Schematically, we calculate the Discrete Fourier Transform using the Butterfly diagram, whose name is depicted from the shape of the diagram. A two-sample Discrete

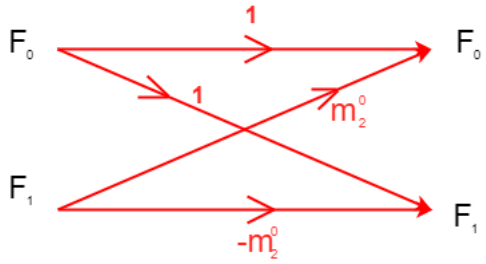

Figure A.1: Butterfly diagram of a two sample Discrete Fourier Transform.

Fourier Transform requires two multiplication accumulates to complete it as shown in Figure A.1.

A four (4) sample Discrete Fourier Transform, implies that $n = 4$, $m_4^2 = e^{-\mathrm{i}(2)2\pi/4} = -m_4^0$, and $m_4^3 = e^{-\mathrm{i}(3)2\pi/4} = -m_4^1$, which can be summerized into the equations below as

$$
\begin{aligned}
F_0 &= f_0 + f_1 + f_2 + f_3 \\
F_1 &= f_0 + m_4^1 f_1 + m_4^2 f_2 + m_4^3 f_3 \\
F_2 &= f_0 + m_4^2 f_1 + m_4^4 f_2 + m_4^6 f_3 \\
F_3 &= f_0 + m_4^3 f_1 + m_4^6 f_2 + m_4^3 f_3
\end{aligned}
$$

Simplifying the equations again, we have

$$
\begin{aligned}
F_0 &= (f_0 + f_2) + m_4^0(f_1 + f_3) = (f_0 + m_2^0 f_2) + m_4^0(f_1 + m_2^0 f_3) = G_0 + m_4^0 H_1 \\
F_1 &= (f_0 - f_2) + m_4^1(f_1 - f_3) = (f_0 - m_2^0 f_2) + m_4^1(f_1 - m_2^0 f_3) = G_2 + m_4^1 H_3 \\
F_2 &= (f_0 + f_2) + m_4^2(f_1 + f_3) = (f_0 + m_2^0 f_2) - m_4^0(f_1 + m_2^0 f_3) = G_0 - m_4^0 H_1 \\
F_3 &= (f_0 - f_2) + m_4^3(f_1 - f_3) = (f_0 - m_2^0 f_2) - m_4^0(f_1 - m_2^0 f_3) = G_2 + m_4^0 H_3
\end{aligned}
$$

The four sample Discrete Fourier Transform depicted in Figure A.2 requires 8 multiply accumulates. The power of m ranges from 0 to 1 which is obtained from $\frac{n}{2} - 1 = \frac{4}{2} - 1 = 2 - 1 = 1$. The Fast Fourier Transform uses $O(n\log_2 n)$ computations, that

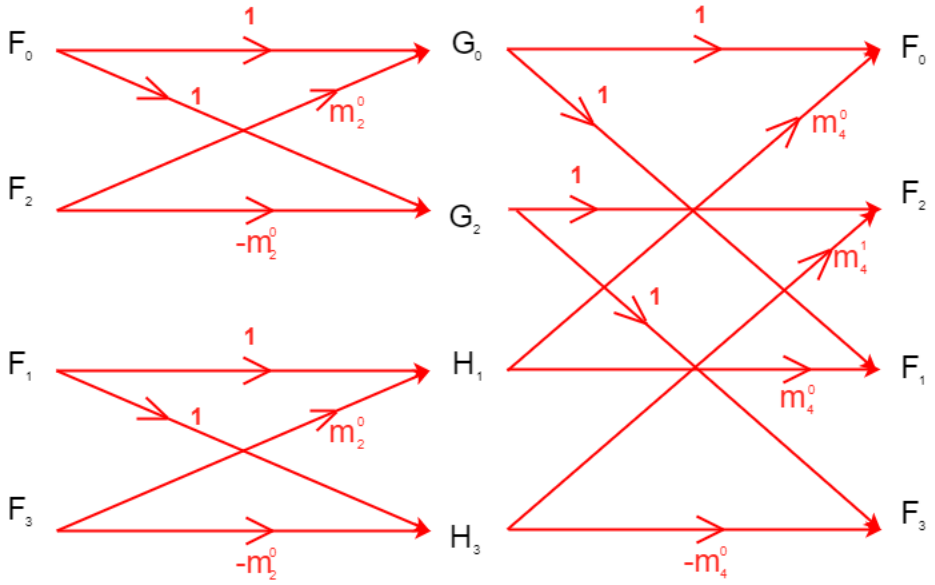

Figure A.2: Butterfly diagram of a four sample Discrete Fourier Transform

is,

$$n = 2^1 \implies 2\log_2 2^1 = 2 \times 1 = 2$$
$$n = 4 = 2^2 \implies 4\log_2 2^2 = 4 \times 2 = 8$$

A.2 Bandpass Filtering

Typically, we desire to eliminate the occurrence of a certain event that happens frequently within a given data set over a period of time. For instance, if you want to study tidal waves in ocean data, you can get rid of the low and high frequencies in the data. In the SSH data that we are studying, we are looking at Kelvin waves. We are interested in signals that have periods between 25 to 95 days. This can be done by removing some signals that have frequencies we are not interested in. The filtering process can be used to sort out information in different ways such as time, frequency, or space, as explained in [41]. This text offers a description of crucial information and mathematical principles utilized in filtering instruments designed for studying the ocean.

If you use a time-based filtering method, the result from the filter is a mix of the input data that is based on the time difference between each data point and the output.

Assume you want to separate or sort data based on time. The output (Y) of the signal is given by

$$Y_k = \sum_{j=0}^{n-1} w(t_i - t_k)X_j, \quad \text{for} \quad k = 0, 1, \cdot, n-1,$$

To find the filter weights, you can use a method called Fourier transformation. This method converts the information from the time domain to the frequency domain. Instead, if you pick a filtering method that uses frequency instead of time, you can convert the series of data into a different form called an unaveraged spectrum using a mathematical process called Fourier transformation. The different frequencies in the spectrum are separated and adjusted using specific weights. The filtered spectrum is transformed again using the Fourier transform to get the signal in the time domain. This can be done mathematically using the formula

$$y_j = \sum_{j=0}^{n-1} W(f_j)x(f_j), \quad \text{for} \quad j = 0, 1, \cdots, n-1,$$

where f is the frequency, x is the Fourier transformed signal, y is the filtered spectrum, and W is the frequency domain's weights. There are three types of filters: lowpass filter, highpass filter, and bandpass filter. A lowpass filter is a type of filter that gets rid of high-pitched sounds above a certain point called the cutoff frequency. It only lets through the low-pitched sounds. The lowpass frequencies are typically used to make a time series appear smoother. It is not too difficult to understand and do within a certain time. The lowpass filter can be done using the different frequencies of a signal instead of using the time it takes for the signal to change. The sounds can be changed using a math process called Fourier transformation. After that, the parts of the sounds that we don't want can be removed completely. You can bring back the filtered signals by using the inverse Fourier transform. The highpass filter is a type of filter that gets rid of low-pitched sounds below a certain frequency, while still keeping the high-pitched sounds. A bandpass filter is a type of filter that only allows certain frequencies in the middle range of the data while getting rid of the really low and high frequencies.

Highpass and bandpass filters are easy to understand and use in the frequency domain because they help get rid of specific frequencies, even though they are mostly used in the time domain. One way to do this is to modify the signals by using the Fourier

transform technique, where we change the intensities of certain frequencies to zero. Then, do the opposite process of Fourier transform to reconstruct the desired signals. Another method to get highpass filtering is by taking away the lowpass signals from the original signals. However, when we try to remove unwanted frequencies from a time series using a simple method, it causes issues in the inverse Fourier transform, similar to the Gibbs phenomenon. If the number of data points in the time series cannot be easily divided by 2, add extra zeros to make it divisible by 2. This is done to ensure that the sample size has a power of 2 ([41]). This means that by using Bandpass filtering, you can choose to ignore or reject specific bands, frequencies, or signals and only let some of them pass through. That's why it's called Bandpass filtering. For instance, if we have information (such as data) If there is a specific frequency that a sound or signal makes, and it goes up and down, I might want to study only some parts of it and not the rest. This information can help us tell apart different events in time for a certain parameter. For example, we can separate what happens in a single day from what happens over a longer period of time like months or years.

From the synthetic signals in the first subplot of Figure A.3, we have frequencies of different waves at 5, 10, 20, and 40 days. The idea is to know how specific signals can be extracted once the frequency and wavelength of the signal are known. Because we want a particular signal at a specific frequency and wavelength, we have to remove these from the synthetic signal. Thus, in preparing the filter, we will instruct the program to keep a particular day and cut off all other days, this line in the code:

CutRate=[1/90 1/30.

This cut-rate will remove all the other time signals and keep only those on 30-90 day oscillations (i.e. the time band allowed to pass through the filter). The Bandpass filter has been designed to avoid problems of the Gibbs phenomenon. The Fourier transform of the filter in terms of frequency can be used to make the filter in terms of time. If you want a bandpass filter to produce a narrow range of frequencies, you need to have a shorter time series. The longer the time series, the narrower the desired range of frequencies must be for the bandpass filter to work effectively.

The bandpass used in filtering the signals in figure A.3 can remove the mean from the data to get the anomalies. The sampling frequency is once daily since the signal is assumed to be daily. The fourth-order Butterworth filter is used; if the order of the Butterworth is too high, the tool may not work well. Double frequency values for the bandpass, for example, CutRate=[1/22 1/18] in the code for 18 to 22 days to

keep only 18 to 22 days and remove all other frequencies as shown in Figure A.3.

```
% Frequency at 5, 10, 20 and 40 days
w=2*pi*[1/5,1/10,1/20,1/40];
 A=1;k=0.1; L=25/11; N=100;
% Creating a surface (3D)
lon = linspace(-40,10,N) ;lat1=linspace(-10,0,N);
lat = linspace(-20,20,N) ;x=lon;y=lat;y1=lat1;
[X,Y] = meshgrid(x,y) ;[X1,Y1] = meshgrid(x,y1) ;
% Sampling everyday for 365 days
t = 1:365; E = zeros(N,N,length(t));
for i = 1:length(t)
    E(:,:,i)= A*exp(-0.5*(Y+8).^2/L^2)*cos(k.*X-w(1)*t)+ ...
              A*exp(-0.5*(Y+16).^2/L^2)*cos(k.*X+w(2)*t)+...
              A*exp(-0.5*Y.^2/L^2)*cos(k.*X-w(3)*t)+...
              A*exp(-0.5*(Y-8).^2/L^2)*cos(k.*X+w(4)*t);
end
% Filtering and viewing 3D signal in 2D
for i = 1:length(t)
    pcolor(x,y,squeeze(shband3(:,:,i))); % shband3 is a filter
    xlabel('Lon');ylabel('Lat');
    title('18 to 22 days bandpass filtering');
end
```

This can be observed in the first subplot of Figure A.3.

A.2.1 Power Spectrum of Synthetic Signal

Spectral analysis is about getting useful information from a set of measurements made over time. - It is utilized for distinguishing waves or signals and detecting significant variations in a sequence of time. Time-changing processes in the ocean can be represented as a combination of many different wave patterns, like the up and down movements of waves. If the functions are at right angles to each other and continue on forever, then the time series or signal can be shown as a combination of sines and cosines. Spectral analysis is helpful in the time and spatial domain, yielding information about periods or frequencies (time scales) and wavelengths (spatial scales)

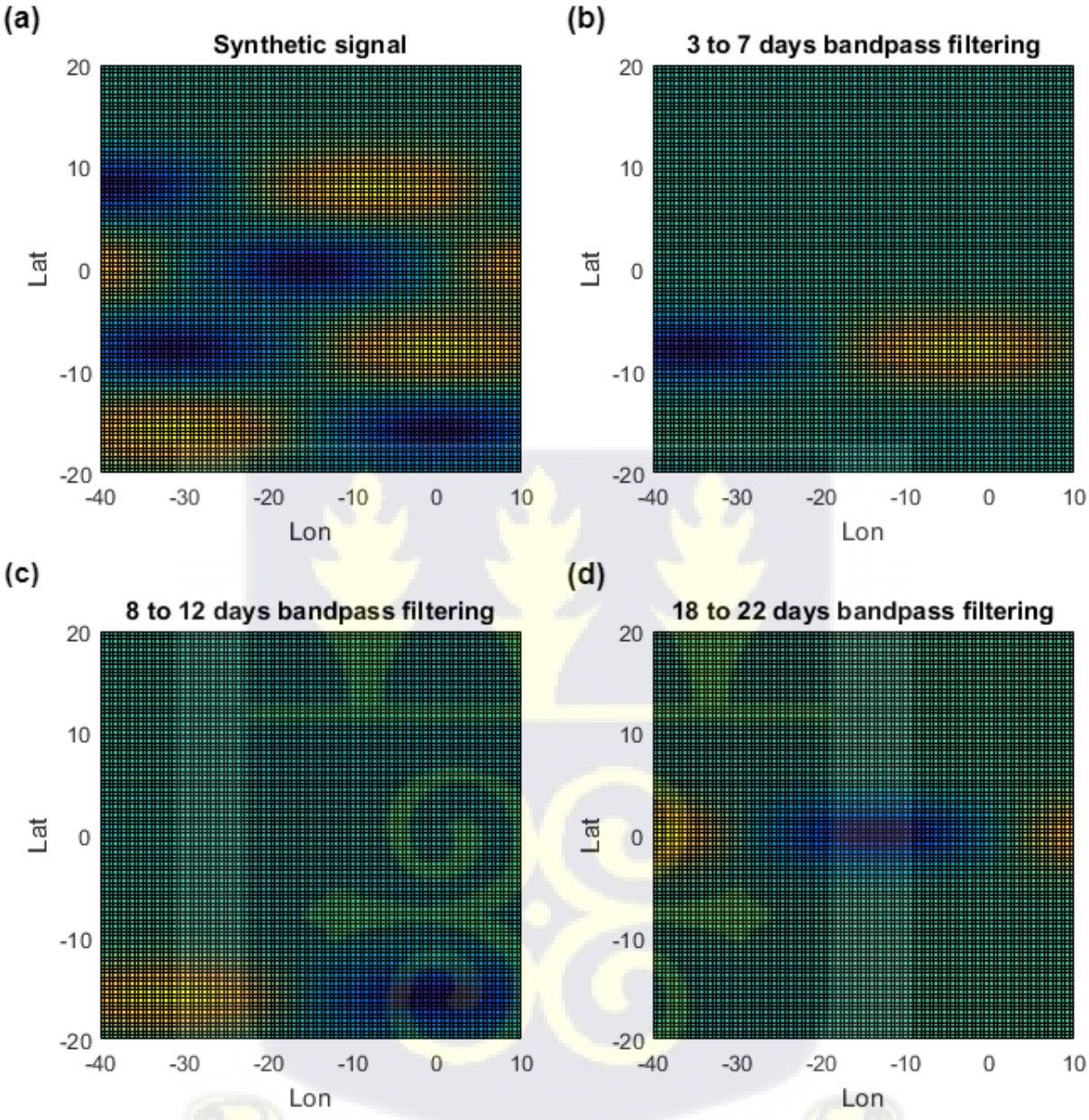

Figure A.3: Bandbass filtering at different frequencies

for characterizing and studying waves. Spectral analysis is a way of decomposing the time series to extract more information from the time series. This process allows the signals or time series to be expressed as sines and cosines using the Fourier transform, a frequency function. The absolute of the Fourier transform multiplied by itself gives the spectral density.

A.2.2 Cross-Correlation of Signals

Cross-correlation is the similarity measure between two signals (time series) at different time lag positions. The idea of cross-correlation is to compare the correlation coefficient of two signals to identify how strongly one signal is present in another signal. The mathematical relation of cross-correlation is given by

$$r_{xy} = \frac{\sum_{i=-K}^{K}(x_i - \bar{x})(y_i - \bar{y})}{\sqrt{\sum_{i=-K}^{K}(x_i - \bar{x})^2}\sqrt{\sum_{i=-K}^{K}(y_i - \bar{y})^2}}. \tag{A.1}$$

Equation (A.1) involves the removal of the mean from the data before finding the correlation coefficient. Cross-correlation can also be defined as

$$r_{xy} = \frac{\sum_{i=-K}^{K}(x_i)(y_i)}{\sqrt{\sum_{i=-K}^{K}(x_i)^2}\sqrt{\sum_{i=-K}^{K}(y_i)^2}}, \tag{A.2}$$

where K is the number of lags in the two signals. Equation (A.2) does not involve the removal of the mean from the data before finding correlation coefficent. It can be computed either by using the Matlab function **crosscorr** or **xcorr**.

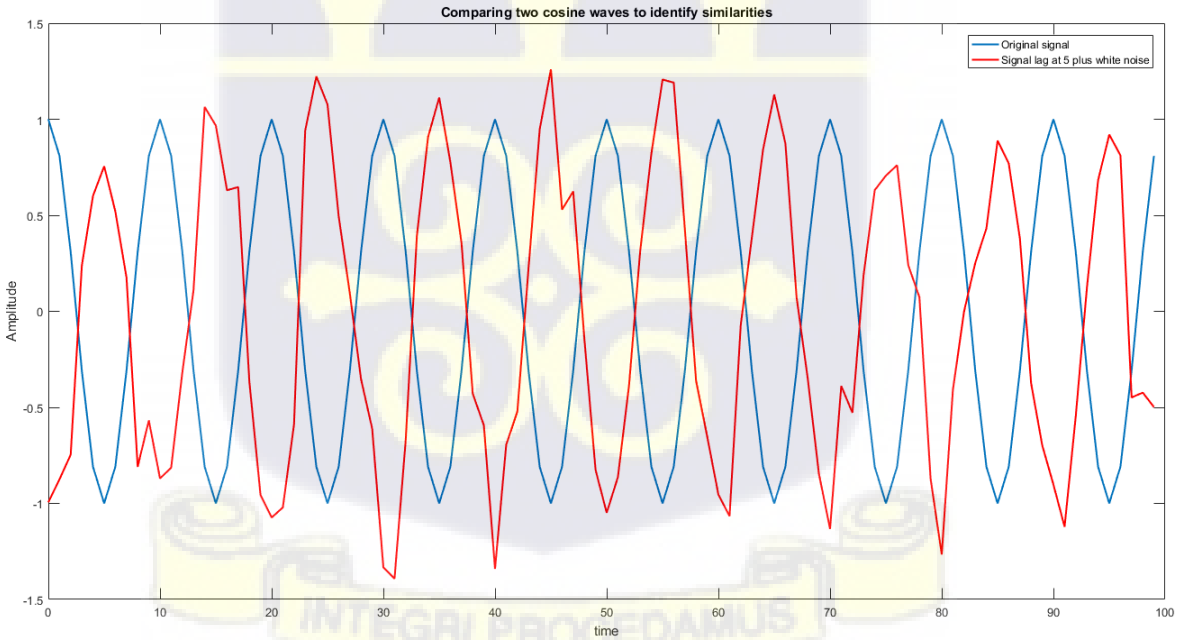

Figure A.4: Comparing the behaviour of two signals

We demonstrate using the cross-correlation sequence to estimate the phase lag be-

tween two cosine signals or waves. Two cosine waves with frequencies of $2\pi/10$ radian per sample are constructed. The starting phase of one cosine wave is 0, while the starting phase of the other cosine wave is $-\pi$ radians. We include a set of random data that follows a typical bell-shaped curve, centered around zero and with a spread of 0. 25 denoted as N(0,0.25^2) which is a white noise. The addition of N(0,0.25^2) white noise to the cosine wave with the phase lag of π radians. The two signals are given by $x = \cos(2\pi/10t(i))$ and $y = \cos(2\pi/10t - \pi) + 0.25 \times \text{randn}(\text{size}(t(i)))$. We cannot tell their similarities by plotting the two signals as shown in Figure A.4. By plotting the cross-correlation sequence as seen in Figure A.5 and marking the known lag between the two cosine waves, we find that the signal from x lags behind the signal from y.

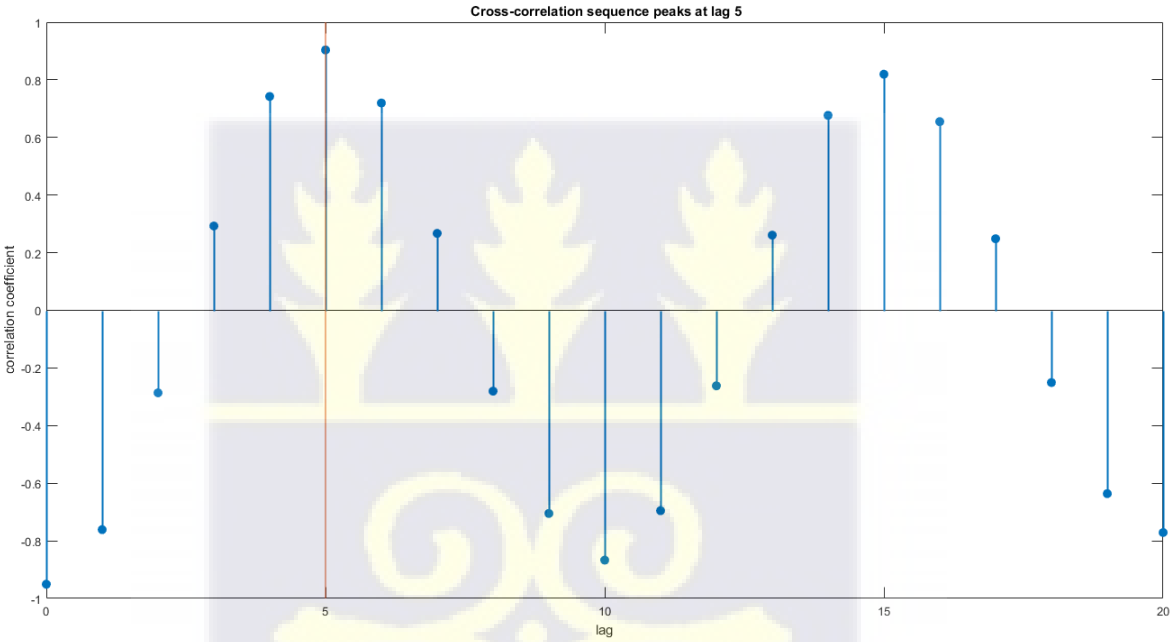

Figure A.5: Lag correlation of the two signals

References

[1] Bakun, A. (1978). *Guinea Current upwelling.* Nature, 271, 147–150, https://doi:10.1038/271147a0.

[2] O'Brien,J.J, Adamec, D., and Moore,D.W. (1978). *A simple model of equatorial upwelling in the Gulf of Guinea.* Geophysical Research Letters, 5, 641–644.

[3] Adamec, D. and O'Brien,J.J. (1978). *The seasonal upwelling in the Gulf of Guinea due to remote forcing.* J. Phys. Oceanogr., 8, 1050–1060.

[4] Picaut, J. (1983). *Propagation of the seasonal upwelling in the eastern equatorial Atlantic.* J. Phys. Oceanogr, 18–37, https://doi.org/10.1175/1520-0485(1983)013<0018:POTSUI>2.0.CO;2.

[5] Polito, P. S., and Cornillon, P. (1997). *Long baroclinic Rossby waves detected by TOPEX/POSEIDON.* J. Geophys. Res., 102, 3215–3235, http://doi:10.1029/96JC03349.

[6] Servain, J., Picaut, J., and Merle, J. (1982). *Evidence of remote forcing in the equatorial Atlantic Ocean.* J. Phys. Oceanogr., 12, 457–463.

[7] Polo, I., Lazar, A., Rodriguez–Fonseca, B., and Arnault, S. (2008). *Oceanic Kelvin waves and tropical Atlantic intraseasonal variability: 1. Kelvin wave characterization.* J. Geophys. Res., 113, C07009, http://doi:10.1029/2007JC004495.

[8] Roundy, P. E. and Kiladis, G. N. (2006). *Observed relationships between oceanic Kelvin waves and atmospheric forcing.* J. Clim., 19, 5253–5271.

[9] Polito, P. S. and Liu, W. T. (2003). *Global characterization of Rossby waves at several spectral bands.* J. Geophys. Res., 108(C1), 3018, http://doi:10.1029/2000JC000607.

[10] Polito, P. S., Sato, O. T., and Liu, W. T. (2000). *Characterization and validation of heat storage variability from Topex/Poseidon at four oceanographic sites.* J. Geophys. Res., 105(C7), 16,911–16,921.

[11] Djakouré, S., Penven, P., Bourlès, B. , Veitch, J., and Koné, V. (2014). *Coastally trapped eddies in the north of the Gulf of Guinea.* J. Geophys. Res. Oceans, 119, 6805–6819, http://doi:10.1002/2014JC010243.

[12] Djakouré, S., Penven, P., Bourlès, B. , Koné, V., and Veitch, J. (2017). *Respective Roles of the Guinea Current and Local Winds on the Coastal Upwelling in the Northern Gulf of Guinea.* American Meteorological Society, 47, 1367–1387, 3018, http://doi:10.1175/JPO\T1\textendashD\T1\textendash16\T1\textendash0126.1.

[13] Djakouré, S., Koné, M., Koffi, K.U., Kouadio, K.Y., Adon, M., Nyadjro, E., and Ta, S. (2023). *Characterization of marine heat waves in the eastern tropical Atlantic Ocean.* American Frontiers in Marine Science, 10, 2023, 2296-7745, http://doi:10.3389/fmars.2023.1293779.

[14] Moore, D.W., Hizard, P., McCreary, J., Merle, J., O'Brien, J.J., Picaut, J., Verstraete, J.M., and Wunsch, C. (1978). *Equatorial adjustment in the eastern Atlantic.* Geophys. Res. Lett., 8, pp. 637–640.

[15] Kouadio, Y.K., Djakouré, S., Aman, A., Ali, E., Kone, V., and Toualy, E. (2013). *Characterization of the Boreal Summer Upwelling at the Northern Coast of the Gulf of Guinea Based on the PROPAO In Situ Measurements Network and Satellite Data.* International Journal of Oceanography, 1687–9406, http://doi:https://doi.org/10.1155/2013/816561.

[16] Oliveira S.C. and Polito, P.S. (2013). *Characterization of westward propagating signals in the South Atlantic from altimeter and radiometer records.* Remote Sensing of Environment, 134 (2013), 367–376.

[17] Tulich, S.N, Kiladis, G.N., and Suzuki–Parker, A. (2009). *Convectively coupled Kelvin and easterly waves in a regional climate simulation of the tropics.* Clim. Dyn., 36:185–203, http://doi:10.1007/s00382\T1\textendash009\T1\textendash0697\T1\textendash2.

[18] Jacox, M.G. and Edwards, C.A. (2011). *Effects of stratification and shelf slope on nutrientsupply in coastal upwelling regions.* JOURNAL OF GEOPHYSICAL RESEARCH, 116, C03019, https://doi.org/10.1029/2010JC006547.

[19] Olaniran, J.M. and Muritala, A.A. (2020). *Seasonality of wind speed, wind shears and precipitation over West Africa.* Journal of Atmospheric and Solar–Terrestrial Physics, 207, 1364–6826, https://doi.org/10.1016/j.jastp.2020.105371.

[20] Philander, S. G. H. (1979). *Nonlinear Coastal and Equatorial Jets. Journal of Physical Oceanography.* Journal of Physical Oceanography, 9 (4). 739–747, https://doi:10.1175/1520\T1\textendash0485(1979)009<0739:ncaej>2.0.co;2.

[21] Wang, B. (2002, April, 16). *Kelvin Waves.* https://www.soest.hawaii.edu/MET/Faculty/bwang/bw/paper/wang_103.pdf.

[22] Abrahams, A., Schlegel, R.W., and Smit A.J. (2021). *Variation and Change of Upwelling Dynamics Detected in the World's Eastern Boundary Upwelling Systems.* Front. Mar. Sci., 8:626411. https://doi:10.3389/fmars.2021.626411.

[23] Lin, L. and Hurlburt, H. (1981). *Maximum simplification of nonlinear Somali Current dynamics.* Monsoon dynamics, pp.541–555.

[24] Wiafe, G. and Nyadjro, E.S. (2015). *Satellite Observations of Upwelling in the Gulf of Guinea.* IEEE Geoscience and Remote Sensing Letters, 12, 1066–1070. https://https://doi.org/10.1109/LGRS.2014.2379474.

[25] Stewart, R. (2008). *Introduction to Physical Oceanography.* Open Textbook Library.

[26] Benoit, C. R. and Beckers, J.M. (2011). *Introduction to Geophysical Fluid Dyanmics.* Academic Press.

[27] Talley, L. D., Pickard, G. L., Emery, W. J., and Swift, J. H. (2011). *Descriptive Physical Oceanography: An Introduction.* Burlington: Elsevier Science.

[28] Dwomfuor, P. (2014). *Theory and applications of conservation laws.* Master's thesis, Institutt for matematiske fag, https://ntnuopen.ntnu.no/ntnu-xmlui/handle/11250/259402.

[29] Knauss, J. A. (1997). *Introduction to physical oceanography.* Waveland Press.

[30] Houghton, R.W. (1976). *Circulation and Hydrographic Structure over the Ghana Continental Shelf during the 1974 Upwelling.* Journal of Physical Oceanography, 6(6), 909–924. Retrieved Jul 22, 2022, from https://journals.ametsoc.org/view/journals/phoc/6/6/1520\T1\textendash0485_1976_006_0909_cahsot_2_0_co_2.xml.

[31] Katz, E.J., Belevitsch, R., Bruce, J., Bubnov, V., Cochrane, J., Duing, W., Hisard, P., Lass, H.U., Meincke, J., DeMesquita, A., Miller, L., and Rybnikov, A. (1977). *Zonal pressure gradient along the equatorial Atlantic.* J. Mar. Res., 35(2), 293–307.

[32] Moore, D. (1968). *Planetary–gravity waves in an equatorial ocean.* Ph.D. Thesis, Harvard University, Cambridge, Mass.

[33] Moore, D.W. and Philander, S.G.H. (1977). *Modeling of the tropical oceanic circulation.* The Sea, Vol. VI, John Wiley Interscience, 319–361.

[34] Bunker, A. F. (1976). *Computations of surface energy flux and annual air–sea interaction cycles of the North Atlantic Ocean.* Mon. Wea. Rev., 104, 1122–1140.

[35] Yoshida, K. (1959). *A theory of the Cromwell Current and of equatorial upwelling.* J. Oceanogra. Soc. Japan, 15, 154–170.

[36] McPhaden, M. J. (2002). *Mixed Layer Temperature Balance on Intraseasonal Timescales in the Equatorial Pacific Ocean.* Journal of Climate, 15(18), 2632–2647. Retrieved Jul 23, 2022, from https://journals.ametsoc.org/view/journals/clim/15/18/1520\T1\textendash0442_2002_015_2632_mltboi_2.0.co_2.xml.

[37] McCreary, J. (1976). *Eastern tropical ocean response to changing wind systems; with application to El Nino.* Journal of Physical Oceanography, 6(5), 632–645.

[38] Hurlburt, H.E. and Thompson, J.D. (1976). *A numerical model of the Somali current* . Journal of Physical Oceanography, 6, 646–664.

[39] Kindle, J.C. and O'Brien, J.J. (1976). *A numerical simulation of the onset of E1 Nino.* Journal of Physical Oceanography, 6, 621–631.

[40] Arnault, S., Menard, Y., and Merle, J. (1990). *Observing the Tropical Atlantic Ocean in 1986–87 from altimetry..* Journal of Geophysical Research, 95, 17,921–17,946.

[41] Thomson, R. E. and Emery, W. J. (2014). *Chapter 5 – Time Series Analysis Methods (Data Analysis Methods in Physical Oceanography (Third Edition)).* Elsevier, 425–591. https://doi.org/10.1016/B978\T1\textendash0\T1\textendash12\T1\textendash387782\T1\textendash6.00005\T1\textendash3, retrieved Jul 27, 2022, from https://www.sciencedirect.com/science/article/pii/B9780123877826000053.

[42] Franca .C., Wainer, I., Mesquita, A. R. and Goni, G. (2003). *Planetary equatorial trapped waves in the Atlantic ocean from TOPEX/POSEIDON altimetry.* Elsevier Oceanography Series, 68, 213–232,946. https://doi.org/10.1016/S0422\T1\textendash9894(03)80148\T1\textendash4.

[43] Arnault, S. and Cheney, R. (1994). *Tropical Atlantic sea level variability from GEOSAT (1985–1989).* Journal of Geophysical Research, 99, 18,207–18,223.

[44] Busalacchi, A. and Picaut, J. (1983). *Seasonal variability from a model of the tropical Atlantic ocean.* Journal of Geophysical Research, 13, 1564–1588.

[45] Arnault, S., Menard, Y., and Merle, J. (1990). *Observing the Tropical Atlantic Ocean in 1986–87 from altimetry.* Journal of Geophysical Research, 95, 17,921–17, 946.

[46] Liu, W.T. (2002). *Progress in scatterometer application.* Journal of Oceanography, vol. 58, no. 1, pp. 121–136. https://doi.org/10.1023/A:1015832919110.

[47] Lamb, P.J. (1978). *Case studies of tropical Atlantic surface circulation pattern during recent sub– Saharan weather anomalies, 1967–1968.* Monthly Weather Review, vol. 106, pp. 482–491.

[48] Ducet, N., LeTraon, P.–Y., and Reverdin, G. (2000). *Global high resolution mapping of ocean circulation from TOPEX/Poseidon and ERS–1/2.* Journal of Geophysical Research, vol. 105, no. C8, pp. 477–498.

[49] Verstraete, J. M. (1970). *The seasonal upwelling in the Gulf of Guinea.* Progress Oceanography, vol. 29, no. 1, pp. 1–60.

[50] Nykjaer, L. and Van Camp, L. (1994). *Seasonal and interannual variability of coastal upwelling along northwest Africa and Portugal from 1981 to 1991.* Journal of Geophysical Research, vol. 99, no. C7, pp. 14197–14207.

[51] Wyrtki, K. (1975). *El Niño–The dynamic response of the equatorial Pacific ocean to atmospheric forcing.* Journal of Physical Oceanography, 5, 572–584.

[52] Binet, D. and Servain, J. (1993). *Have the recent hydrological changes in the Northern Gulf of Guinea induced the Sardinella aurita outburst?.* Oceanologica Acta, vol. 16, no. 3, pp. 247–260. Retrieve from https://archimer.ifremer.fr/doc/00099/21052/18678.pdf.

[53] Wiafe, G., Yaqub, H. B., Mensah, M. A., and Frid, C. L. J. (2008). *Impact of climate change on long–term zooplankton biomass in the upwelling region of the Gulf of Guinea.* ICES Journal of Marine Science, Volume 65, Issue 3, Pages 318–324. https://doi.org/10.1093/icesjms/fsn042.

[54] Rayner, N. A., Parker, D. E., Horton, E.B., Folland, C. K., Alexander, L. V., Rowell, D. P., Kent, E. C., Kaplan, A. (2003). *Global analyses of sea surface temperature, sea ice, and night marine air temperature since the late nineteenth century.* Journal of Geophysical Research,Vol. 108, No. D14, 4407 https://doi:10.1029/2002JD002670.

[55] *GLOBAL OCEAN GRIDDED L4 SEA SURFACE HEIGHTS AND DERIVED VARIABLES REPROCESSED (COPERNICUS CLIMATE SERVICE).* E.U. Copernicus Marine Service Information. https://doi.org/10.48670/moi\T1\textendash00145.

[56] Zhang H., Menemenlis, D., and Fenty, I. (2018). *ECCO LLC270 ocean–ice state estimate.* http://doi.org/1721.1/119821, also available at https://ecco.jpl.nasa.gov/drive/files/Version5/Alpha/doc/ECCO_LLC270.pdf.

[57] Zhang H., Menemenlis, D., and Fenty, I. (2018). *ECCO LLC270 ocean–ice state estimate.* http://doi.org/1721.1/119821, also available at https://ecco.jpl.nasa.gov/drive/files/Version5/Alpha/doc/ECCO_LLC270.pdf.

[58] Forget, G., Campin, J.–M., Heimbach, P., Hill, C. N., Ponte, R. M., and Wunsch, C. (2015). *ECCO version 4: an integrated framework for non–linear inverse modeling and global ocean state estimation.* Geoscientific Model Development, 8, 3071–3104,http://doi:10.5194/gmd\T1\textendash8\T1\textendash3071\T1\textendash2015.

[59] Hersbach, H., Bell, B., Berrisford, P., Biavati, G., Horányi, A., Muñoz Sabater, J., Nicolas, J., Peubey, C., Radu, R., Rozum, I., Schepers, D., Simmons, A., Soci, C., Dee, D., and Thépaut, J–N. (2018). *ERA5 hourly data on single levels from 1959 to present. Copernicus Climate Change Service (C3S) Climate Data Store (CDS).* (Accessed on 22–Oct–2020), https://doi:10.24381/cds.adbb2d47.

[60] Reynolds, R. W., Smith, T. M., Liu, C., Chelton, D. B., Casey, K. S., and Schlax, M. G. (2007). *Daily High–resolution Blended Analyses for sea surface temperature.*

J. Climate, 20, 5473–5496. Reynolds, R.W. 2009. What's new in version 2. Available online at http://www.ncdc.noaa.gov/oa/climate/research/sst/papers/oisst_daily_v02r00_version2\T1\textendashfeatures.pdf.

[61] Reynolds, R. W., Banzon, V. F., and NOAA CDR Program (2008). *NOAA Optimum Interpolation 1/4 Degree Daily Sea Surface Temperature (OISST) Analysis*. Version 2. NOAA National Climatic Data Center. https://doi:10.7289/V5SQ8XB5. Accessed on 20th January 2021.

[62] Huang, B., Liu, C., Banzon, V. F. Freeman, E., Graham, G., Hankins, B., Smith, T. M., and Zhang, H.–M. (2020). *NOAA 0.25–degree Daily Optimum Interpolation Sea Surface Temperature (OISST)*. Version 2.1. [https://www.ncei.noaa.gov/data/sea\T1\textendashsurface\T1\textendashtemperature\T1\textendashoptimum\T1\textendashinterpolation/v2.1/access/avhrr/]. NOAA National Centers for Environmental Information. https://doi.org/10.25921/RE9P\T1\textendashPT57. Accessed on 20th October 2021.

[63] Ingham, M. (1970). *Coastal upwelling in the northwestern Gulf of Guinea*. Bull. Mar. Sci., 20, 1–34.

[64] Colin, C. (1988). *Coastal upwelling events in front of the Ivory Coast during the FOCAL program*. Oceanol. Acta, 11, 125–138.

[65] Binet, D. (1997). *Climate and pelagic fisheries in the Canary and Guinea Currents 1964–1993: The role of trade winds and the Southern Oscillation*. Oceanol. Acta, 20, 177–190.

[66] Katz, E., and Garzoli, S. (1982). *Response of the western equatorial Atlantic Ocean to an annual wind cycle*. J. Mar. Res., 40, 307–327.

[67] Garzoli, S. L., and Katz, E. J. (1983). *The forced annual reversal of the Atlantic North Equatorial Countercurrent*. J. Phys. Oceanogr., 13, 2082–2090, https://doi:10.1175/1520\T1\textendash0485(1983)013<2082:TFAROT>2.0.CO;2.

[68] Philander, S. G. H., and Pacanowski, R. C. (1986). *A model of the seasonal cycle in the tropical Atlantic Ocean*. J. Geophys. Res., 91, 14 192–14 206, https://doi:10.1029/JC091iC12p14192.

[69] Clarke, A. (1979). *On the generation of the seasonal coastal upwelling in the Gulf of Guinea*. J. Geophys. Res., 84, 3743–3751, https://doi:10.1029/JC084iC07p03743.

[70] *Data Buoy Cooperation Panel.* OceanOPS 2001–2022. Retrieve from https://www.ocean\T1\textendashops.org/dbcp/platforms/types.html on 23rd October, 2022.

[71] *The Prediction and Research Moored Array in the Atlantic (PIRATA).* Retrieve from https://www.brest.ird.fr/pirata/pirata.php on 23rd October, 2022.

[72] Rhein, M., Rintoul, S.R., Aoki, S., Campos, E., Chambers, D., Feely, R.A., Gulev, S., Johnson, G.C., Josey, S.A., Kostianoy, A., Mauritzen, C., Roemmich, D., Talley, L.D., and Wang, F. (2013). *Observations: Ocean. In: Climate Change 2013: The Physical Science Basis. Contribution of Working Group I to the Fifth Assessment Report of the Intergovernmental Panel on Climate Change [Stocker, T.F., D. Qin, G.–K. Plattner, M. Tignor, S.K. Allen, J. Boschung, A. Nauels, Y. Xia, V. Bex and P.M. Midgley (eds.)].* Cambridge University Press, Cambridge, United Kingdom and New York, NY, USA, https://www.ipcc.ch/site/assets/uploads/2018/02/WG1AR5_Chapter03_FINAL.pdf.

[73] Alory, G., Da-Allada, C. Y., Djakouré, S., Dadou, I., Jouanno, J., and Loemba, D. P. (2021) *: Coastal Upwelling Limitation by Onshore Geostrophic Flow in the Gulf of Guinea Around the Niger River Plume,* Front Mar Sci, 7, 607216, https://doi.org/10.3389/fmars.2020.607216,2021.

[74] Brandt, P., G. Alory, F. M. Awo, M. Dengler, S. Djakouré, R. A. Imbol Koungue, J. Jouanno, M. Körner, M. Roch, and M. Rouault (2023). *Physical processes and biological productivity in the upwelling regions of the tropical Atlantic,* Ocean Sci., 19, 581-601, https://doi:10.5194/os-19-581-2023,2023.

[75] Illig, S., Bachèlery, M. L., and Cadier, E. (2018a) *: Subseasonal coastal-trapped wave propagations in the southeastern Pacific and Atlantic oceans: 2. Wave characteristics and connection with the equatorial variability,* J Geophys Res-Oceans, 123, 3942-3961, https://doi.org/10.1029/2017JC013539.

[76] Illig, S., Cadier, E., Bachèlery, M. L., and Kersale, M. (2018b) *: Subseasonal coastal-trapped wave propagations in the southeastern Pacific and Atlantic oceans: 1. A new approach to estimate wave amplitude,* J Geophys Res-Oceans, 123, 3915-3941, https://doi.org/10.1029/2017JC013540.

[77] Bachèlery, M. L., Illig, S., and Rouault, M. (2020) *: Interannual coastal trapped waves in the Angola-Benguela upwelling system and Benguela Niño and Niña*

events, J Marine Syst, 203, 103262, https://doi.org/10.1016/j.jmarsys.2019.103262,2020.

[78] Bachèlery, M. L., Illig, S., and Dadou, I. (2016a) *: Interannual variability in the South-East Atlantic Ocean, focusing on the Benguela Upwelling System: Remote versus local forcing,* J Geophys Res-Oceans, 121, 284-310, https://doi.org/10.1002/2015jc011168,2016a.

[79] Imbol Koungue, R. A. and Brandt, P. (2021) *: Impact of intraseasonal waves on Angolan warm and cold events,* J Geophys Res-Oceans, 126, e2020JC017088, https://doi.org/10.1029/2020JC017088,2021.

[80] Bordbar, M. H., Mohrholz, V., Schmidt, M., (2021) *: The Relation of Wind-Driven Coastal and Offshore Upwelling in the Benguela Upwelling System,* Journal of Physical Oceanography, 51:3117-3133, https://doi.org/10.1175/jpo-d-20-0297.1.

[81] Imbol Koungue, R. A., S. Illig, and M. Rouault (2017), *Role of interannual Kelvin wave propagations in the equatorial Atlantic on the Angola Benguela Current system,* J. Geophys.Res. Oceans, 122, 4685–4703, https://doi.org/10.1002/2016JC012463.

[82] Topé G.D.A., Alory G., Djakouré S., Da-Allada C.Y., Jouanno J. and Morvan G. (2023), *How does the Niger river warm coastal waters in the northern Gulf of Guinea?,* Frontiers in Marine Science, 10, 1187202. https://doi.org/10.3389/fmars.2023.1187202.